University of Alberta

Tearing Fracture of Energy Pipelines under Monotonic Loading Conditions

by

Mehmet Aydin ©

A thesis submitted to the Faculty of Graduate Studies and Research in partial fulfillment of the requirements for the degree of Master of Science

in

Structural Engineering

Department of Civil & Environmental Engineering

Edmonton, Alberta
Spring, 2007

Your file Votre référence
ISBN: 978-0-494-29934-0
Our file Notre référence
ISBN: 978-0-494-29934-0

ABSTRACT

Buried pipelines are primarily used by petrochemical industry in North America for transporting oil and derivatives. However, these pipelines are subjected to large deformations resulting from various factors such as: geotechnical movements, temperature effects, internal fluid pressure. Exceeding the critical deformation limit of the pipes initiates wrinkles and further increase may result in tearing type failure.

This research program was designed to simulate the tearing fracture of the pipes. Therefore, six specimens with two types of pipes having different wall thickness, length and diameter were tested under axial load, bending moment and internal pressure. Initially pressurized pipes were bended to create a wrinkle on the compression face and curvature was locked at a specific value. After that, pipes were loaded axially under constant curvature and pressure, to grow the wrinkle around the circumference and create a tearing type of failure.

ACKNOWLEDGEMENTS

I would like to extend my thanks to TransCanada Pipeline Ltd. and Tokyo Gas for providing financial support and testing specimens. Without their support this research project would not have been possible.

I would like to extend my thanks to my supervisor Dr. J.J. Roger Cheng for his guidance, support and patience throughout this project. Also my co-supervisor Dr. Mohammad Behbahanifard's contributions on finite element analysis are greatly appreciated. Thanks to the fellow graduate student Jianmin Zhang for his help and support during conducting the experiments.

The technical assistance from Mr. Richard Helfrich and Mr. Larry Burden of I.F. Morrison Structural Engineering Laboratory of University of Alberta is greatly appreciated.

TABLE OF CONTENTS

LIST OF TABLES

LIST OF FIGURES

List of Symbols

A_i Cross-sectional area of the water chamber inside the pipe wall

A_s Cross-sectional area of the pipe on an undeformed normal cross section

D Nominal diameter of pipe specimen

D/t Diameter-to-thickness ratio of pipe

E Elasticity Modulus

FEA Finite element analysis

F_j The jack force

L_{pipe} Overall length of pipe

LVDT Linear variable differential transducer

M_g Global end moment

M_{max} Experimental maximum moment

p_i Internal water pressure

P_{max} Maximum axial load capacity of pipe segment

P_{MTS} MTS load

p_y Internal pressure that causes yielding in the hoop direction

RVDT Rotational variable differential transducer

SMYS Specified minimum yield strength

t Wall thickness of pipe

Greek Symbols

ϕ_g Global curvature

ϕ_L Local curvature

σ_y Yield stress

θ_{top} Top rotation angle

θ_{bottom} Bottom rotation angle

$\theta_{ave.}$ Average rotation angle

δ_{LVDT} Horizontal displacement of a given cross section taken from LVDT measurements

Δ Deflection

ε_{cr} Critical buckling strain

ν Poission's ratio

$\mu\varepsilon$ Unit of microstrain (10^{-6} strain)

1. INTRODUCTION

1.1. Statement of the Problem

In Arctic and sub-Arctic regions of Canada, buried pipelines have proven to be one of the most effective ways of transporting oil and natural gas resources to urban regions. However, field observations of buried pipelines show that it is not uncommon for geotechnical movements and temperature effects to impose large displacements on buried pipelines that may result in localized deformations in the pipe wall, i.e. local buckling or wrinkles. The local buckling may eventually result in fracture of the pipe at wrinkle locations.

The geotechnical movements and temperature difference create axial force and bending moment on the pipelines. Axial force may result form temperature difference and soil-pipe interaction. It is known that pipeline construction in Northern parts of Canada normally takes place during winter time when the temperature is around -30°C or lower, but the operating temperature for pipelines in the summer can be around +15°C. This temperature difference of 45°C will impose axial force on the pipeline. In addition to temperature effects, internal pressure may also result in axial force on the pipe due to Poisson's effect. Furthermore, buried pipelines are not free to expand or contract because surrounding soil constrains the pipe movement. Soil friction results in compressive strains on the pipe. On the other hand, geotechnical movements such as soil settlements impose bending moment on the pipe, when combined with the axial forces/strains can fail in local deformations or buckling. If the axial force and bending moment continue to increase, the pipe can fail in tearing fracture, as shown in Figure 1.1

(Das et al., 2002). However, there is no existing research program studying this unique failure mechanism.

1.2. Objectives and Scope

An experimental program was designed to simulate the behavior of pipelines failed by tearing fracture under combination of internal pressure, bending moment and axial load. The program is designed to address the following two objectives related the tearing failure:

- To investigate under what loading conditions the tearing fracture can occur in a wrinkled pipe.
- To determine limiting strain or deformation values at the wrinkle location that may result in fracture or significant change in pipeline geometry which can disrupt pipeline safety or integrity.

To achieve these objectives full-scale tests were conducted under constant internal pressure and curvature with monotonically increased axial load in the test program. Two different sizes (406 mm and 508 mm) of pipes with D/t ratios of 34 and 79, respectively, were used in the test specimens. The steel grades of X60 (SMYS = 414 MPa) and X65 (SMYS = 448 MPa) were used in 406 mm and 508 mm diameter specimens, respectively. A total of six specimens/tests were conducted in the program, which includes three tests from each of pipe size.

It is known that in oil and natural gas pipelines maximum internal operating pressure is controlled by the hoop stress permitted and the hoop stress is limited to a fraction of the SMYS (Mohareb et al. 2001).All specimens were pressurized with 40%

of the specified minimum yield stress (SMYS) to avoid the diamond shape wrinkle(Figure 1.2). Also, an initial axial load was applied on the pipes to reduce the stress on the top and bottom end welds of the pipe. Then, bending moment was applied monotonically to the pipes until bulge type wrinkle was formed on the compression side of the specimens. The specimens were then loaded continuously by gradually increasing the curvature on the pipes until a desired curvature was reached and sizable wrinkle was formed in the specimens. The specimens were then loaded under a monotonically increasing axial load and constant curvature, either with zero internal pressure or 40% of SMYS internal pressure depending on the test parameter of each specimen, until tearing was occurred in the pipe.

1.3. Organization of Thesis

The body of the thesis is broken into five chapters. Chapter one is the introduction part of the thesis.

Chapter two summarizes the research findings related to the pipeline fracture under constant curvature. However, this research project is the first of this new research area so limited number of literature was reviewed. The FEA which was conducted by Dr. Behbahanifard and PhD. Candidate Jianmin Zhang to determine the loading sequences of the tests is included in this section.

Chapter three includes the explanation of testing setup and test procedures that were followed during the testing of the six full-scale specimens. The chapter also includes the observed parameters and detailed explanation of the instrumentation used in the experimental program.

Chapter four gives the reduced data obtained from the experiments. The behavior of each pipe during testing was explained. This chapter includes detailed discussion of each pipe to the corresponding loading sequences and experimental procedures. Also, in this chapter test specimens were compared to each other to interpret the effect of various parameters on tearing behavior.

Chapter five provides summary, conclusions and recommendations obtained from this study.

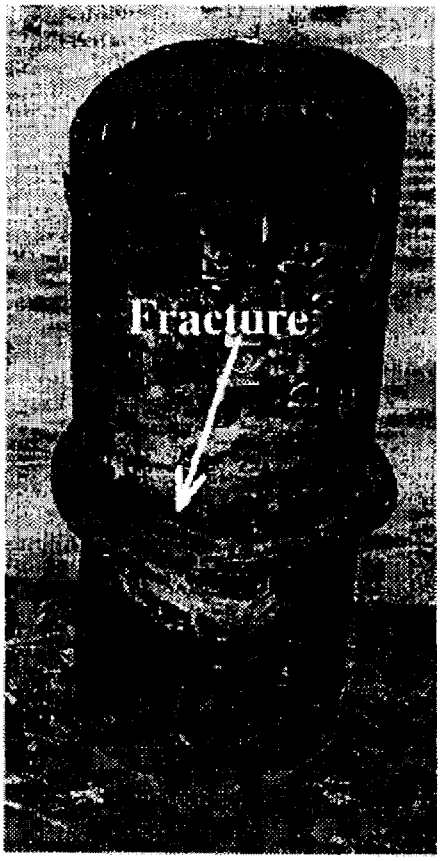

Figure 1.1 Fractured Linepipe specimen of WestCoast Energy Inc

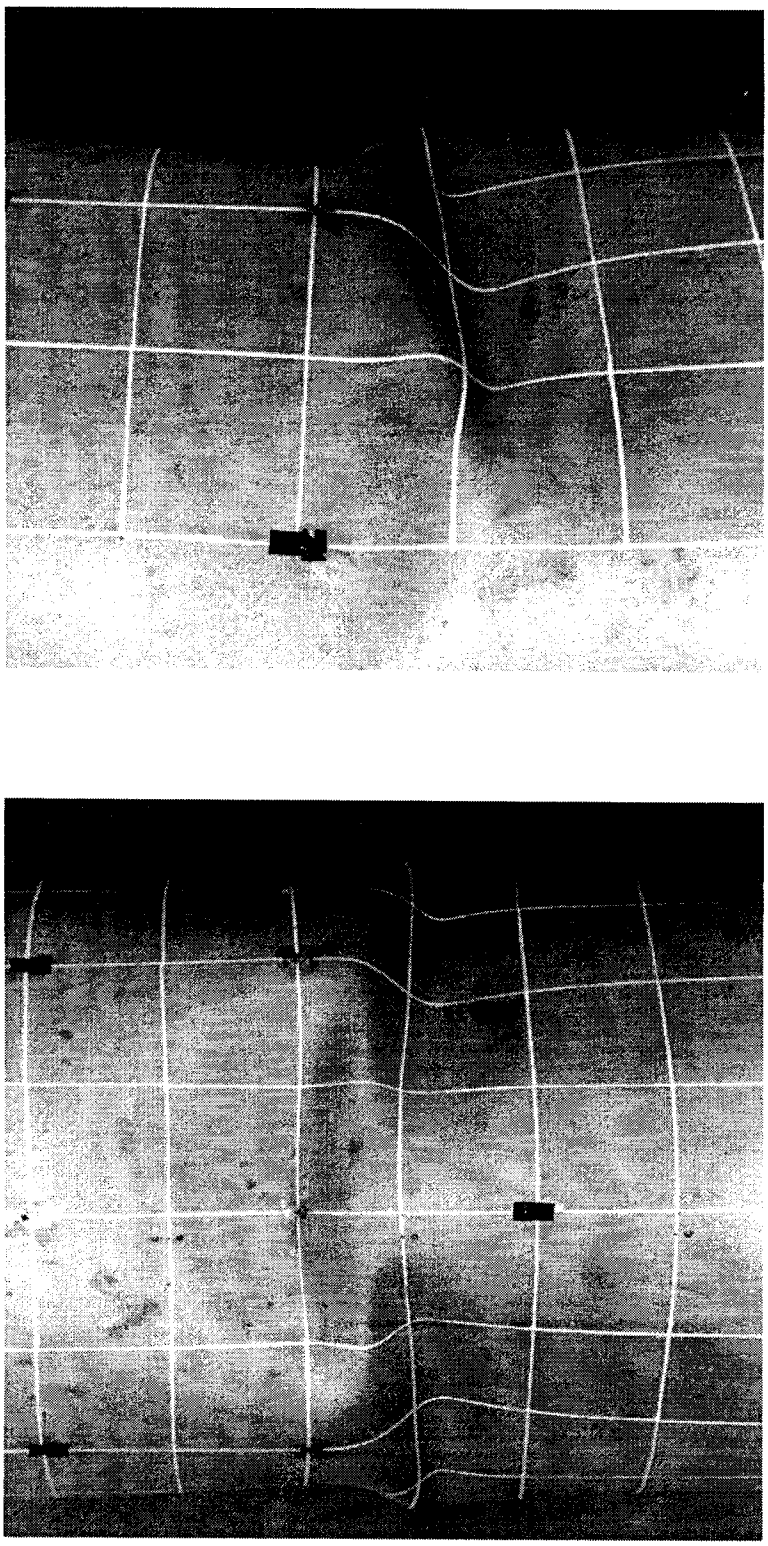

Figure 1.2 General view of a Diamond shape buckle

2. LITERATURE REVIEW

2.1. Introduction

This chapter reviews the existing literature on behavior of buried pipelines under harsh environmental conditions. The majority of the research done on buried pipelines are related to the wrinkling (local buckling) behavior, i.e. onset of buckling. However, the main objective of this project is to understand the post-buckling behavior until tearing or fracture of a wrinkled pipe. Therefore, limited amount of literature was found related to this new area.

The main focus of this research program is to provide experimental data to assess the potential tearing failure of a pipeline. For that reason, numerical analysis will not be covered in this study nor will the literature review.

2.2. Related Research

2.2.1. J.G. Bouwkamp and R.M. Stephen (1973)

Bouwkamp and Stephen (1973) were probably the first ones to conduct full-scale pipeline experiment in this area. They studied the combined effect of the axial load, bending moment and internal fluid pressure on the structural behavior of 48 inches diameter pipes, the wrinkling of the pipe wall and the ultimate rupture of the pipe. The results of the experiment were used in establishing operational limits as affected by the local buckling of the pipe wall and safety limits necessary to prevent rupture of the pipe.

The loading sequence used by Bouwkamp and Stephen (1973) applied constant internal pressure, followed by constant axial load and the monotonically increasing bending moment. During the experiments they applied 95% of p_y of internal pressure

initially for 8 hours and then drop it to testing pressure level. Pressurization was followed by the application of the axial load which was the sum of the forces resulted from temperature difference, Poisson's effect and cap forces on the pipe due to the internal pressure. Finally, bending was created by the loading yokes and cables acting at the four points on the specimens. They tested a total number of seven specimens having an overall length of 31.5 feet. All the pipe specimens were a grade of X60. The test setup was a four point bending system where the pipes were tested in a vertical position.

Bouwkamp and Stephen (1973) obtained valuable observations and conclusions from those set of experiments. Basically, according to the test results, the 48 inches pipes showed excellent ductility with forming wrinkle without rupturing the pipe wall. The displacements at time were 20 times larger than those under which buckling occurred. One important result obtained was that, highly pressurized pipes had much higher critical buckling strains than pipes with low internal pressure. It was also observed internal pressure had an effect on the type of buckling of the pipes. Under high levels of pressurization buckling was in a shape of outward bulge, where as in for low pressure cases, pipe wall buckling took the form of diamond-shape.

Another important conclusion is that, neutral axis shifted towards tension zone under bending. It was also observed that for the pressurized case wrinkles extend over at least 2/3 of the circumference.

2.2.2. *M. Mohareb, S.D.B Alexander, G.L. Kulak and D.W. Murray (1993)*

The objective of the research of Mohareb et al. (1993) was to observe the deformation of pipeline under large inelastic deformation in order to provide experimental database to establish techniques for design and assessment of pipe performance when subjected to imposed geotechnical settlements. The test setup was designed to provide basis to evaluate the numerical predictions of large deformation elastic-plastic local buckling of buried pipelines. Full-scaled tests were carried out and two types of pipes were used: (a) 508 mm x 7.9 mm (outside diameter (OD) x thickness) Grade X56 (386 MPa); and (b) 324 mm x 6.25 mm Grade X52 (359 MPa).

When compared to Bouwkamp et al. (1973), Mohareb et al. (1993) used a totally different test setup. The test setup used by Mohareb et al. (1993) was similar to the arrangement that was used to investigate the strength and behavior of beam-columns. The pipe was first welded at both ends to the two end plates by circumferential groove weld and then, the pipe was connected to two horizontal moment arms. The pipe stood in the vertical position between the moment arms. The application center of the axial load (by a universal testing machine) passed through the center of the pipe. The bending moment was created by a hydraulic jack located between the moment arms. This setup allowed Mohareb et al. (1993) to use shorter specimens than Bouwkamp et al. (1973).

Previous research discovered that pipe behavior was dependent on material properties, residual stresses, fabrication techniques and initial imperfections. Therefore, stub column and tension coupon tests were carried out to observe the effect of those parameters. Unlike a coupon test, stub column tests provided the material response up to peak loading including the effect of initial imperfections and residual stresses.

Besides, the loading procedure for the test specimens was to first apply the axial load, then apply the internal pressure and last, to impose curvature on the pipe by opening the moment arms by an eccentric jack.

The experimental arrangement used by Mohareb et al. (1993) was more effective and efficient to obtain deformational characteristics of a pipeline than the one used by Bouwkamp et al. (1973). It was concluded from the moment vs. curvature response of the pipes that, internal pressure reduced the axial load carrying capacity but increased its ductility (i.e. critical compressive strain).

2.2.3. S.Das, J.J.R. Cheng and D.W. Murray (2003)

The research work, conducted by Das et al., was targeted to provide information required for the assessment of the fracture risk at the wrinkle locations of the buried pipelines. For that reason, 12 full-scale specimens, which were operated by Norman Wells pipeline and Enbridge Pipeline Inc. were tested. Determination of the loading conditions that can result in fracture, limit strain values at buckle location and the assessment of the fracture criteria to determine the remaining fatigue life of a wrinkled pipe are the main objectives of this research.

First two specimens of the experimental program were loaded by continuously increasing axial load and constant internal pressure. However, it was observed that, fracture does not occur under such loading history. Therefore, for the remaining specimens strain reversals were created in the wrinkle locations either by loading/unloading of axial load or moment under constant internal pressure.

It was concluded from the test of 12 specimens that, fracture can occur in the wrinkled location with very few cycles due to the low-cycle fatigue. On the other hand, monotonically increasing axial load does not create fracture.

2.2.4. B. Myrholm, J.J.R. Cheng and D.W. Murray (2001)

The objectives of the research by Myrholm et al. (2001) included, expanding the database on pipeline behavior under constant internal pressure, axial load and increasing curvature. Another objective was to understand the behavior at wrinkle location under cyclic loading. Eight full scale pipes having OD of 508 mm were tested. Four of them had a D/t ratio of 62 and the rest had 85. Also, six of the pipes had a girth weld at their mid-section. The test setup used by Mohareb et al. (1993) was used for this project. The axial load was delivered by a universal testing machine and the curvature was created by an eccentric jack.

Similar to previous research, it was observed that in case of pressurized pipes bulge type wrinkle occurred and for unpressurized case diamond-shape buckle was formed. It was also observed that, D/t ratio affects the location of the wrinkle, for D/t ratio of 85 wrinkles intersected the girth weld at mid-height and small fractures occurred. However, for D/t ratio of 62, wrinkles did not intersect with the girth weld and the fractures were formed in the circumferential direction at the crest of the wrinkle. Besides, pipes having lower D/t ratio showed higher peak moment values. The girth welded pipes having same D/t ratios showed lower critical strain values than non-girth welded pipes.

2.2.5. S. Das, J.J.R. Cheng and D.W. Murray (2002)

Two full scale tests applying axial load and shear load with different boundary conditions were carried out on NPS12 pipe by Das et al. (2002). According to the diagnoses of a fracture at a wrinkle location of a pipeline operated by WestCoast Energy Inc. it was found that failure was resulting from monotonic application of axial load not aligned with the axis of the pipe. In order to simulate the field failure, two pipes having 324 mm (12.75") OD, 6.84 mm thickness and Grade X52 were used for this testing program. The test setup used was a very simple arrangement; pipe was welded to two end plates at both ends of the pipes. The axial load was applied by a universal testing machine and lateral force was applied by a hydraulic jack at a desired location. The testing procedure includes three parts; first concentric axial load was applied until the wrinkle was formed around mid height of the pipe when the specimen boundary conditions were fixed against rotation. As a second stage, axial load was unloaded and end conditions were changed into pin-pin situation. After that, axial load was increased up to previous level and lateral load was applied 30 mm below the wrinkle location until desired rotation and lateral deflection formed between upper and lower parts of the pipe. As a final stage, end conditions were brought back to clamped-clamped condition, which was followed by the application of axial load. During this stage, as the axial load was increased, the wrinkle folded on the compression side and upper part of the specimen began to telescope into the bottom part of the specimen. Finally, the pipe was failed by the tearing fracture.

In conclusion, it was observed from this test series that, in presence of telescoping action, monotonic loading can result in tearing type of failure.

2.3. FEA for Simulation of Tearing Failure under Monotonic Loading Conditions

Buried pipelines are usually subjected to geotechnical movements, internal pressure and temperature effects. These load combinations can result to localized buckling and wrinkling of a pipe. From an operational point of view, the buckling/wrinkling may restrict product flow or may prohibit the passage of in-line inspection tools, e.g. Geopig, required for proper maintenance. Under specific circumstances, the increase in deformations at buckling/wrinkling locations may cause fracture of the pipe wall, which will affect the pipeline integrity.

Previous research conducted at the University of Alberta has shown that large deformations resulting from monotonically applied loads generally lead to an accordion type wrinkle, but fracture does not occur, unless strain reversals exist at the wrinkle location due to the application of cyclic loads (Das et al., 2002).

Under a specific loading condition, severe strain reversal may occur at a wrinkle location, which can result in fracture of pipeline. An experimental program conducted at the University of Alberta (Das et al. 2002) successfully simulated a tearing failure in a pipeline, similar to field fracture by using only monotonically applied loads.

Although the test at the University of Alberta was considered monotonic, the loading sequence used in the experiment consisted of axial loading (30 mm axial stroke to create a wrinkle at the mid-height of the specimen), an unloading (to allow for the insertion of the knife edges in the loading apparatus) and then a reloading sequence (up

to failure of the pipe wall). While not fully reversed, the load-unload reload sequence does represent a cyclic loading sequence (of at least one cycle) and not a truly monotonically increasing loading sequence. The effect of this can be seen in either the load displacement or the stress-displacement plots where two reversals are evident (Das et al. 2002).

The objective here in this investigation is to modify the testing procedure, implemented by Das et al. 2002, in order to simulate a fracture in a wrinkled pipe by applying only a monotonic loading (no load-unload-reload sequence). The finite element analysis to investigate the objective that was mentioned above was conducted by Dr. Behbahanifard and PhD. Candidate Jianmin Zhang. The test procedure in this simulation is based on the followings steps:

1) Developing a bulged type wrinkle in a segment of pipeline by applying a combination of axial force, bending moment and internal pressure.

2) At a specific wrinkle size and curvature (or a specific ratio of compressive strain to critical strain), the rotations at both ends of pipe will be locked. The locking of the end rotation as part of the testing procedure is to simulate the effect of soil constraint in a buried pipeline.

3) While the end rotations are locked the axial deformation of the pipe increased until a fracture develops in the pipe at the wrinkle location.

The objective of the present finite element analysis in this phase of the project is to propose a testing procedure based on the above steps considering the limitation of the facilities at the University of Alberta.

2.3.1. Finite Element Model

ABAQUS version 6.3 was used as the finite element program. The details of the finite element model outlined following:

1) The shell element S4R was used to model the pipe. The S4R is a general purpose 4-node doubly-curved shell element with reduced integration.

2) Because of symmetry, only one half of the pipe along the longitudinal axis was modeled.

3) A mesh size of 40 by 100 elements was used (40 elements in circumferential direction).

4) End plates were modeled using 3-node shell elements. The end plates were 75 mm thick and were modeled as an elastic material.

5) The end plates were connected by rigid links to the pivot points at both ends to simulate rigid sections at both ends (with the rotational degree of freedom at the pivot points).

6) Hinged boundary conditions were used at both ends and only the axial degree of freedom released at one end.

7) Displacement control was used for application of end moments (Boundary type-displacement in ABAQUS).

8) Collars were used at both ends of the pipe to prevent end buckling. The collars were modeled using a thicker plate and elastic material properties.

9) 5% of pipe thickness was used as an imperfection at the mid-length of the pipe.

2.3.2. *Material Properties*

Material properties of the 16 inches pipe were obtained by conducting a standard tension test on a longitudinal strip obtained from the pipe. Figure 2.1 shows the engineering stress-strain curve and the mechanical properties are shown in Table 2.1. The material properties obtained from a tension coupon test are nominal values, i.e., engineering stress and engineering strain, which are defined in terms of an initial gauge length and initial cross sectional area of the coupon. The finite element analysis uses true stress (Cauchy stress) and logarithmic strain as stress and strain measures regardless of the type of analysis. To obtain the true stress (σ_{true}) and logarithmic plastic strain ($\varepsilon_{\ln}^{pl}$) the following transformations are applied to the tension coupon data

$$\sigma_{true} = \sigma_{nom}(1+\varepsilon_{nom})$$

$$\varepsilon_{\ln}^{pl} = \ln(1+\varepsilon_{nom}) - \frac{\sigma_{true}}{E}$$

where, E is the modulus of elasticity; σ_{nom} is the nominal (engineering) stress; and ε_{nom} is the nominal (engineering) strain obtained from material tests. Figure 2.2 shows the material input for the finite element analysis.

2.3.3. *Finite Element Analysis for 16 inch Pipes*

In order to come up with a testing procedure to simulate fracture of a wrinkled pipe under monotonic loading many finite element analyses under different loading conditions were conducted. Some of the procedures resulted in different failure modes (i.e. end wrinkle or accordion type failure) and for some of the analysis the loading demands exceeded the capacity of the equipment that were available at the structural engineering lab at University of Alberta. In the following only the result of the finalized

FE procedure that was used as a base for simulation of tearing under moronic loading is presented.

2.3.3.1.Pressurized Pipe

Based on the results of finite element analysis, the following steps are proposed in order to simulate a tearing under monotonic loading:

1) Apply 40% of p_y of internal pressure (11.9 MPa). Internal pressure is mainly applied to develop a bulge type wrinkle. An axial force of 1373 kN is also applied to compensate the effect of pressure on the cap plates.

2) Apply 2000 kN extra axial compressive force by MTS. The total axial force at this stage is 3373 kN (see Figure 2.3).

3) Apply End rotations to create a bulge wrinkle around the mid height of the pipe (see Figure 2.4). The size of wrinkle has significant effect in success of the experiment. Based on FEA results, minimum rotation of 0.085 radians should be used in order not to exceed the MTS capacity (6000 kN) during the application of axial stroke.

4) Lock the rotation at both ends of pipe. During the experiment this can be achieved by modifying the force in the jack. Variation of the jack force throughout the experiment while the end rotations were locked can be seen in Figure 2.5.

5) Increase the axial displacement of the specimen (Using MTS) to create another bulge wrinkle on the opposite side of the original wrinkle (at tension face, see Figures 2.6 and 2.7) and keep increasing the axial displacement to develop a tearing type failure at mid height of the specimen.

2.3.3.2. Unpressurized Pipe

The wrinkle in un-pressurized pipe has a diamond shape. Following the procedure established in previous section starting with no internal pressure resulted to a failure mode shown in Figure 2.8. For practical reasons and feasibility of the test to fail in tearing, a bulge wrinkle is preferred for the initial wrinkle. As a result the procedure for un-pressurized test will be similar to the pressurized test except that after locking the end rotation at a specific angle, the internal pressure is released and then axial stroke will be applied to the specimen. The MTS force versus the axial stroke is shown in Figure 2.9 for a zero pressure situation (The pressure was only applied to create an initial wrinkle).

2.3.4. Finite Element Analysis for 20 inch Pipes

Basically the same procedure as 16 inches pipes was used for the 20 inches pipes. The only differences were the level of axial load and the rotation angle. The procedure is as follows:

1) Apply 40% SMYS (5.31 MPa) internal pressure and at the same time applying 1021 kN axial load to compensate the effect of internal pressure on cap plate.
2) Apply 520 kN extra axial load (10% of yield strength).(see Figure 2.10)
3) Apply end rotations to create a bulge wrinkle around the mid height of the pipe (see Figure 2.11). Based on FEA results, minimum rotation of 0.0871 radians should be used in order not to exceed the MTS capacity (6000 kN) during the application of axial stroke.

4) Lock the rotation at both ends of pipe. During the experiment this can be achieved by modifying the force in the jack. The change of jack force during the experiment is given in Figure 2.12.

5) Increase the axial displacement of the specimen (using MTS) to create another bulge wrinkle on the opposite side of the original wrinkle (at tension face, see Figures 2.13 and 2.14) and keep increasing the axial displacement to develop a tearing type failure at the mid-height of the specimen.

2.3.5. General Notes

1) Application of 2000 kN axial force reduces the demand on hydraulic jack for developing a bulge wrinkle (for 16 inches pipes). Under combination of axial force and bending moment, wrinkle was initiated at 600 kN compressive jack load. However, in Figure 2.15 the same wrinkle is developed under pure bending condition and the required jack force is increased to 838 kN.

2) Since the rotations at both ends of specimen are locked, increasing the axial deformation of the pipe might trigger formation of another wrinkle at the ends of the pipe (see Figure 2.16). Adding more collars at the beginning of the experiment or after formation of first wrinkle at the middle will prevent this issue and all the deformation will be concentrated at the original wrinkle location.

3) By modifying the force in hydraulic jack, the average rotation at the specimen ends can be locked. The end moments will change the sign during the test in order to keep the end rotation constant. During the test the hydraulic jack force will be in

compression and eventually it will be in tension. A double acting jack with proper connection detail should be considered in the design of test set up.

4) By comparing Figures 2.3 and 2.17 (the MTS force vs. MTS stroke) it can be concluded that regardless of the amount of axial force for developing the initial wrinkle, the maximum MTS force and stroke is similar for developing the second wrinkle in tension face of the specimen.

5) The point for locking the end rotation will affect the MTS demand for creation of second wrinkle. Higher the angle reduces the MTS demand and also increasing the possibility of a sever strain reversal the wrinkle location and fracture of the pipe.

The above testing protocol is based on the limitation of the testing facility in the laboratory. Based on the results of this experiment a comprehensive parametric study should be conducted to investigate the effect of the above parameters on tearing resistance of pipelines. The finite element model should be modified by including contact elements at the wrinkle location in the model and also inclusion of a suitable fracture material model to simulate the tearing.

Table 2.1 Mechanical Properties of 16 inch Pipes

Thickness (mm)	E (GPa)	Proportional Limit (MPa)	Static Yield (MPa)	Dynamic Yield (MPa)	Static Ultimate (MPa)	Dynamic Ultimate (MPa)	Final Elong. (%)
11.9	193.5	226	489	507	543	572	33.5

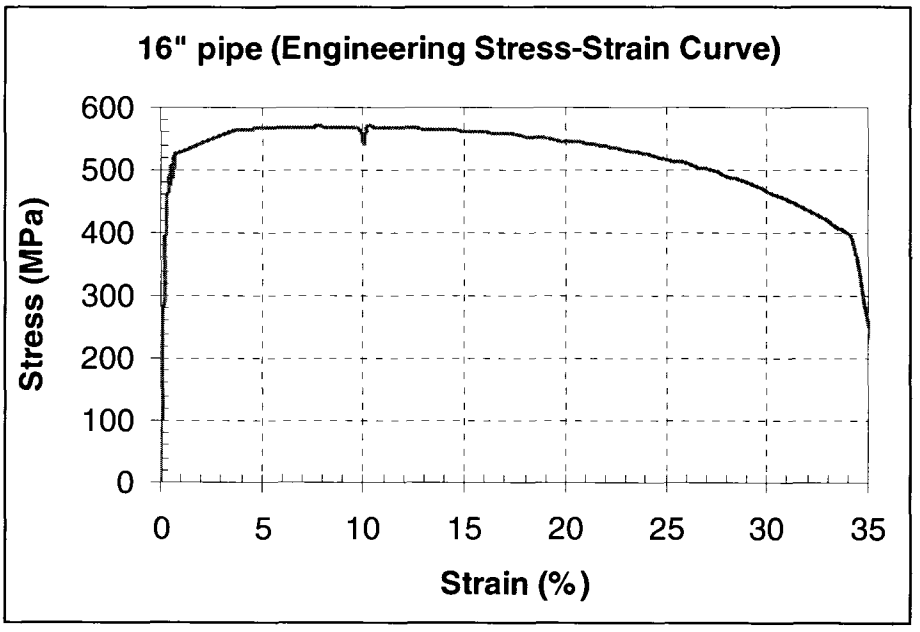

Figure 2.1 Engineering Stress-Strain curve for 16 inch pipes
(Obtained from a longitudinal strip coupon)

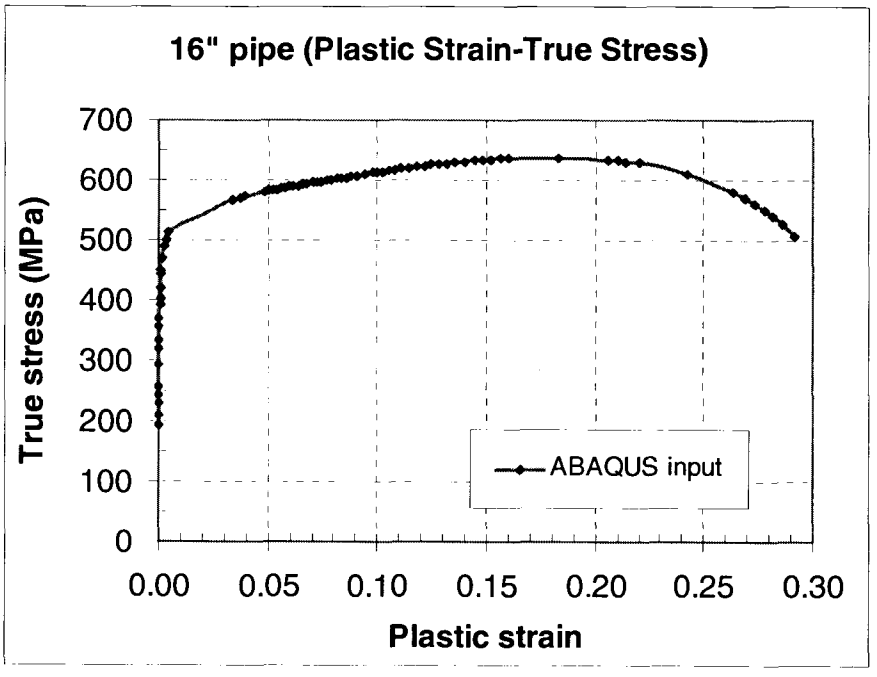

Figure 2.2 True Stress-Plastic Strain prepared as an input for ABAQUS

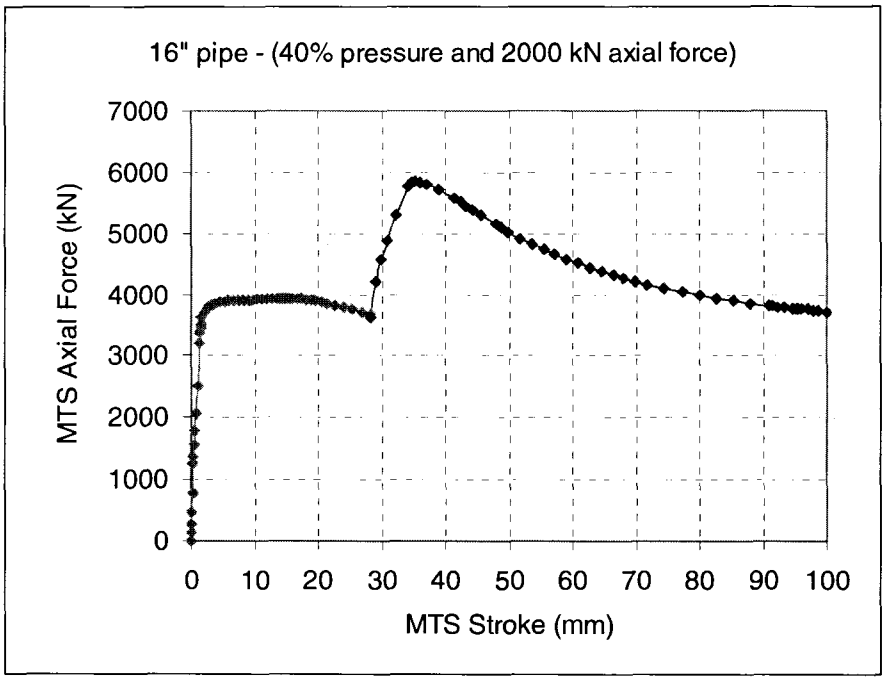

Figure 2.3 MTS force vs. MTS stroke

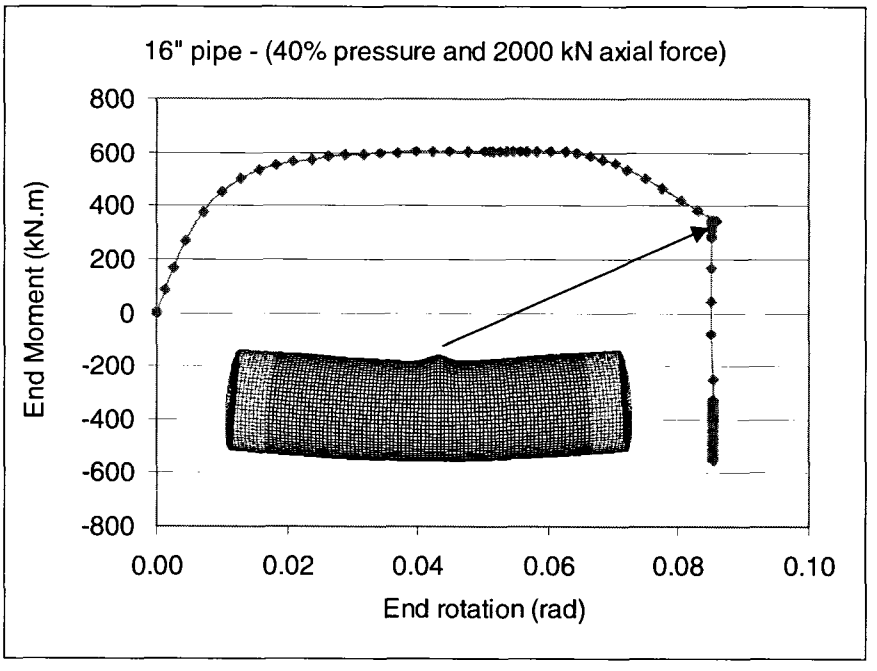

Figure 2.4 Initiation of wrinkle at the mid-height of a 16 inch pipe
(Under the combination of internal pressure, axial load and bending moment)

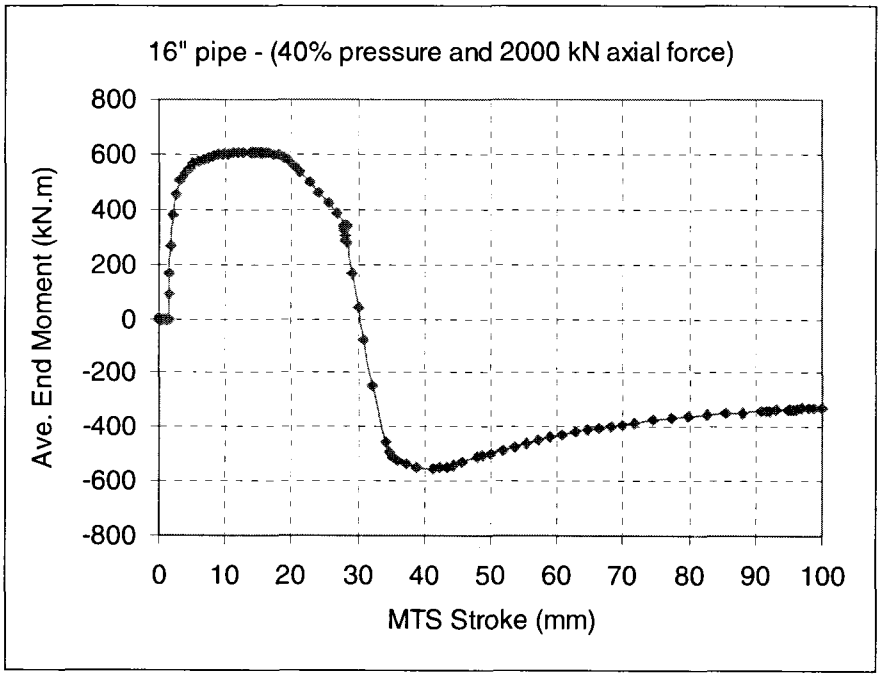

Figure 2.5 End Moment vs. MTS stroke

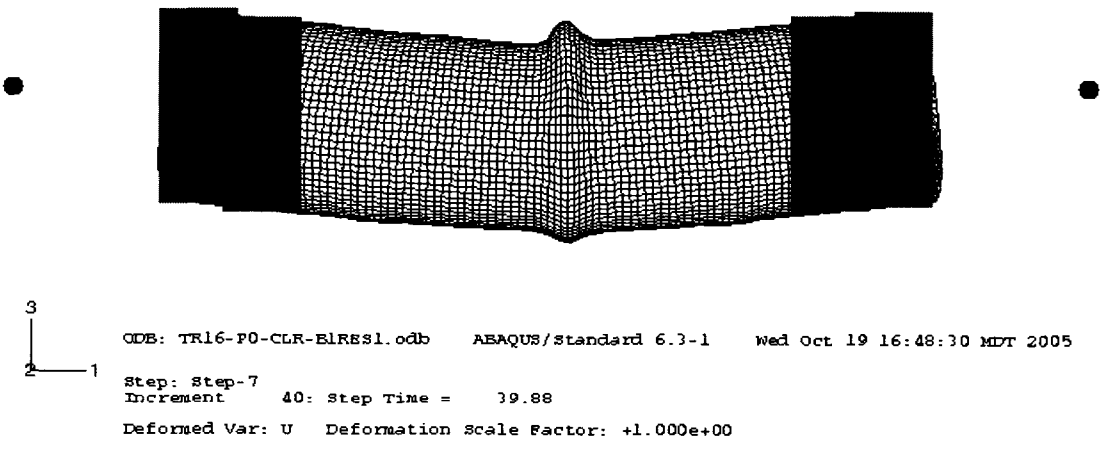

Figure 2.6 Growing wrinkle around the circumference-16 inch pipe
(Rotation is locked and MTS stroke is being applied)

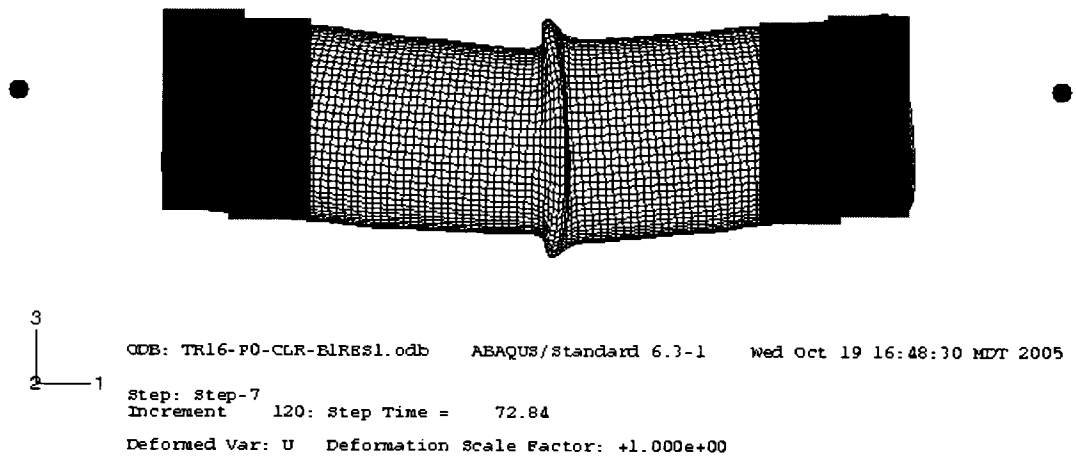

Figure 2.7 Significant deformation and strain reversal at the wrinkle location

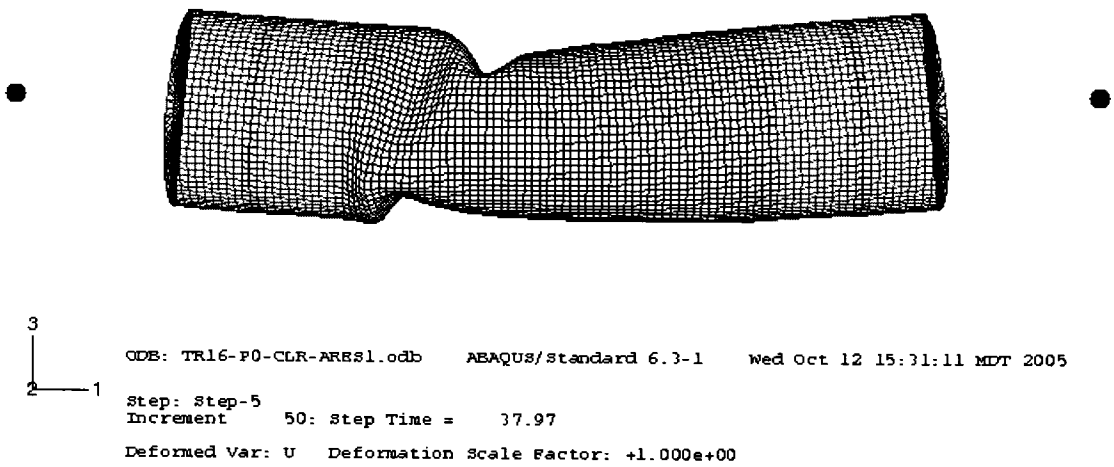

Figure 2.8 Deformed shape of a pipe under zero internal pressure

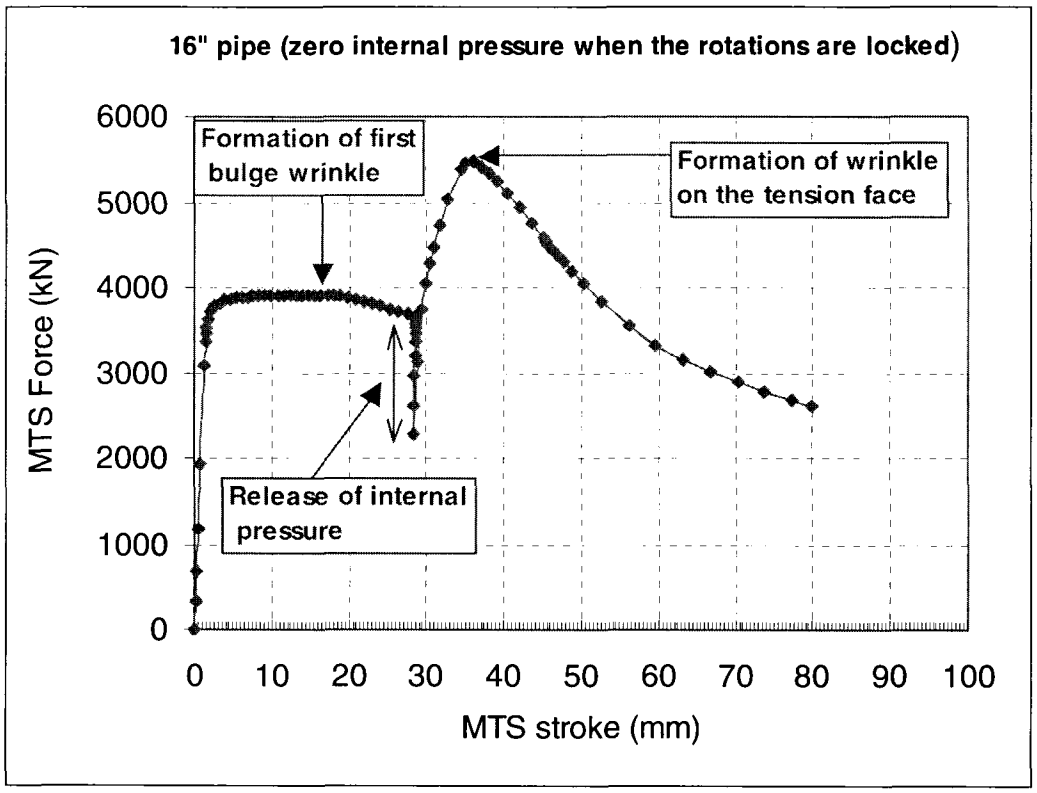

Figure 2.9 Relation between axial load vs. axial shortening and buckling behavior of a pipe

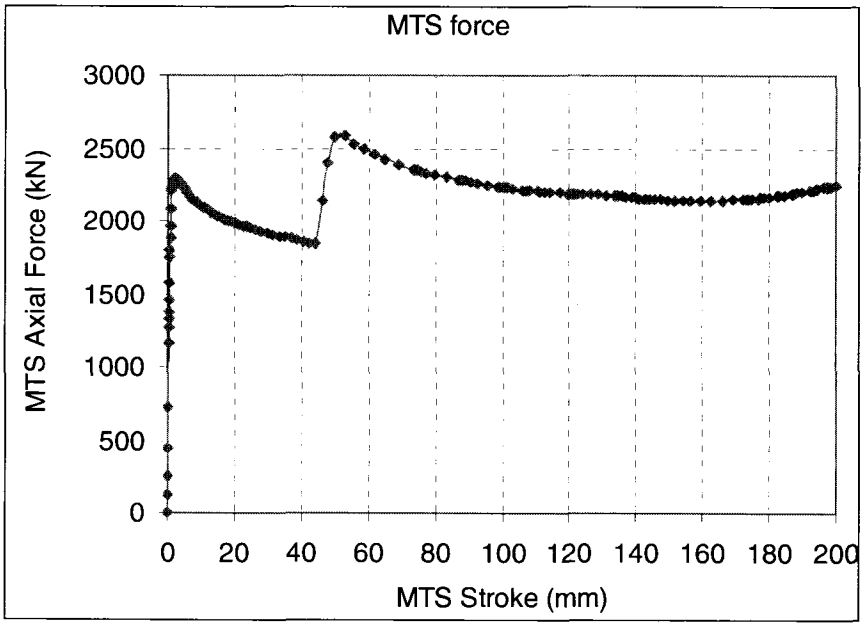

Figure 2.10 MTS Force vs. MTS Stroke

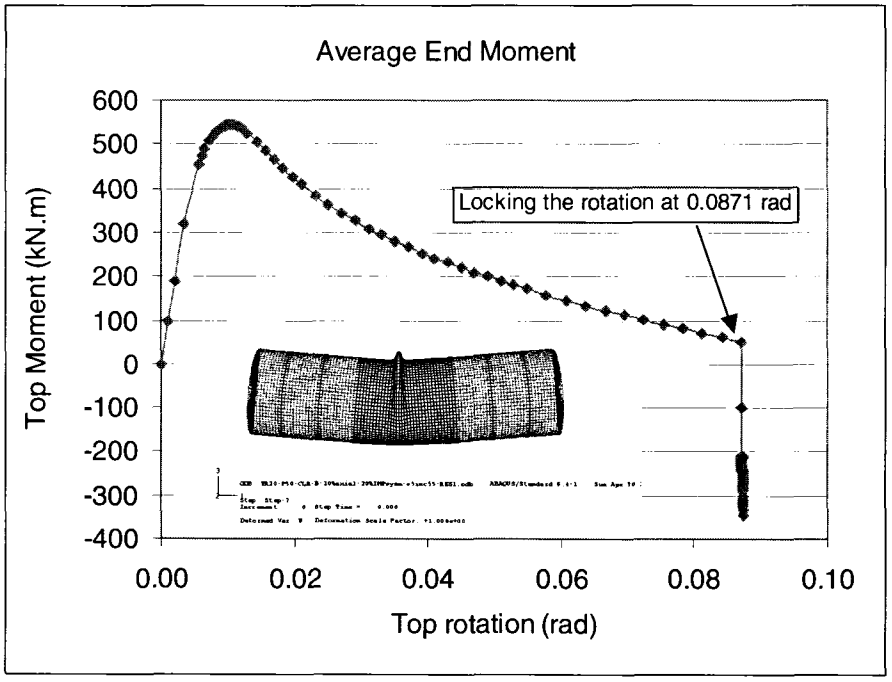

Figure 2.11 Initiation of wrinkle at the mid-height of a 20 inch pipe (Under internal pressure, axial load and bending moment)

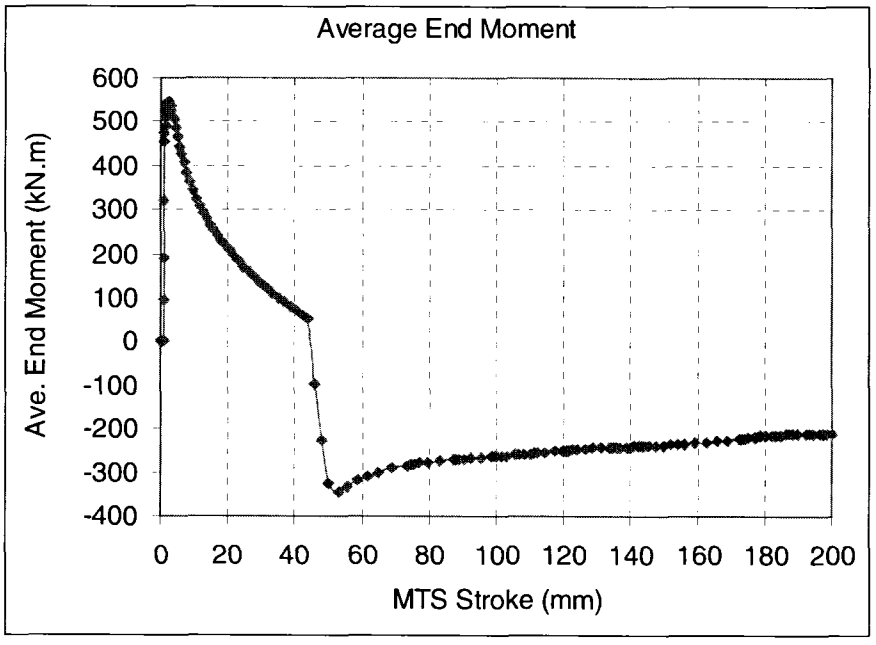

Figure 2.12 End Moment vs. MTS Stroke

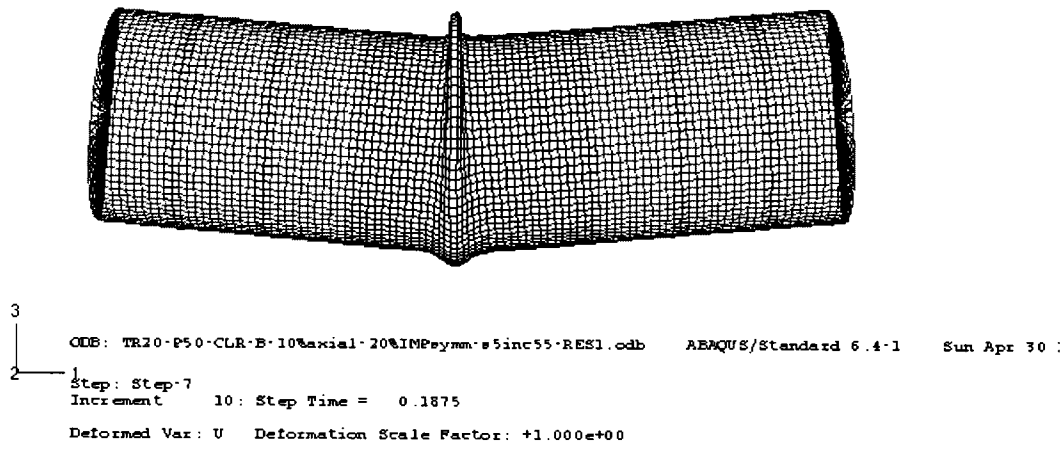

Figure 2.13 Growing wrinkle around the circumference-20 inch pipe (Rotation is locked and MTS stroke is being applied)

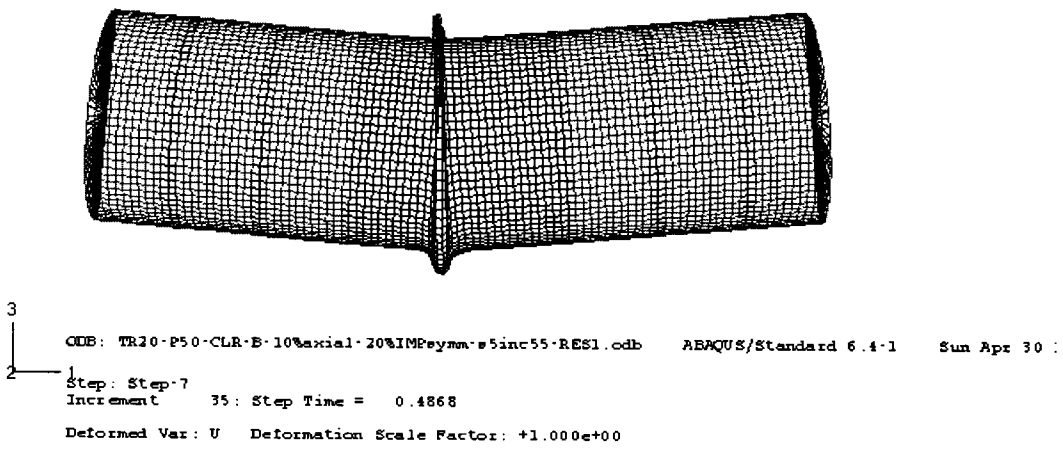

Figure 2.14 Significant deformation and strain reversal at the wrinkle location

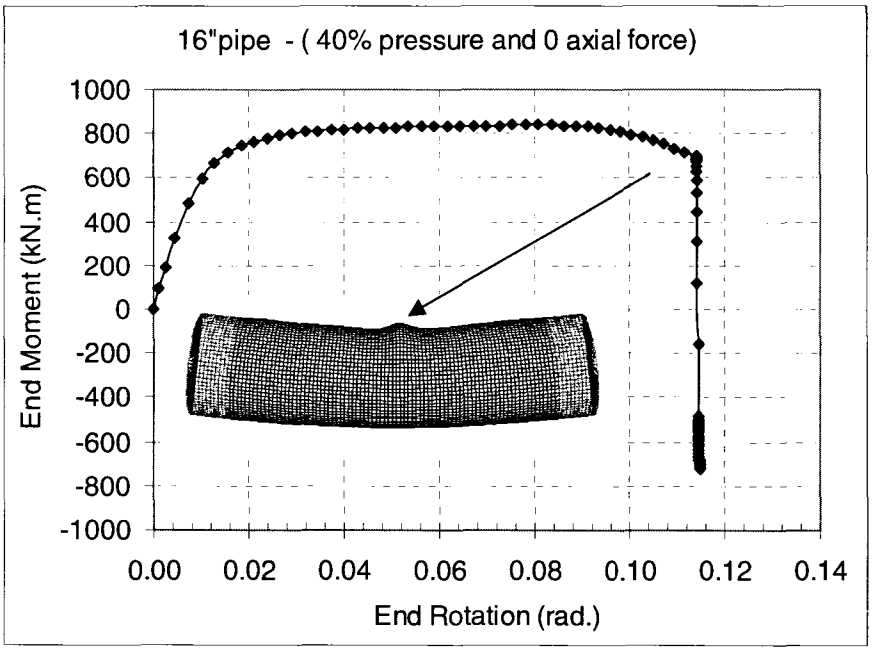

Figure 2.15 Initiation of a wrinkle at mid-height of the specimen under internal pressure and bending moment (no axial force)

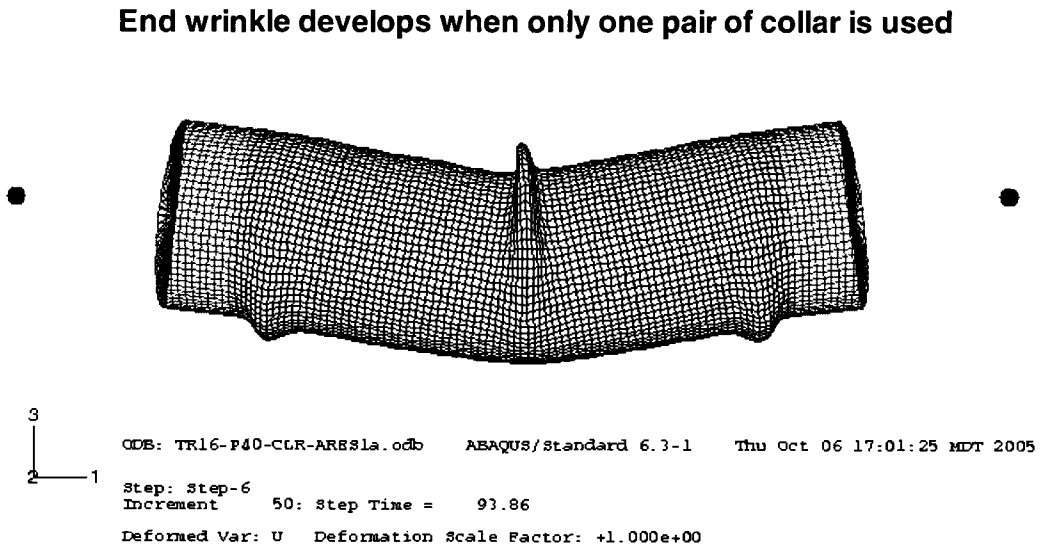

Figure 2.16 End wrinkle development due to the insufficient use of end collars

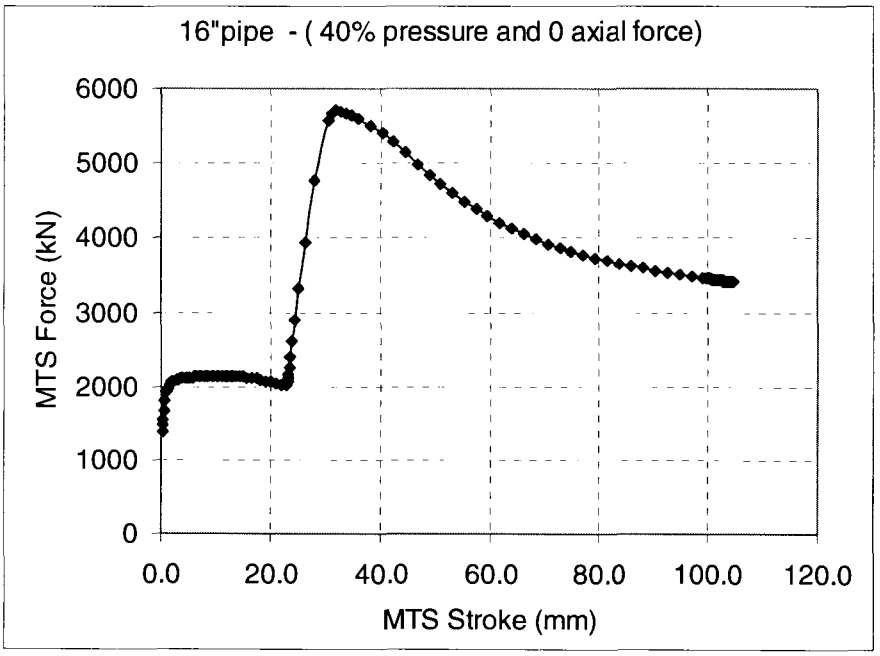

Figure 2.17 MTS force vs. MTS stroke
(no axial force for the formation of initial wrinkle)

3. EXPERIMENTAL PROGRAM

3.1. Introduction

In order to study the buckling and post-buckling behavior of pipelines up to fracture, a full-scale test set setup was designed. A total of six full-scaled tests were tested at I.F. Morrison Structural Laboratory, University of Alberta. Two types of specimens having different D/t ratios were used. Over the last two decades much research was done to understand the behavior of buried pipelines under combined loading conditions. The first and the only research conducted on rupture related to wrinkling was done by Das et al. (2002). It was proved that under monotonically increasing axial load and constant curvature, tearing fracture may occur at the wrinkle location. However, the loading sequence used by Das et al. (2002) was not exactly monotonic because during changing the boundary conditions of the test setup, loading and unloading of the axial load were introduced to the specimens. The main objective of this project was to improve the previous test setup by Das et al. (2002) and to simulate the tearing fracture of wrinkled energy pipelines under monotonically increasing axial load. To achieve this goal, several modifications were done on the test frame which was used by previous full-scale pipe tests by Dorey et al. (2000). The most important modification to the existing setup was the addition of the lateral bracing system to allow the growing of the wrinkle around the circumference of the pipe under monotonically increasing axial load. The loading program to simulate the fracture of a buckled pipe was designed using finite element analysis (FEA) software ABAQUS. The details of loading program and preliminary FEA are explained in Section 3.10.

3.2. Test Specimens

Two types of pipes (NPS16 and NPS20) were used in this experimental program with a total number of six specimens. The NPS 16 pipes were supplied by Tokyo Gas Ltd. had a nominal outside diameter of 406.4 mm and a thickness of 11.9 mm and a grade of X60 (414 MPa). The NPS 20 pipes supplied by TransCanada Pipelines Ltd. and had a nominal outside diameter of 508 mm and a thickness of 6.4 mm and a grade of X65 (448 MPa). The nominal geometrical properties of the specimens are given in Table 3.1. Before delivering to the I.F. Morrison Structural Engineering Laboratory at University of Alberta, the pipes were cut to an adequate length which is approximately equal to three times the OD of each specimen. The ends of the pipes were prepared to a bevel angle of 45° to satisfy the weld penetration between the base plate and the pipe.

Each specimen was given by a designation based on its physical properties and the load case as shown in Table 3.1. The following designation is used to identify each test specimens: **DaaPbbAcc-#**,

Daa – indicates the pipe outside diameter, e.g. D16 is a 16 inches diameter pipe;

Pbb – indicates the level of hoop stress induced by the internal pressure as a percentage of the SMYS, e.g. P40 is a 40% SMYS internal pressure;

Acc – indicates the level of locking angle in degree;

– indicates the test specimen number.

For example, D16P40A5-2 stands for a 16 inches pipe with an internal pressure that induces 40% SMYS hoop stress and has a 5° rotation angle. It is the second specimen in the test program.

3.3. Pretest Measurements

Various geometric dimensions of each specimen were measured before it was welded to the end plates. Therefore, in order to facilitate the presentation of the test results, the angular coordinate system shown in Figure 3.1 is adopted. The circumference of the pipe section was divided into four quadrants of 90^{o} (which is equal to 319 mm for 16 inches pipes and 399 mm for 20 inches pipes). All measurements for the seam weld position were taken as an offset of approximately 35 mm. During this stage, thickness, length and outside diameter of each pipe was measured.

Thickness of each pipe was measured along each quadrant (0^{o}, 90^{o}, 180^{o} and 270^{o}) at fourteen locations by an ultrasonic thickness gauge. However, thickness of the 20 inch pipe was also measured by a caliper in order to exclude the effect of the green coating on the pipes. As a result, when the measurements obtained from an ultrasonic device and a caliper were compared; it was observed that green coating has a negligible effect on the measurements which can be seen in Table 3.2.

The outside diameter of each pipe was measured at six locations (between 0^{o}-180^{o}, 30^{o}-210^{o}, 60^{o}-240^{o}, 90^{o}-270^{o}, 120^{o}-300^{o} and 150^{o}-330^{o}) at top and bottom of the pipe with a 24 inches caliper. The length of each specimen was measured along four locations (0^{o}, 90^{o}, 180^{o} and 270^{o}) with a measuring tape. The measured dimensions of the full scale pipes are also given in Table 3.2

3.4. Initial Imperfection Measurements

The effect of the geometric imperfections on the buckling resistance of thin shells has long been recognized. This effect has been studied since the mid-1960. The imperfection measurements were taken across the inside surface of each specimen by a

measuring device that was designed by Dorey et al. (2001) at the University of Alberta. The device basically consists of three parts: high-precision machined rail, tailor fitted carriage for LVDT (linear variable differential transducer) and adjustable end supports. Figure 3.2 and Figure 3.3 show the general view of the imperfection measurement device that was used for both specimens.

The imperfection measurement sequence was as follows. First, the pipe was located on the adjustable support. By the help of two bulbs which were mounted at the top of the pipe, 90° apart from each other, the adjustable tripod support of the imperfection measurement device was leveled to maintain the vertical position of the specimen. Once the specimen was leveled, then the high precision machine rail that carries the LVDT carriage was aligned with the center of the pipe. This rail is a special piece of vertical metal that assumed perfectly vertical and it allows the LVDT carriage move up- down through the inside surface of the specimen. Also, it can rotate around its axes at each elevation of the LVDT. When locating the rail system to the center of the pipe, the voltage values from the LVDT were observed at 0°, 90°, 180° and 270° locations. When the values at opposite locations were equalized then it was assumed that pipe was located at the center. This procedure was done for both top and bottom ends of the pipes. Finally, the upper end of the machined rail system was clamped to the top end of the pipe. After completing the preparations, the specimen is ready for taking measurements. Two types of instrumentations were used in this device, LVDT and RVDT (rotational variable differential transducer). The LVDT can move up and down and rotate at each elevation on the carriage. For the 16 inches pipes, readings were taken at every 4 inches and for 20 inches pipes 5 inches increments were used. And at every

elevation, readings were taken at 22.5° increments. So, the RVDT was used to monitor the rotation angle of the LVDT carriage at each elevation of the pipes. At every level, 16 readings were taken by rotating LVDT.

Since this research project is focused on the behavior and results of full-scale test specimens, the imperfection measurement results are not included in this study. However, it was observed during the experiments that imperfections had a larger effect on the 20 inches pipes because of the larger D/t ratio and smaller thickness of the specimens.

3.5. Installation of the Pipe in the Test Setup

After measuring the actual geometric dimensions and the initial geometric imperfections, the specimen is ready to place in the test setup. These steps were followed during this project:

1) Once the imperfection was measured, the pipe was transferred to a roller system in a horizontal position. The purpose of this was to mount the strain and demec gauges.
2) The bevel surface was grinded for the welding to create better fusion between the base plate and the pipe.
3) The upper moment arm was placed on the floor in a position that, pipe can sits on the base plate which was bolted to the moment arm. Then, the moment arm was shimmed to make the upper base plate leveled horizontally before the pipe was welded.
4) The upper end of the pipe was placed on the upper base plate in such a way that center of the pipe and center of the axial load coincides during the experiment.

5) The pipe was shimmed after locating on the base plate to make it perpendicular to the base plate along all directions. Once the pipe was centered and aligned vertically, it was welded to the top end plate.

6) The bottom moment arm was positioned and shimmed under the MTS machine where the center of the axial load passes through the center of the bottom base plates. (**Note:** Before connecting the base plates to the moment arms, the centers of base plates and moment arms were aligned in order to make sure that MTS load could be transferred through the center of the upper plate, pipe and bottom plate. So that, no eccentricity was created in and out of plane directions.)

7) After completing the welding and the inspection of the upper end of the pipe, top moment arm and the pipe was lifted and rotated to the upside down position. The assembly was transferred under the MTS machine by the over head crane. Then positioned and leveled so that the centers of the pipe and bottom base plate were matched and pipe was perpendicular to the bottom base plate.

8) Bottom end of the pipe was welded to the bottom base plate. After completing the welding of the bottom end, the weld was inspected. Once the welds were passed the inspection, then the remaining components and the instrumentations of the system was mounted.

3.6. Welding Information

The pipes were connected to the moment arms by high strength top and bottom plates where they were welded by circumferential groove welds. The plates were Grade X70 pressure vessel steel. According to the calculations, it was decided to weld the pipe on 3 inches thick base plates by a full penetration groove weld with a matching

electrode of X60. After completing welding of the first specimen (D16P0A4.5-1), according to the UT inspection of the weld, lack of fusion problem was found between the base plate and the pipe. Therefore, pipe is cut-out of the setup and base plates were cured by a procedure called "*Buttering*", which is depositing a layer of weld metal onto the face of a weld surface which will then form part of a welded joint. The surface of the base plate after buttering is shown in Figure 3.4

3.7. Test Setup

The behavior of buried pipelines has been studied at University of Alberta since 1994. For this project, a previous setup was used with some modifications. Initially, the loading assembly had a "knife edge" which aligned the axial load with the center of the pipe. However, during testing the D16P0A4.5-1 out-of-plane bending of the specimen was observed, after forming the wrinkle on the compression side and increasing the axial load on the pipe. It was decided to prevent this action for the rest of the testing program and, modifications were made. First of all, the knife edge between the MTS loading head and the bearing plate at the top of the loading arm was removed. And, system was supported from top and bottom moment arms by lateral bracing systems which can be seen in Figure 3.5 and Figure 3.6. The schematic view of the initial and modified test setup is shown in Figures 3.7 and Figure 3.8. Another difference of this setup from the previous one is that, a double acting hydraulic jack was used to create end moments on the specimens.

3.7.1. MTS6000

The axial load was applied by an MTS6000 universal testing machine. The system has a capacity of 6000 kN of axial compressive load. The expected axial shortening for the 16 inches specimens was larger than the 20 inch pipes. For that reason, maximum stroke capacity, which is 300 mm, of the system was used for the 16 inches and 150 mm of the stroke capacity was used for the 20 inch pipes. The load and stroke values imposed by the MTS6000 were recorded through a digital data acquisition system.

3.7.2. Hydraulic Jack

The previous experiments discussed in Chapter 2 investigated the effect of monotonically increasing curvature which was created by a compressive hydraulic jack. But in this project, the fracture behavior of wrinkled pipe under constant curvature and monotonically increasing axial load was studied. Therefore, the only way of keeping curvature constant was to use a double-acting hydraulic jack. Thus, the boundary conditions were modified by special jack fixtures and spacers to accommodate a double action hydraulic jack, as shown in Figure 3.8. The hydraulic jack was connected to the moment arms by pin ends to allow its rotation in plane direction.

The jack has a maximum tensile capacity of 940 kN and maximum compressive capacity of 1100 kN with a stroke capacity of 15 inches. The level of the load applied through the jack was recorded by a load cell which was also connected to the digital data acquisition system.

3.7.3. Pneumatic Air Pump

Full-scale tests of pipes were carried out with two levels of internal pressures: unpressurized and 40% SMYS. The pipes were filled with water at least one day before the experiments and then, during the experiments internal pressure was applied through a manually controlled pneumatically driven pump. During the experiments, level of internal pressure was monitored by a pressure transducer that was connected to a digital data acquisition system.

3.8. Instrumentations

It was planned to take various electronic and manual measurements during the tests, for that reason, basically two types of instrumentations were used: Demec gauges and strain gauges were used to record the strains. In addition, rotations and deflections were monitored by RVDT's, LVDT's and cable transducers. List of the instrumentations used during the project can be seen in Table 3.3 and Table 3.4

3.8.1. Strain Gauges

Strain gauges having 120Ω resistance and 5 mm gauge length were used to measure the strain in longitudinal and hoop directions. Longitudinal strain gauges were mounted along the line at north, south, west (compression) and east (tension) locations of each pipe. The locations of the lines around the pipes can be seen in Figure 3.1. The seam welds on the pipes were located near the north side and shifted about 35 ~ 40 mm.

Two types of strain gauge arrangement were used for the experiment of 16 inch pipes. The main reason for that was, first experiment was done with two sets of collars at top and bottom of the pipe. However, it was observed during the test that winkle was

formed near the top end of the pipe. As a result of adding extra sets of collars two types of layouts were created for 16 inches specimens. For the first test, on compression and tension faces, longitudinal strain gauges were placed at 101.6 mm intervals, starting at 368.6 mm from both ends of the pipe. On the north and south faces, longitudinal strain gauges were placed at 203.2 mm intervals, starting at 368.6 mm from both ends. Hoop strain gauges were mounted at top, middle and bottom levels of the pipe at 0^{o}, 90^{o}, 180^{o} and 270^{o} locations. Schematic view of the strain gauge lay out and their corresponding designation is shown in Figure 3.9.

The modified layout of strain gauges is not very different from the initial one. For the modified layout; along tension and compression sides, longitudinal strain gauges were placed at 101.6 mm intervals as well. However, they were started at 470.2 mm from both ends of the pipe. Also on the north and south sides, longitudinal strain gauges were placed at 203.2 mm, starting at 571.8 mm from the both ends of the pipe. Furthermore, hoop strain gauges were mounted at top, middle and bottom levels of the pipe at 0^{o}, 90^{o}, 180^{o} and 270^{o} locations as well. The only difference is that they were located at 571.8 mm from the both ends of the pipe. The schematic view of the strain gauge lay out and their corresponding designation is shown in Figure 3.10.

For 20 inches pipes, only one type of strain gauge layout was used. At compression and tension faces, longitudinal strain gauges were placed at 127 mm intervals, starting at 646 mm from the both ends of the pipe. On the north and south faces, longitudinal strain gauges were placed at 254 mm intervals, starting at 646 mm from the both ends. Hoop strain gauges were mounted at the middle of the pipe at 0^{o},

90°, 180° and 270° locations. The schematic view of the strain gauge lay out and their corresponding designation is shown in Figure 3.11.

3.8.2. Demec Gauges

Average strains between two demec points along tension and compression sides of specimens were measured by mechanical demec gauges of different gauge lengths.

For 16 inches specimens two types of demec gauge layouts were used. For the first test, 203.2 mm demec gauges were employed for the measurement of strain on the compression and tension sides of the pipe. However, for the following tests it was decided to use 200 mm demec gauges because of the inconsistency between the strain gauge strain and the demec gauge (having 203.2 mm gauge length) strain. The locations of the demec points and their corresponding designation on the compression and tension sides are shown in Figures 3.12 and 3.13. Demec points were shifted 8 mm apart from the adjacent strain gauge at the corresponding locations. Punch holes were stamped beside demec points. The reason for the punch holes is that, if a demec point drops off during the test, the distance between the punch holes can be measured by a divider and a caliper at the punched holes. Thus, the strain can be calculated according to the punch mark measurements. In addition, when the distance between the demec points was out of range of the Demec gauge, the distance was measured by a divider and a caliper. Demec readings were recorded over the pre-buckling range in order to verify the consistency between the electronic strain gauge measurements and manually recorded demec measurements, which in turn would provide confidence on the post-buckling manual readings for which there is no confirming electronic strain gauge data.

For 20 inches pipes 254 mm demec gauge was used for the measurement of strain on the compression and tension sides of the pipe. Similar to the 16 inches pipes, caliper and a divider was used to measure the strain when the demec points were out of range. The locations of the demec points and their corresponding designation for 20 inches pipes are shown in Figure 3.14

3.8.3. LVDT (Linear Variable Differential Transducer)

LVDT's were located on the compression and tension sides of the pipes to measure the lateral movement of the specimens. LVDT's were mounted on a support frames on the tension and compression sides of the specimen. For 16 inches pipes, two ±1 inch LVDT's were placed on the compression face on the mid-thickness of the base plates. Three pairs of ±3 inches LVDT's were located along the compression and tension sides. One pair was located at the mid-section of the pipe and other two were placed 203.2 mm above and below the mid-height. The schematic view of the LVDT layout can be seen in Figures 3.15 and 3.16.

On the other hand, for 20 inches pipes almost the same layout was used. Only ±1 inch LVDT's on the base plates were changed with ±3 inches ones and transducers were located 254 mm apart from each other on compression and tension sides.

3.8.4. RVDT (Rotational Variable Differential Transducer)

RVDT's were of great importance during the tests because the locking angles of the pipes were monitored through them. Therefore, for 16 inches specimens total number of 7 RVDT's were used to measure the rotation of the end plates and the pipe. On each end plate and at the tip of each moment arm a rotation meter was mounted.

Also, three rotation meters were placed at mid-height, 203.2 mm below and above elevations. Basically, RVDT's on the top and bottom base plates were used to calculate the global curvature of the test specimen. The RVDT lay out is shown in Figure 3.15. In addition, for the 20 inches pipes 7 RVDT's were used as well. However, rotation meters at the tip of the moment arms were cancelled and one of them were used to monitor the out of plane movement and the other was used to catch the rotation of the jack. The schematic view of the layout of RVDT's for the 20 inches pipes can be seen in Figure 3.16.

3.8.5. Cable Transducers

Six cable transducers were mounted on the bottom end plate. Three of them were positioned between the underside of the bottom end plate and the strong floor, and the other three were located between the top and bottom end plates. The purpose of these cable transducers was to determine the relative rotations of the base plates in-plane and out-of-plane directions, and measure the shortening of the pipes. Besides, an overall cable transducer was used to measure the sum of pipe shortening and moment arms opening. Therefore, one end of that was hooked to the MTS head and the other end was connected to the tip of the bottom moment arm. The schematic explanation of cable transducers is shown in Figures 3.15 and 3.16.

3.8.6. Load History Measurements

Load history measurements including axial load, eccentric jack load, internal pressure and axial deformation were recorded electronically during the tests. The MTS load was measured by a load cell, the internal pressure with a pressure transducer, the

jack load with a load cell, and the axial deformation through MTS stroke and cable transducers.

3.9. Loading Procedure

All the specimens involved in this experimental program were tested under monotonically increasing loading type. In order to simulate the failure type which is, tearing fracture under constant curvature and monotonically increasing axial load, the FEA was conducted by Dr. Behbahanifard and PhD. candidate Jianmin Zhang to determine the proper loading procedure. According to the FEA which was discussed in section 2.3, the loading procedure to create tearing type failure includes four basic steps:

1) Application of internal pressure and initial axial load;
2) Application of bending moment until the pipe buckled;
3) Increasing curvature to a predetermined level;
4) Increasing axial load under constant curvature.

Loading properties, such as internal pressure, initial axial load, maximum jack loads, maximum axial load and locking rotation of each specimen are given in Table 3.5.

3.9.1. Application of Internal Pressure and Axial Load

It was proved that buckling modes of pipes depend on the existence of the internal fluid pressure inside the pipe. In the case of zero internal pressure wrinkle forms in a buckling mode called "*Diamond-Shape Buckle*". However, under adequate amount of internal pressure pipe wrinkles in a mode called "*Outward-bulge*" which is desired for this experimental program. Moreover, after forming the wrinkle on the compression

face, by keeping the curvature constant and increasing the axial compressive load monotonically, it was tried to grow the wrinkle around the circumference and create strain reversals at wrinkle location and fracture the pipe at compression side. For that reason every specimen was pressured at the beginning until forming a bulge wrinkle on the compression type. Except the last pipe every specimen was pressurized by 40% SMYS and the last one was by 80% SMYS. For 16 inches pipes the actual yield strength obtained from the tension coupon tests is 480 MPa. Therefore;

$$p_y = \frac{2 \times \sigma_y \times t}{D_i} = 31.1 MPa$$

$$40\% \times p_y = 12.45 MPa = 1805 psi$$

where

p_y: internal pressure that cause yielding in hoop direction,

σ_y: yield strength,

t: thickness of the pipe,

D_i: inside diameter of the pipe.

p_y was calculated for the 20 inches pipes in the same way but the only differences were D_i and t.

During this stage, the cap force created by the internal pressure was compensated by increasing the MTS load. For 16 inches pipes the cap force was calculated as follows:

$$P_{cap} = 40\% \times p_y \times \frac{\pi \times D_i^2}{4} = 1424 kN$$

Apart from the internal pressure, during this stage some initial axial load was applied on the specimens to reduce the demand on the hydraulic jack force. Also, this axial force reduces the stress on the weld between the pipe and base plate. Therefore, for

16 inches specimens this load was chosen as 2000 kN which was based on the preliminary FEA. However, for 20 inches pipes it was taken as 10% of the yield load of the material which is 520 kN.

In conclusion, during this stage internal pressure and the axial load were applied simultaneously on the pipes. For 16 inches specimens, at the end of this stage, internal pressure raised up to 1805 psi and the axial load on the specimens was 3424 kN. Axial load is the sum of the 2000 kN initial load and the cap fore which is 1424 kN. For 20 inches specimens the same procedure was followed with different values. The internal pressure increased up to 770 psi for 40% SMYS and 1540 psi for 80% SMYS. And, the sum of the axial load and the cap force was 1541 kN and 2562 kN, respectively.

During this stage the collars at the top and bottom of the pipes should be kept in snug tight position in order to allow the pipe to expand freely under increasing internal pressure and axial load, without any constraints.

3.9.2. Application of Bending Moment

Next step of the loading procedure increased of the end rotations by means of applying eccentric jack load until the pipe buckled and a desired amount of rotation was reached. The rotation was controlled by watching the average of RVDT readings mounted to top and bottom base plates, which is:

$$\theta_{average} = \frac{\theta_{top} + \theta_{bottom}}{2}$$

During this stage, while increasing the eccentric jack force the net axial load and internal pressure were kept constant. Therefore, while pushing the jack, internal pressure was released and MTS load was increased to keep them constant. By further increasing

the jack force, an outward bulge type wrinkle was formed on the compression side and jack stroke was kept increasing until adequate curvature was formed. While bending the pipe, collars were checked to keep them in snug tight position and after forming the wrinkle on the compression face of the pipe the closest collars to the wrinkle were removed. Otherwise, while increasing the axial load after locking the rotations, the wrinkle on the compression side can not grow around the circumference of the pipe because collars constrain that action.

3.9.3. Application of Axial Load under Constant Curvature

The "rotation locking" phenomenon is fundamentally means, keeping the $\theta_{average}$ at a specific value by adjusting the jack force. That's why a double acting jack was used, which can apply tension or compression forces. After reaching a desired rotation, according to the testing parameters of the experiment the internal pressure was released. If the test was an unpressurized one, then the internal pressure was released to zero by keeping the $\theta_{average}$ constant. Relaxing internal pressure is equivalent of applying axial load on the pipe. For that reason, MTS load and jack load was reduced while releasing internal pressure. However, for pressurized tests the internal pressure was kept constant until the test was over. After the internal pressure was released (for the unpressurized pipes), the MTS load was increased incrementally by keeping the average rotation at locking rotation until the pipe was torn or fractured. Also for the pressurized specimen after locking rotation, the MTS load was increased incrementally by keeping the internal pressure at the specific value, until the pipe was torn or fractured.

Table 3.1 Nominal Physical Properties of Specimens

Specimen	D mm	t mm	D/t	L mm	L/D	Grade
D16P0A4.5-1	406.4	11.9	34	1550	3.8	X60(414MPa)
D16P0A5-2	406.4	11.9	34	1550	3.8	X60(414MPa)
D16P40A7-3	406.4	11.9	34	1550	3.8	X60(414MPa)
D20P40A3.5-4	508	6.4	79	1800	3.5	X65(448MPa)
D20P0A5-5	508	6.4	79	1800	3.5	X65(448MPa)
D20P804-6	508	6.4	79	1800	3.5	X65(448MPa)

Table 3.2 Actual Physical Properties of Specimens

Specimen	D(mm)	t(mm)		D/t	L(mm)	L/D
D16P0A4.5-1	406.85	12.38		33	1518*	122
D16P0A5-2	407.13	12.35		33	1546	125
D16P40A7-3	407.38	12.38		33	1549	125
	D (mm)	t(mm)		D/t	L (mm)	L/D
		ultrasonic	caliper			
D20P40A3.5-4	509.44	6.713	6.516	77	1806.5	3.5
D20P0A5-5	509.565	6.705	6.331	78	1802.875	3.5
D20P80A4-6	508.67	6.74	-	75	1802	3.5

Table 3.3 List of Instrumentations for 16 inch Pipes

Instrumentation Type	Number	
Electronic Strain Gauge	For 2 pairs of collars	For 3 pairs of collars
	36	28
Demec Gauge	For 2 pairs of collars	For 3 pairs of collars
	18	14
LVDT	2 - ±1 inch 6 - ±3 inches	
RVDT	7	
Cable Transducer	6 - 10 inches 1 - 25 inches	
Pressure Transducer	1	
Load Cell	2	

Table3.4 List of Instrumentations for 20 inch Pipes

Instrumentation Type	Number
Electronic Strain Gauge	20
Demec Gauge	10
LVDT	8 - ±3 inches
RVDT	7
Cable Transducer	6 - 10 inches 1 - 25 inches
Pressure Transducer	1
Load Cell	2

Table 3.5 Loading properties

Specimen	Internal Pressure (psi)	P_{cap} (kN)	Initial Axial Load (kN)	P_{jack} (kN)		P_{MTS} (kN)	Locking Rotation (degrees)
				Compression	Tension		
*D16P0A4.5-1	1805	1424	3424	697	403	5500	4.5
*D16P0A5-2	1805	1424	3424	694	599	5245	5
D16P40A7-3	1805	1424	3424	700	758	5700	7
D20P40A3.5-4	770	1020	1540	490	268	2800	3.5
*D20P0A5-5	770	1020	1540	550	307	2150	5
D20P80A4-6	1440	2040	2560	320	263	3000	4.05

*These pipes were pressurized to %40p_y initially however after locking rotation pressure was released.

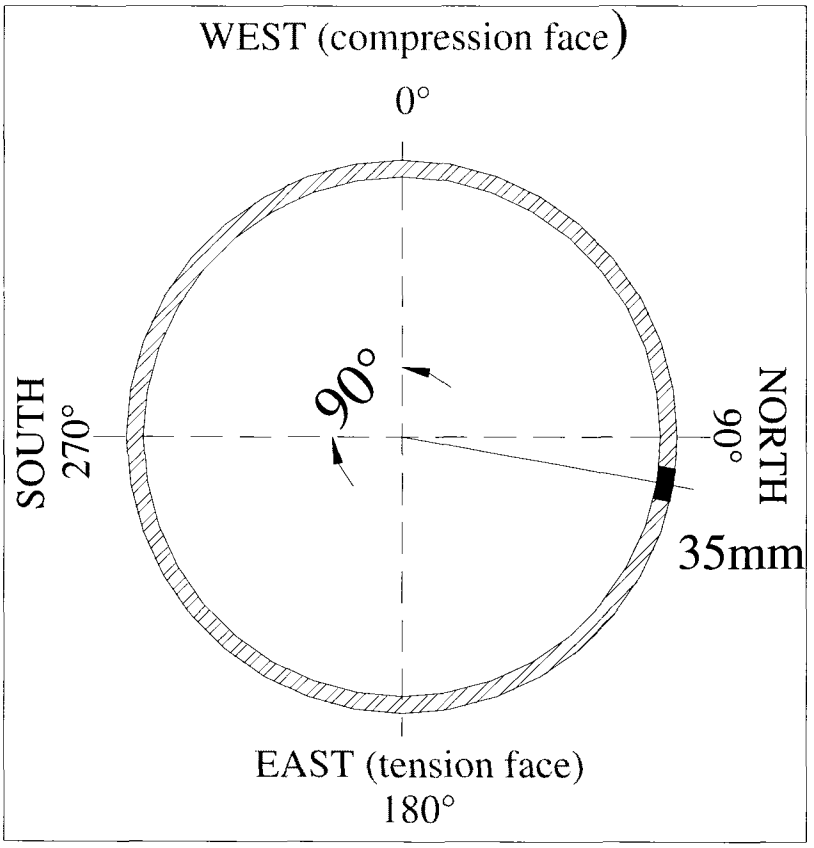

Figure 3.1 Angular Coordinate System

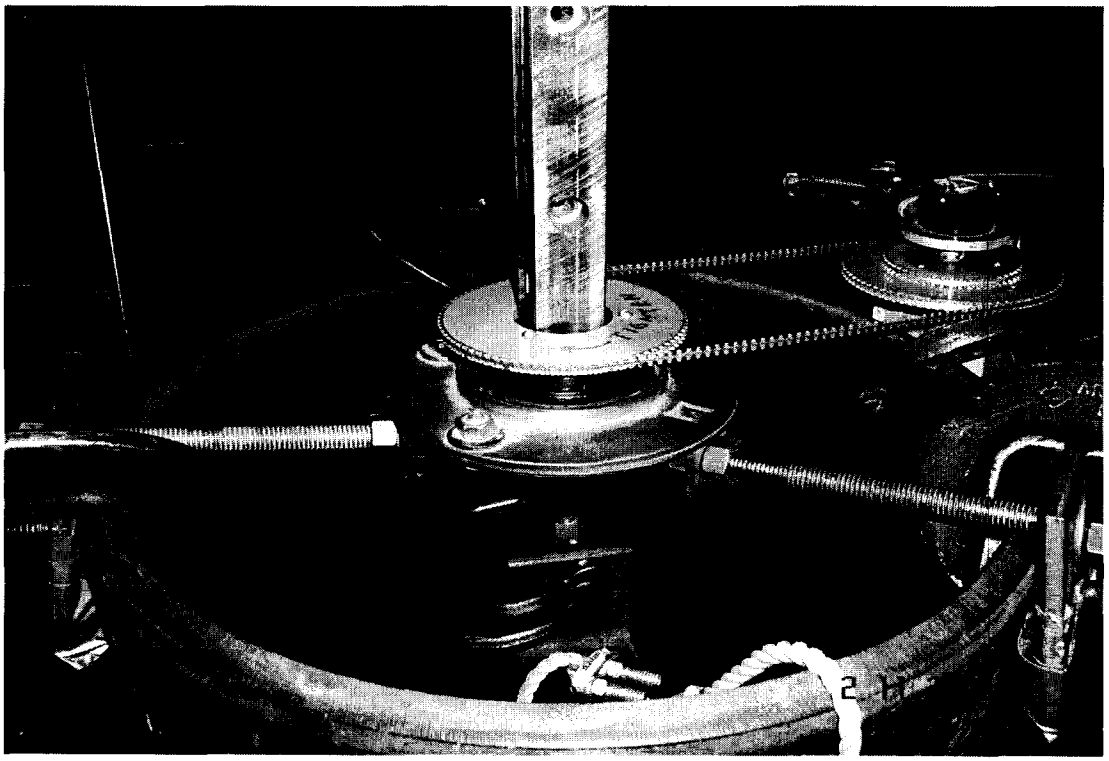

Figure 3.2 Top View of the Imperfection Device

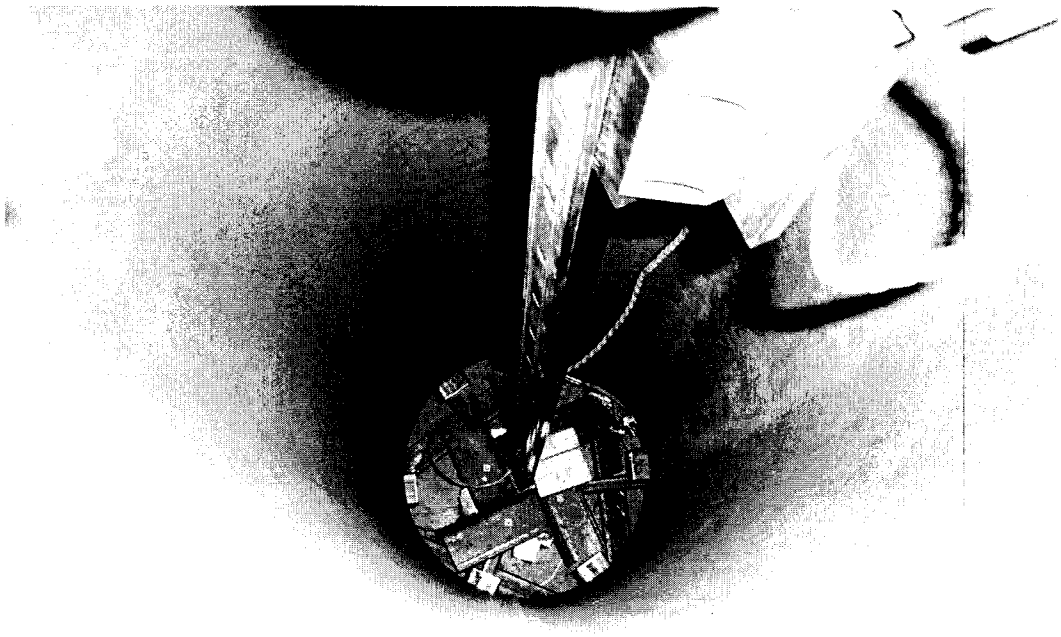

Figure 3.3 High Precision Machine Rail and LVDT Carriage

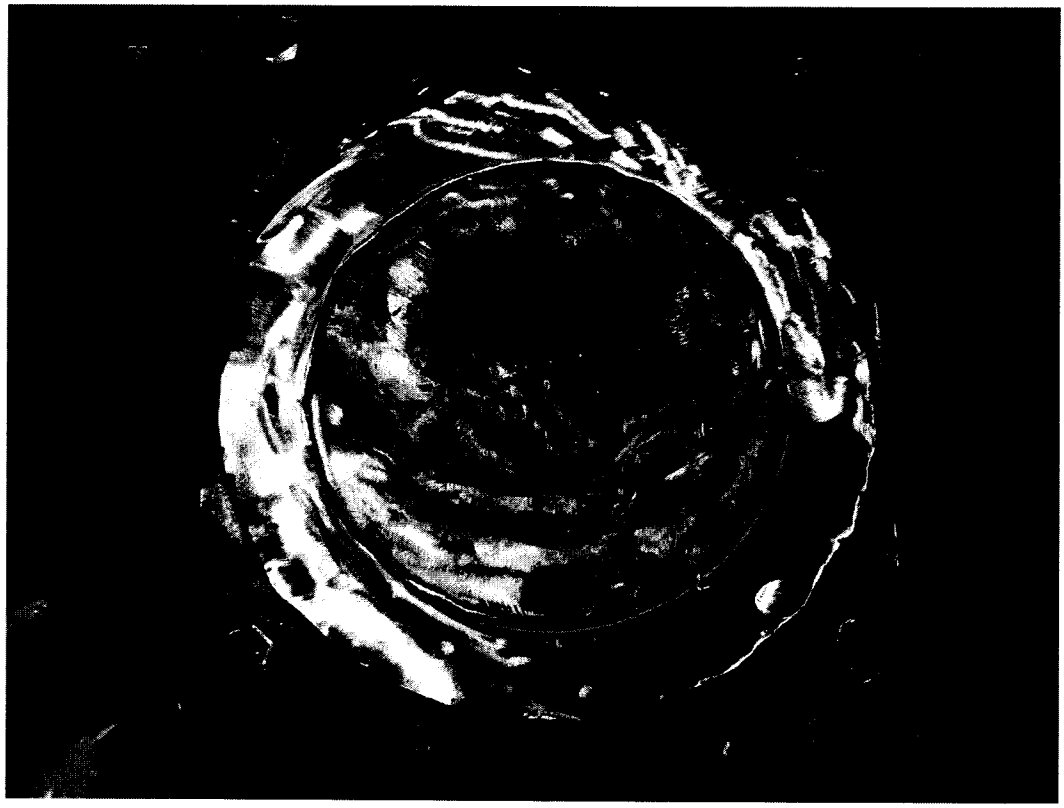

Figure 3.4 View of Base Plate after "Buttering"

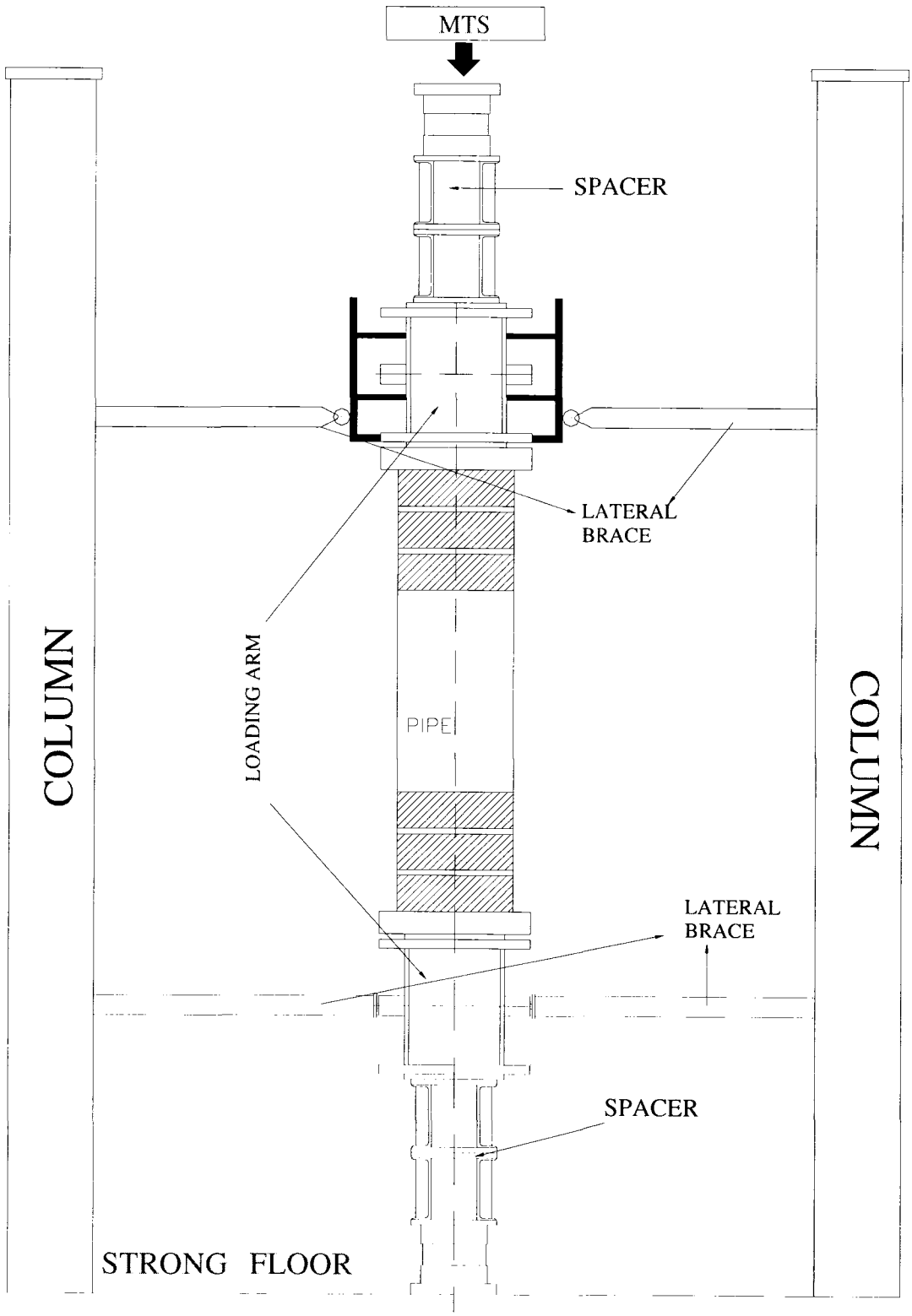

Figure 3.5 Schematic View of the Lateral Bracing System

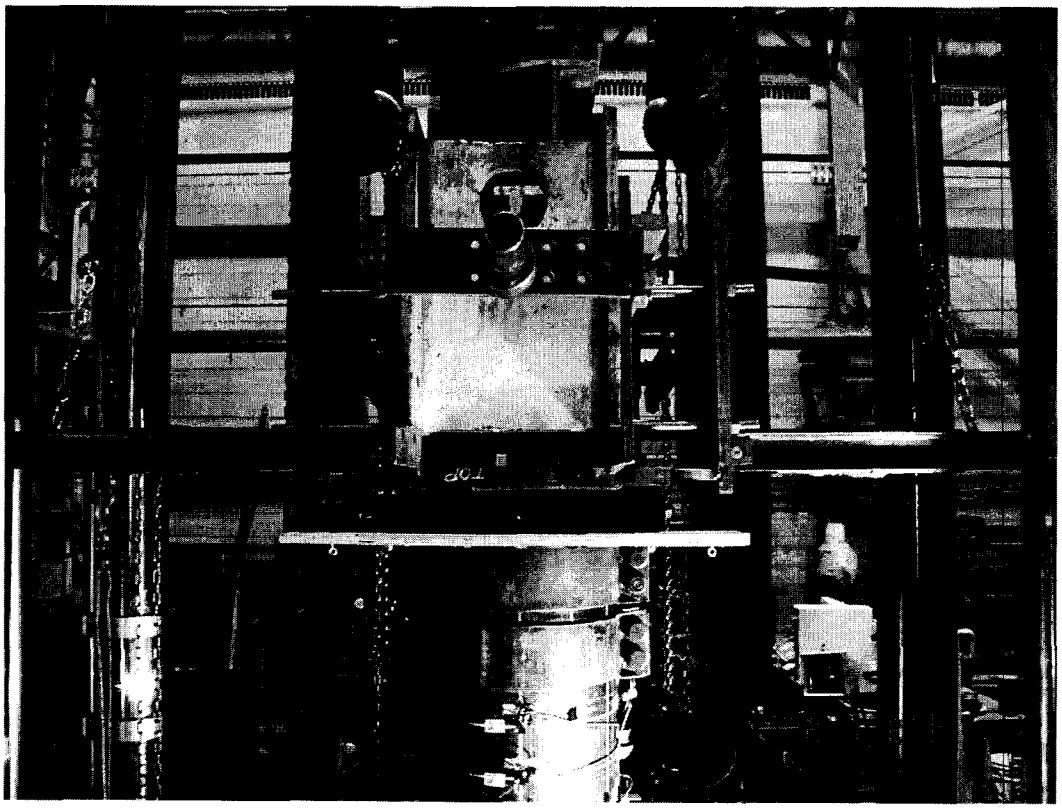

Figure 3.6 Lateral Bracing System

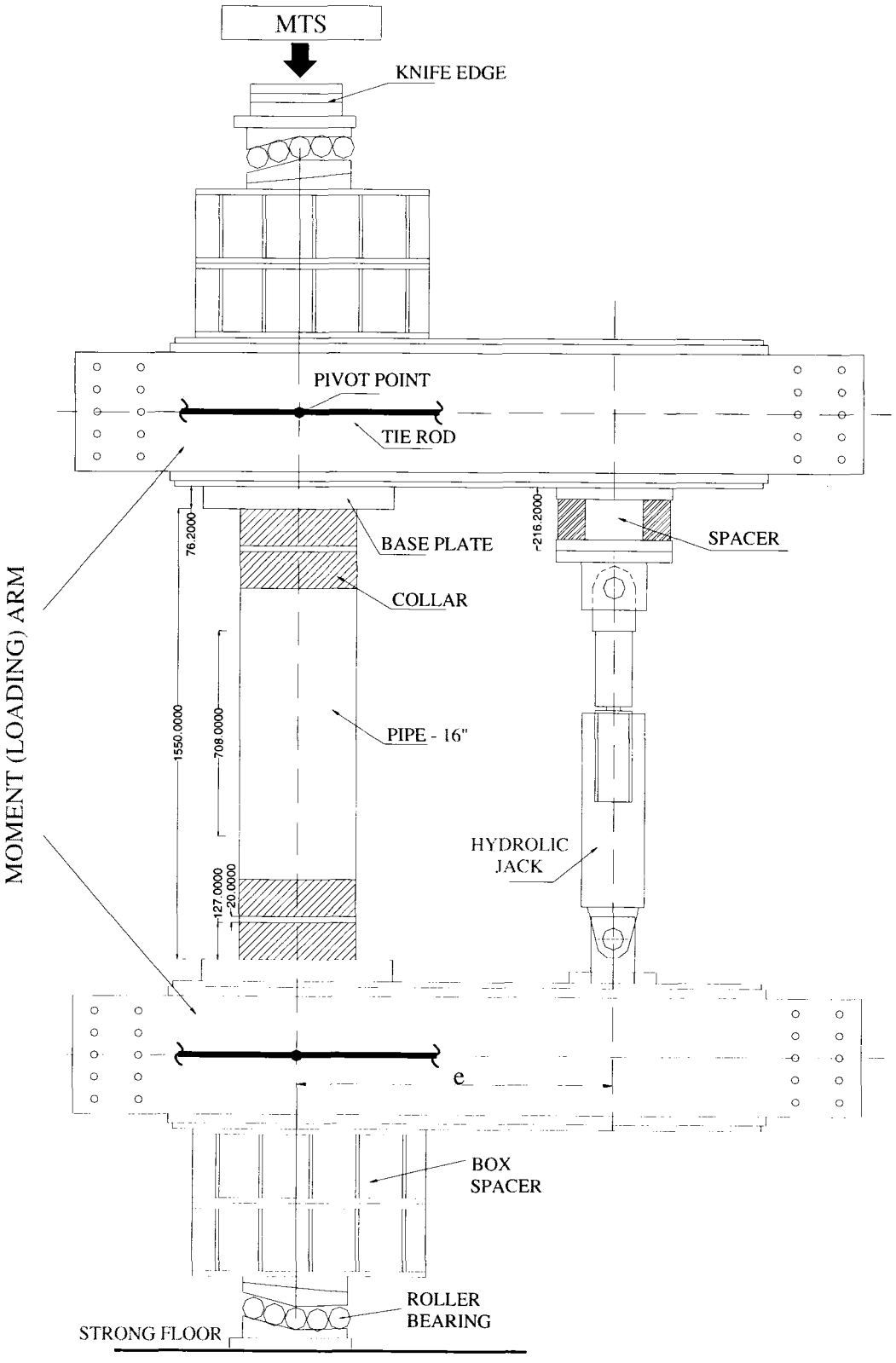

Figure 3.7 Test Setup - Initial

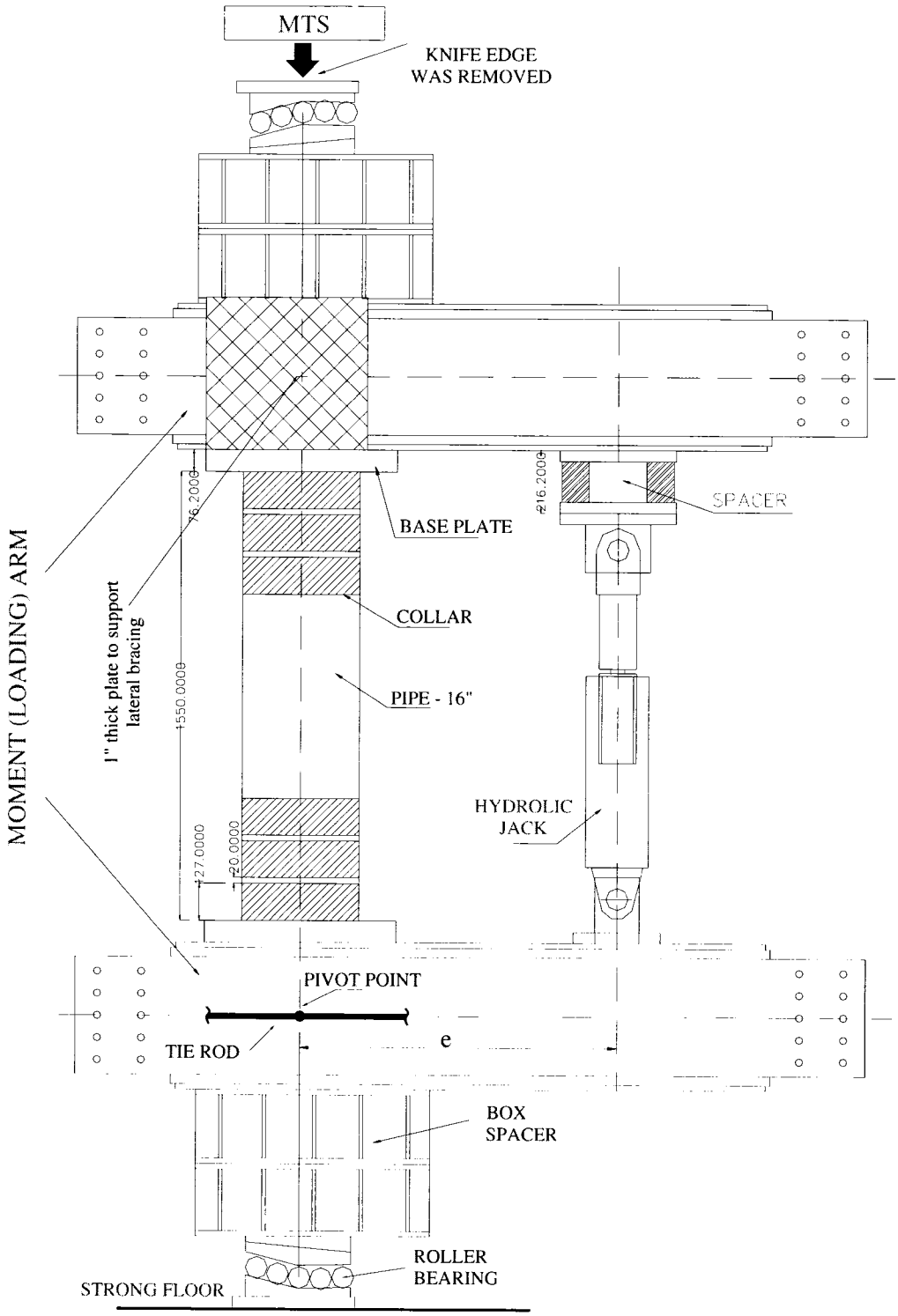

Figure 3.8 Test Setup - Modified

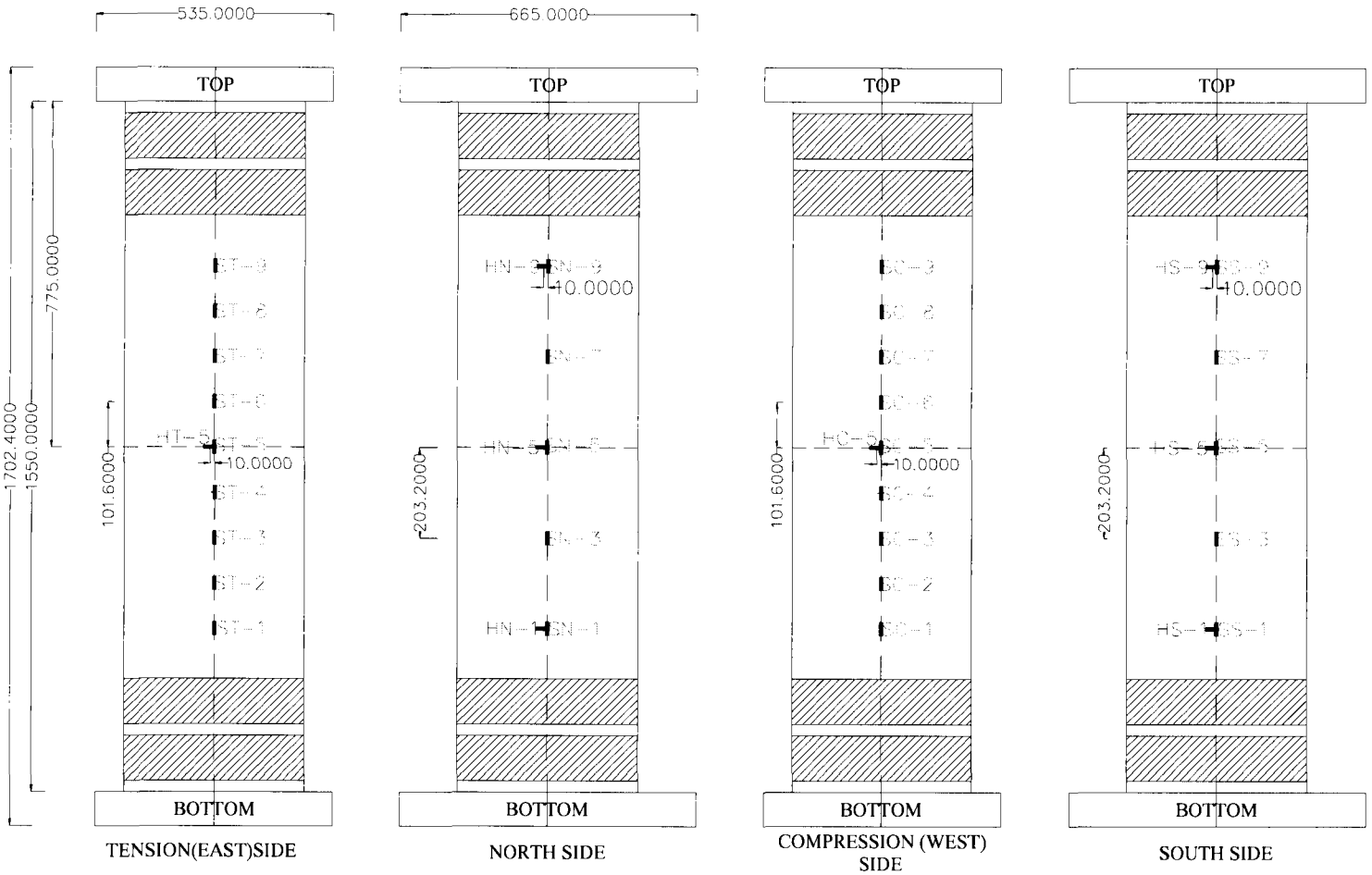

Figure 3.9 Strain Gauge Layout for 16 inch Pipes - Initial

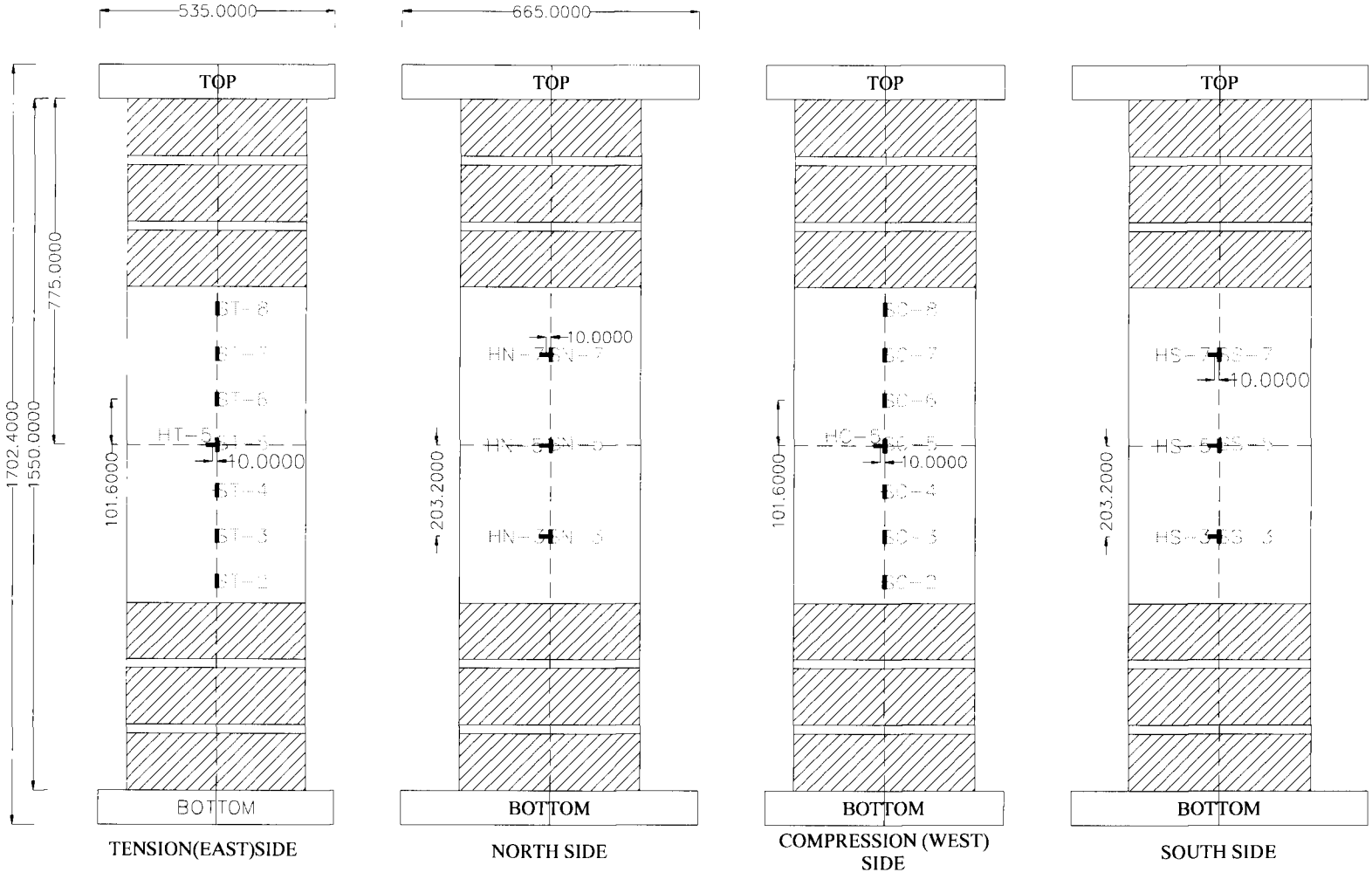

Figure 3.10 Strain Gauge Layout for 16 inch Pipes - Modified

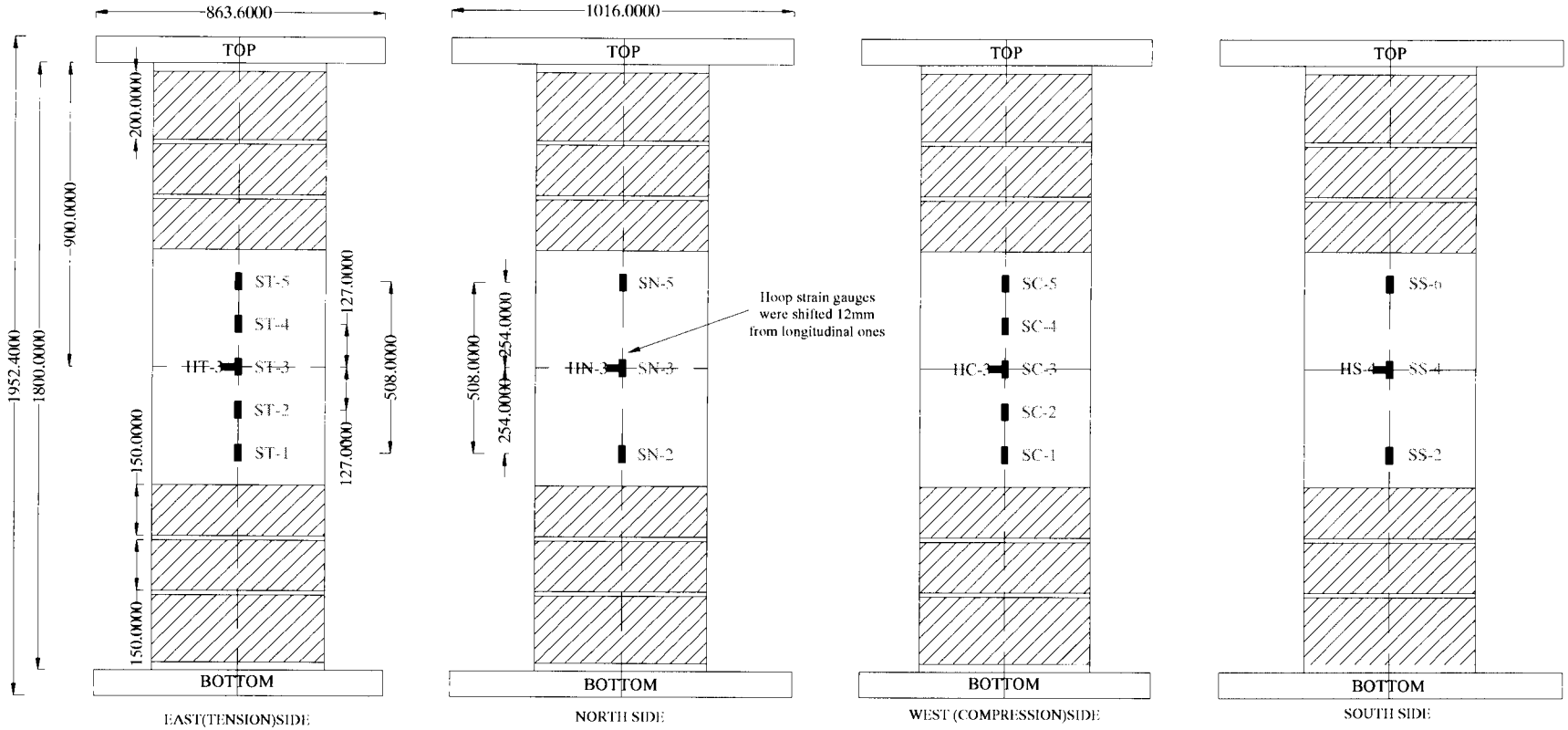

Figure 3.11 Strain Gauge Layout for 20 inch Pipes

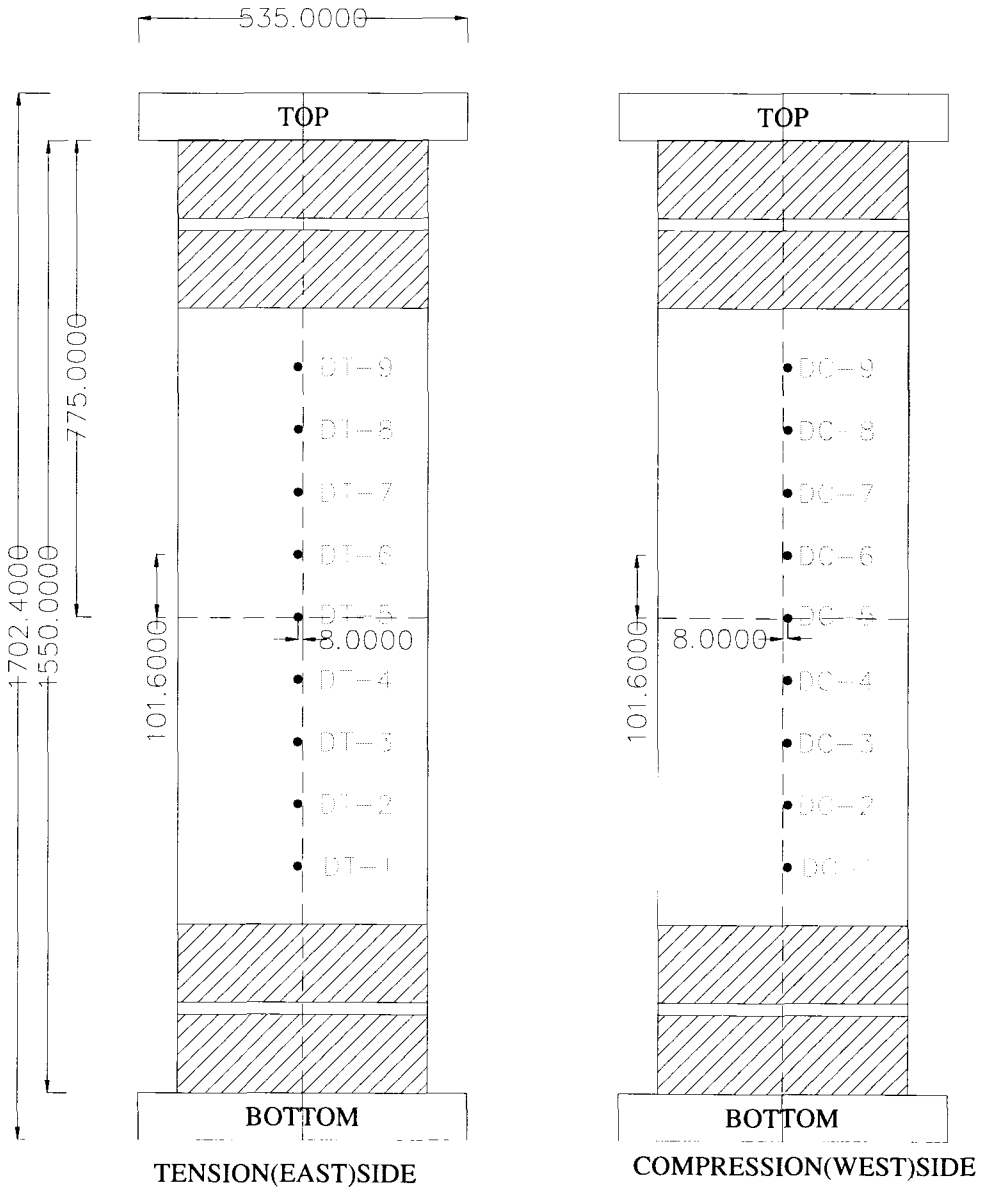

Figure 3.12 Demec Layout for 16 inch Pipes - Initial

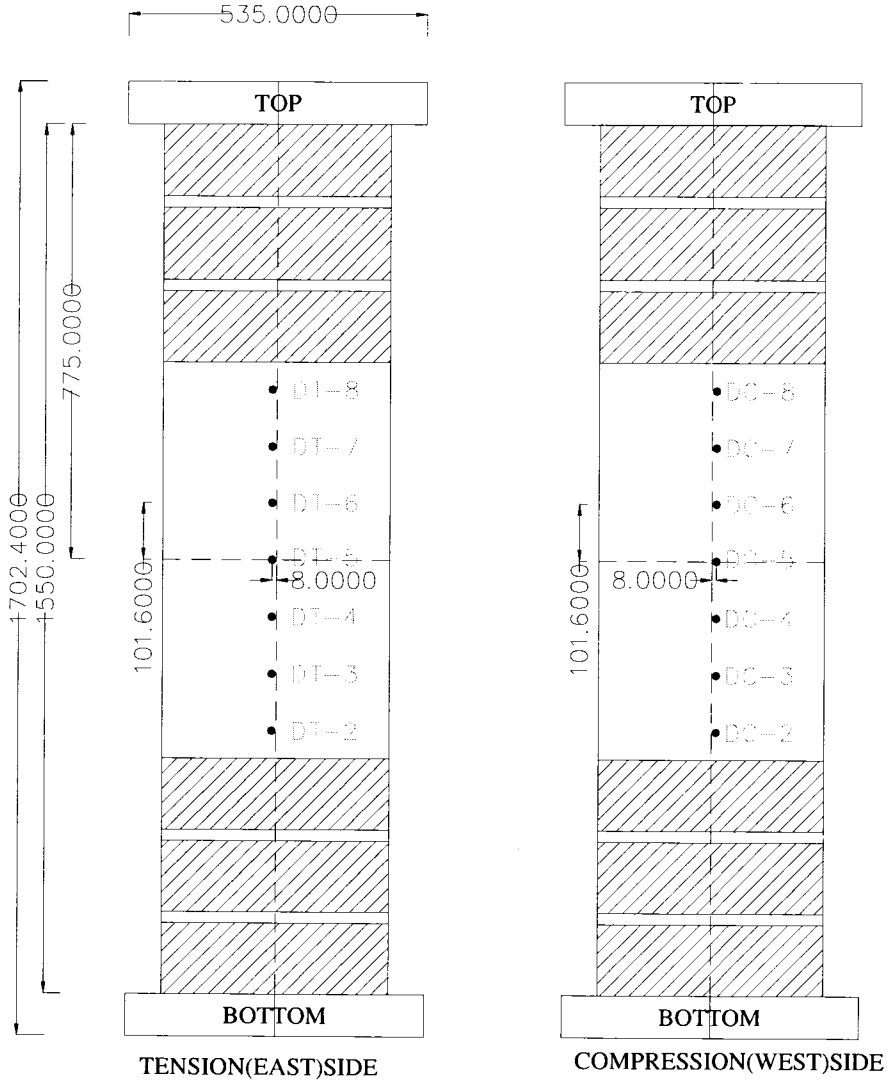

Figure 3.13 Demec Layout for 16 inch Pipes - Modified

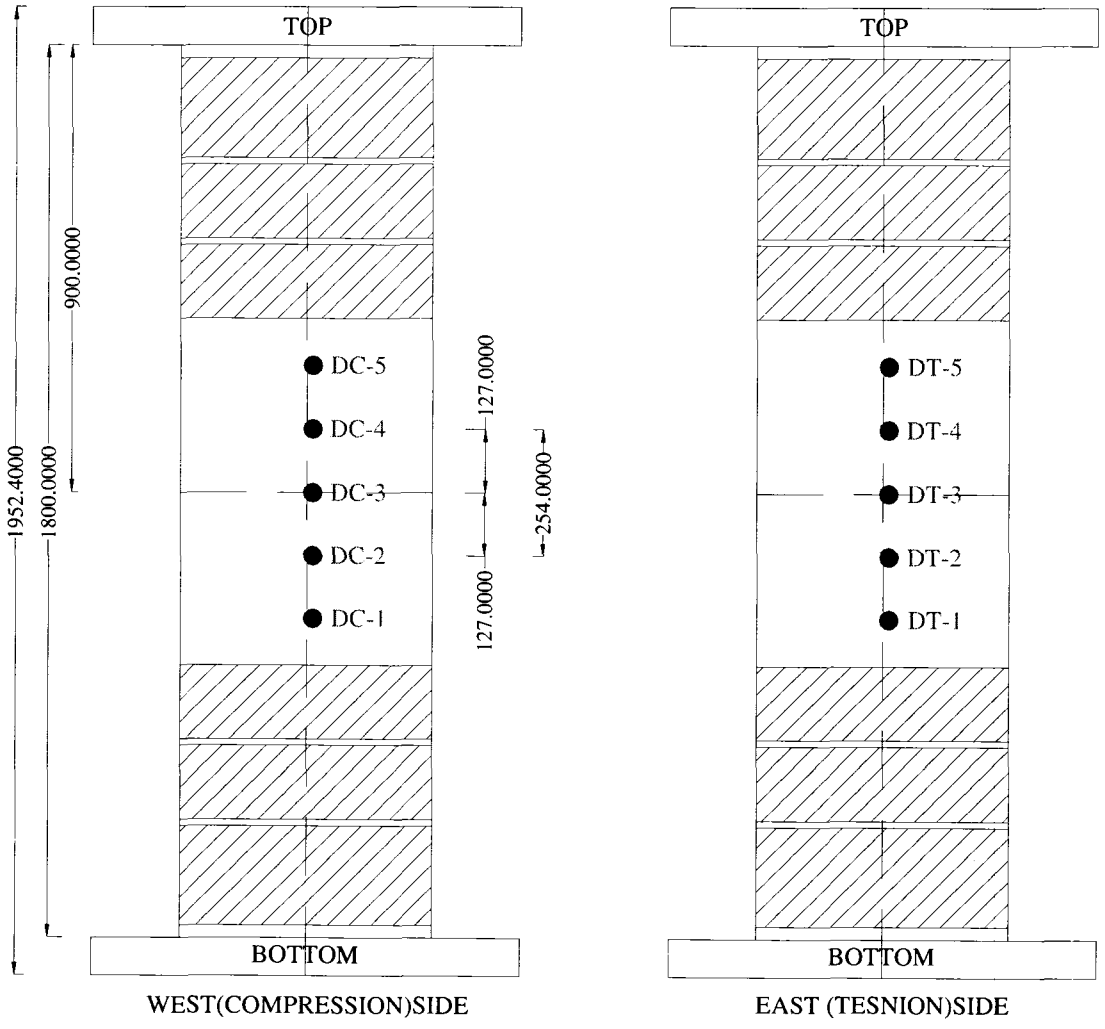

Figure 3.14 Demec Layout for 20 inch Pipes

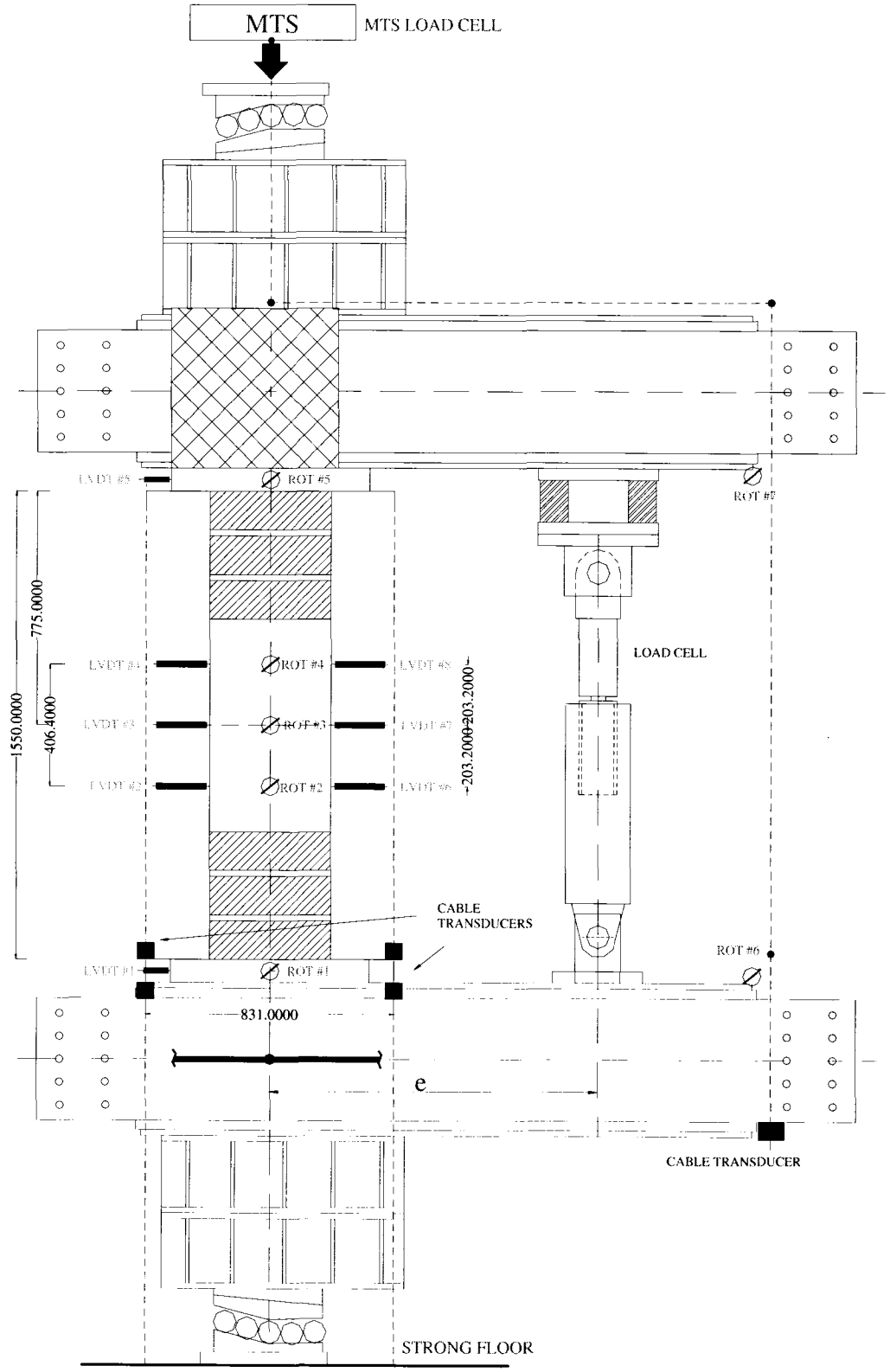

Figure 3.15 LVDT-RVDT-Cable Transducer Layout for 16 inch Pipes

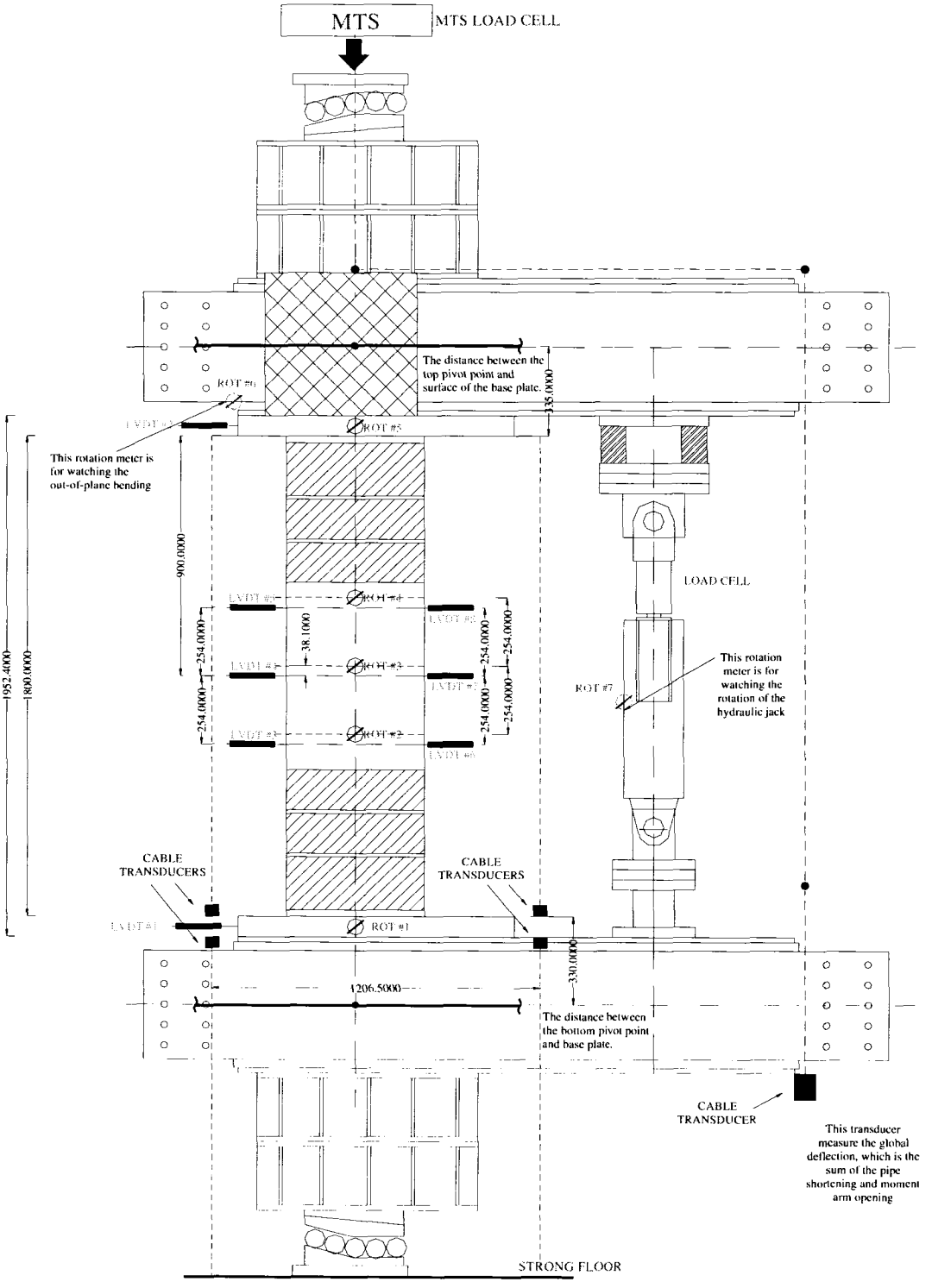

Figure 3.16 LVDT-RVDT-Cable Transducer Layout for 20 inch Pipes

4. DISCUSSION OF EXPERIMENTAL RESULTS

This research project has two main objectives: first one is to simulate the deformational behavior of a pipe in laboratory following the finite element simulation and second is to extend the database about wrinkling behavior in post buckling region, and hopefully fail the pipe in tearing. It was observed during the testing stage of six specimens that first goal was achieved successfully. However, they failed to obtain the tearing of the pipes under monotonic axial deformation. In this chapter, how the wrinkle behaves under large plastic deformations, level of maximum axial load and maximum moment, the strain values and other experimental data that may be helpful on understanding the behavior of the pipes were discussed.

It was observed that pipes are highly ductile and they can sustain large axial deformation. However, under constant curvature and monotonically increasing axial load, the pipes failed to fracture at the wrinkle location. Nevertheless, the strain reversals at the wrinkle location on compression face did produce significant through thickness cracks. Each specimen is investigated separately in this section to make a comparison between them.

4.1. Reduction of Experimental Data

All the data except demec readings were collected electronically by using a data acquisition system and stored in the computer. However, the data has to be reduced in order to make some comparisons between the specimens. This section includes the procedures to reduce the raw data collected during the experiments. Initial set of

readings were used both for manually and electronically collected data by subtracting them from the data collected at each count number.

4.1.1. Global End Moment

The global end moment is defined as the average of the end moments created on the specimens during the test. The free body diagram of the upper moment arm that was used to calculate the global end moment is given in Figure 4.1. It was assumed that the moment arm and the jack fixtures are infinitely rigid. By increasing the jack force, moment arm rotated around the pivot point and line of action of the axial and eccentric load shifted. Thus, by summing the end moments about the center of the base plates, the average end moment was calculated by the following formulae:

$$M_{top} = P_{jack}\left[\cos\theta_{top} \cdot e + \sin\theta_{top} \cdot (d_2 - d_1)\right] + P_{MTS} \cdot \sin\theta_{top} \cdot d_1$$

M_{top} : top end moment,

P_{jack} : eccentric jack load,

P_{MTS}: axial load,

d_1: distance between the surface of the base plate and the moment arm center,

d_2: distance between the application point of the jack load and moment arm center,

θ: rotation angle.

4.1.2. Global End Curvature

The ratio of the average rotation of top and bottom ends of the pipe to the overall length of the pipe is called the average global curvature and it is calculated as follows:

$$\phi_{global} = \frac{\theta_{top} + \theta_{bottom}}{L_{overall}}$$

where

ϕ_{global}: the global curvature,

θ_{top}: rotation of the top end of the specimen,

θ_{bottom}: rotation of the bottom end of the specimen,

$L_{overall}$: effective length of the pipe taken as the overall length.

4.1.3. Local Moment

Local end moments were calculated as taking into account the effect of the lateral deflection, Δ, of the pipe. The method that was used to get the Δ is adopted from Dorey et al. (2001). By the help of the LVDT's located along the pipe on tension and compression faces, lateral movement of the outside surface of the pipe was obtained for each loading step. Then, those deformation values were put in a spread sheet and best curve was fitted to those points. As the equation of the curve was obtained, then the deflection at the wrinkle location was calculated for any count number. However, this method gives the deformation approximately because the ovalization of the pipe was not considered. Also, the mathematical equation creates some error on the results.

The free body diagram of a deformed specimen was given in Figure 4.2. Local end moment may be calculated by summing the moments about the center of the cross section where the wrinkle was formed which is given by the formulae:

$$M_{local} = P_{MTS}.\Delta + P_{jack}.(e.\cos\theta + d_2.\sin\theta - \Delta)$$

4.1.4. Local Curvature

Local strains were measured by using a manually operated Demec Gauges. When the deformations exceed the capacity of the Demec gauges, strains between the consequent points were measured by a pair of divider and a caliper. Once the strains

were obtained, local curvatures were calculated as shown in Figure 4.3, which is the change of the angle per unit length:

$$\phi_{local} = \frac{|\varepsilon_c| + |\varepsilon_t|}{D}$$

where

ϕ_{local}: local curvature

ε_c: average compressive strain

ε_t: average tensile strain

D: diameter of the specimen

4.2. Discussion of Behavior of D16P0A4.5-1

During the testing of this specimen some undesirable situations occurred. First, the axial load on the specimen had to be unloaded three times during the test due to the technical problems with the MTS6000 testing machine. Then, the test had to be stopped prematurely before the pipe had fractured because out-of-plane bending was observed on the buckled pipe. The out-of-plane bending was caused by the pipe wrinkle and the existence of a knife edge between the loading head of the MTS6000 and the upper loading arm that allows the pipe to rotate around the axis in west-east direction.

The buckled shapes of D16P0A4.5–1 are shown in Figures 4.4 to 4.6. The wrinkle was first formed between the demec points Dc7 and Dc9, as indicated in Figure 4.4. Since 40% of SMYS internal pressure was presented while the buckle was first formed, outward bulge type wrinkle was observed. The center elevation of the buckle was located 454.2 mm from the top of the specimen. The height of the wrinkle was approximately 21 mm when the rotation was locked at 4.5° at each end of the pipe. After locking the rotation, the pipe was depressurized to zero pressure. The axial load was

then increased monotonically to extend the wrinkle around the circumference of the pipe. However, due to lack of lateral bracing and presence of the knife edge at the top of the loading assembly, the pipe was bended in the out-of-plane direction as shown in Figure 4.6. Therefore, the growth of the wrinkle around the pipe could not be achieved for this test. The final buckled shape in the compression side is shown in Figure 4.6.

The reduced test results for D16P0A4.5–1 are given in Figures 4.7 to 4.13. The comparison between strain gauge and demec gauge readings at two different load levels are shown in Figure 4.7, in which the strain gauge readings were showing higher values then the demec gauge readings. However, the strain gauge readings exhibited constant distribution along the entire specimen before buckling; the demec gauge readings indicated inconsistent results. The rotation meter readings at top and bottom of the specimen are shown in Figure 4.8. As can be seen in the figure, at the time of locking rotation angle of an average of 4.5°, the top end rotation was around 5° while the lower end was 4°.

The peak moment and the corresponding critical buckling strain can be obtained from Figures 4.9 to 4.11. As shown in Figure 4.9, the peak moment and the local buckling strain of the test specimen were of 770 kN.m and 19408με (1.94%). The axial force in the pipe wall and eccentric jack loads were around 3400 kN and 698 kN, respectively, at the time of pipe buckle (Figures 4.12 and 4.13). The axial load from MTS6000 stayed around 4000 kN, which is the addition of the jack force and the net force in the pipe wall, after the pipe buckled. The deformations were localized in the wrinkle location under increased bending moment. The local strain (curvature) grew rapidly under increase curvature to about 10% before the pipe was locked at an average

rotation angle of 4.5°, as shown in Figures 4.12 and 4.13.

Subsequently, the internal pressure was released after locking the rotations and the axial force on the pipe was increased while keeping the curvature at a constant level. The axial load was reached to 5556 kN (Figure 4.12) before the sideways deflection of the pipe was observed.

Consequently, the results from this test were used to modify the test setup and test procedures for the following tests. The most important modification was the addition of the lateral bracing system to the testing assembly to prevent out-of-plane instability. The lock rotation angle was also increased at a higher level for the remaining of two tests. In addition, since the demec strain values showed inconsistent results as compared with the strain gauge values, a new 200mm demec gauge was used in the remaining tests instead of 8 inches demec gauge.

4.3. Discussion of Behavior of D16P0A5-2

The buckled shapes of D16P0A5–2 are shown in Figures 4.14 to 4.18. The wrinkle was first formed between the demec points Dc3 and Dc4, as indicated in Figure 4.14. Since 40% of SMYS internal pressure was presented while the buckle was first formed, outward bulge type wrinkle was observed. Also, adding an extra pair of collars to each end of the pipe pushed the wrinkle closer to the mid-height. The crest of the buckle was located 623 mm from the bottom end of the specimen, approximately 150 mm below the mid-height of the pipe. The height of the wrinkle was approximately 29 mm when the rotation was locked at an average rotation angle of 5° at the end of the pipe. After locking the rotation, the pipe was depressurized and the axial load was then increased monotonically to extend the wrinkle around the circumference of the pipe. No

lateral deformation was observed for this experiment throughout the test. Due to zero pressure in the pipe, the wrinkles (in south and north sides) at the 90° directions to the initial local buckling location (in west side) were deformed inward at the initial buckled section. The final deformation shapes in different views are shown in Figures 4.15 and 4.16. The test was terminated after the winkle in the tension side (east side) folded and the axial load started to increase again. No tearing was observed during the test. The failed specimen was cut at the wrinkled segment after the test, as shown in Figures 4.17 and 4.18. Close inspection of the cut segment, showed no fracture on inside of the failed specimen.

The reduced test results for D16P0A5–2 are given in Figures 4.19 to 4.27. The comparison between strain gauge and demec gauge readings at two different load levels are shown in Figure 4.19. Good agreement was observed between two measurements. The strain readings exhibited constant distribution along the entire specimen before buckling. The rotation meter readings at top and bottom of the specimen are shown in Figure 4.20. As can be seen in the figure, at the time of locking rotation angle of an average of 5°, the top end rotation was around 4.7° while the lower end was 5.3°.

Similar to D16P0A4.5–1, this specimen was also pressurized at 40% SMYS until forming an outward bulge wrinkle on the compression side. The peak moment and the corresponding critical buckling strain can be obtained from Figures 4.21 and 4.23. As shown in Figure 4.21, the peak moment and the local buckling strain of the test specimen were of 706 kN.m and 19497με (1.94%). If the point where the slope changes from the global curvature versus local compressive strain plot was used (Figure 4.23), a local buckling strain of 16452με (1.65%) was obtained. Up to this point of test, the

behavior of the test specimen was almost identical to D16P0A4.5–1. The local strain (curvature) grew rapidly under increased curvature to about 14% before the pipe was locked at an average rotation angle of 5°, as shown in Figure 4.23. Besides, under constant curvature and monotonically increasing axial load, pipe was deflected laterally towards east direction of around 85 mm that has created a P-Δ moment of 860 kN.m, as shown in Figure 4.22.

Subsequently, the internal pressure was released after the average rotation from both ends reached 5°, and the axial force on the pipe was increased while keeping the curvature at a constant level. The peak axial load reached 5081 kN before the load drop, as shown in Figure 4.25. While increasing the axial load the third pairs of collars at each end was removed to allow extension of the wrinkle around the pipe circumference. However, it is suspected that the timing for removing the collars might not be adequate so that they could constrain the growth of the wrinkle outward below the wrinkle location (see Figure 4.15). The axial load was dropped to approximately 2000 kN with increase of the magnitude of the wrinkle around the section. However, the axial load increased again after the lips of the wrinkle were formed a contact, the test was terminated after the axial load increased to around 4000 kN (Figure 4.25).

The axial load and jack load versus shortening of the specimen curves are shown in Figures 4.26 and 4.27, respectively. The final shortening of the pipe reached 250 mm over the specimen length of 1546 mm, which represented a significant axial ductility of 16% without fracture. In order to maintain a 5° locking rotation angle at the ends of the specimen, the jack load had to provide a reverse moment to the pipe while formatting the wrinkle around the circumference of the specimen, as shown in Figure 4.27.

However, after the wrinkle around the pipe had formed, the constraining moment from the jack load would be relaxed until the axial load increased again due to the contact force generated from the folded wrinkles.

Based on the results from this test, couple of modifications was adopted in the third test, D16P40A7-3. It was decided to increase the locking rotation angle to 7^{o} to accommodate formation of tearing. The timing of removing third set collars was changed to right after the formation of initial wrinkle to minimize the radial constraint at the vicinity of the wrinkle.

4.4. Discussion of Behavior of D16P40A7-3

The buckled shapes of D16P40A7–3 are shown in Figures 4.28 and 4.29. The wrinkle was first formed between the demec points Dc6 and Dc7, as indicated in Figure 4.29. Since 40% of SMYS internal pressure was presented while the buckle was first formed, outward bulge type wrinkle was observed. Also, adding an extra pairs of collars to the each end of the pipe pushed the wrinkle closer to the mid-height. The crest of the buckle was located 625 mm from the top end of the specimen, approximately 150 mm above the mid-height of the pipe. The wrinkled shapes viewed from the compression (west) and tension (east) sides, when the rotation was locked at an average rotation angle of 7° at the end of the pipe, are shown in Figure 4.29. After locking the rotation, the axial load was then increased monotonically while the internal pressure was kept at 40% of SMYS, to extend the wrinkle around the circumference of the pipe. No lateral deformation was observed for this experiment throughout the test. The test was terminated after the winkle in the tension side (east side) folded and the axial load started to increase again. No tearing was observed during the test. However, significant

cracking was observed in the folded winkled on the compression side, as shown in Figure 4.30. After inspection of the cut segments it was found that significant cracking was occurred around the wrinkle location due to the folding of the buckle. It is clear in Figure 4.31, pipe was tearing due to the folding action of the wrinkle under monotonically increasing axial load. But, crack was not tearing apart completely due to the sealing of the buckle lips under axial load.

The reduced test results for D16P0A7–3 are given in Figures 4.32 to 4.40. The comparison between strain gauge and demec gauge readings at two different load levels are shown in Figure 4.32. Excellent agreement between two measurements was obtained. The strain readings exhibited constant distribution along the entire specimen before buckling. The rotation meter readings at top and bottom of the specimen are shown in Figure 4.33. As can be seen in the figure, at the time of locking rotation angle of an average of 7.1°, the top end rotation was around 7.9° while the lower end was 6.3°.

Similar to D16P0A4.5–1 and D16P0A5-2, this specimen was also pressurized at 40% SMYS until forming an outward bulge wrinkle on the compression side. The peak moment and the corresponding critical buckling strain can be obtained from Figure 4.34. As shown in Figure 4.34, the peak moment and the local buckling strain of the test specimen were of 705 kN.m and 21181με (2.12%). If the point where the slope changes from the global curvature versus local compressive strain plot was used (Figure 4.36), a local buckling strain of 17912με (1.79%) was obtained. Both the peak moment and critical buckling strain are almost identical to previous two tests. The third pair of collars was removed before additional curvature was applied to the pipe. The local strain (curvature) grew rapidly under increased curvature to about 27% before the pipe was

locked at an average rotation angle of 7°, as shown in Figure 4.36. It also indicated when the rotation angle reached 7° the pipe bending capacity had dropped to zero, i.e. the jack force was approaching zero. On the other hand, the lateral deflection of D16P40A7-3 was 119 mm and the P-Δ moment was 882 kN.m (Figure 4.35).

Subsequently, after the average rotation was reached 7°, the axial force on the pipe was increased monotonically while the curvature was kept at a constant level. The major difference of this test from the previous two was the internal pressure was kept constant of 40% of SMYS throughout of the test. The peak axial load reached 5036 kN before the load drop, as shown in Figure 4.38. The axial load was dropped to approximately 3700 kN (including 1424 kN end reaction from the 40% SMYS internal pressure) with increase of the magnitude of the wrinkle around the section. However, the axial load increased again after the lips of the wrinkle in the tension side were formed a contact, the test was terminated after the axial load increased to over 5000 kN (Figure 4.38).

The axial load and jack load versus shortening of the specimen curves are shown in Figures 4.39 and 4.40, respectively. The final shortening of the pipe reached 265 mm over the specimen length of 1549 mm, which represented a significant axial ductility of 17% without fracture. In order to maintain a 7° locking rotation angle at the ends of the specimen, the jack load had to provide a reverse moment to the pipe while formatting the wrinkle around the circumference of the specimen, as shown in Figure 4.40. The jack load increased to approximately 800 kN in tension until the formation of wrinkle around the circumference of the pipe. However, after the wrinkle around the pipe had formed, the constraining moment from the jack load would be relaxed until the axial

load increased again due to the contact force generated from the folded wrinkles in the tension side.

Although no tearing was observed at the end of the test, significant cracks have been observed during the increase of monotonic axial load from MTS6000. It is believed that the specimen was close to fracture at the wrinkle location. The reasons that no tearing was observed in the test could be attributed to several factors, such as the ductile behavior of the material, locking rotation angle at 7°, and monotonic loading history.

4.5. Discussion of Behavior of D20P40A3.5-4

Fundamentally the same testing procedure and setup was followed for the 20 inches sets of specimens. Under the combination of monotonically increasing axial load, constant curvature and 40% of SMYS internal pressure, D20P40A3.5-4 was deformed in modes which were shown in Figures 4.41 to 4.43. The pipe was pressurized 40% of p_y initially and an outward bulge type wrinkle was formed on the compression side of the pipe. The wrinkle was formed between the demec points Dc1 and Dc2, as indicated in Figure 4.41. Initially, thee pairs of collars were mounted to each end of the pipe to push the wrinkle across the mid section. The closest collar to the wrinkle was immediately removed just after the realizing the wrinkle on the compression side in order to allow the wrinkle to grow freely without any constraint. However, due to the presence of initial imperfections on the pipe wall, wrinkle was formed slightly above the closest bottom collar. The crest of the buckle was located 1192 mm from the top end of the specimen, approximately 292 mm below the mid-height of the pipe. The final shape of the wrinkle when the rotation of the pipe was located at an average angle of 3.5 was shown in Figure 4.42. After locking the rotation, the 40% internal pressure was kept and

axial load was increased monotonically to grow the wrinkle around the circumference of the pipe. During this stage, by the help of the RVDT located in the moment arm which was working in the out-of-plane direction, no sideways movement was observed in the test setup due to the help of the lateral bracings. Moreover, while increasing the axial load, a crack was formed under the wrinkle on the compression side (Figure 4.43). But, as the wrinkle folds, lips of the buckle touched and the load carrying capacity of the pipe increased again. So, tearing action could not be seen and the similar deformed configuration with the D16P0A5-2 was occurred.

The reduced data are given in Figures 4.44 to 4.51. Different from 16 inches specimens, for 20 inches pipes demec reading were taken by a 10 inches demec gauge. The comparison between strain gauge and demec gauge readings at two different load levels are shown in Figure 4.44. Excellent agreement between two measurements was obtained. The strain readings exhibited constant distribution along the entire specimen before buckling. The variation of the rotation of the top and bottom ends of the pipe was given in Figure 4.45. According to the graph, at the time of locking rotation angle, which is 3.5°, the top end rotation was around 2.7° and the bottom end rotation was 4.3°.

The pipe was pressurized to 40% of SMYS initially and this pressure was kept until completing the test. The moment vs. curvature relationship of the specimen was given in Figures 4.46 and 4.47. Similar to the previous pipes, peak moment and the corresponding critical buckling strain was obtained from Figure 4.46. According to the Figure 4.46, moment capacity was 630kN.m and the critical strain was 4941με (0.49%). If the point where the slope changes from the global curvature versus local compressive strain plot was used (Figure 4.48), a local buckling strain of 8550με (0.85%) was

obtained. The third pair of collar was removed immediately just after the wrinkle was formed initially. Prior to locking the curvature (angle), the local compressive strain was grown rapidly to 16%, as shown in Figure 4.49. When the rotation was locked, the moment value was dropped to 7% of the capacity of the section, as shown in Figure 4.46. On the other hand, the pipe was deflected 55 mm in the east direction and the moment vs. global curvature relationship that includes the P-Δ effect is given in Figure 4.47.

Furthermore, once the end rotations were reached to 3.5°, the axial load on the pipe was increased monotonically to tear the pipe. The axial load hit up to 2500 kN which was the axial load capacity of the buckled section and it dropped to 1870 kN while growing the wrinkle around the circumference of the pipe. During this stage, internal pressure was adjusted simultaneously with axial load to keep around 40% of p_y. And, as the axial load increase, wrinkle was folded and strain reversals created the tearing action. In contrary, wrinkle lips touched before the section completely fractured and the axial load carrying capacity was increased to 2480 kN (Figure 4.50). After realizing the increase of the axial load, experiment was terminated.

The axial load and eccentric jack load versus shortening of the specimen curves are shown in Figure 4.51. D20P40A3.5-4 showed an axial shortening of 141 mm over an overall length of 1806.5mm, which represented an axial ductility of 8% without fracture. The wrinkle was created and developed around the pipe by adjusting the jack load in tension or compression directions. The jack force increased up to 596 kN in compression to create a bulge wrinkle on the west side and it turned into 273 kN in

tension while increasing the axial load to expand the wrinkle all the way around, as shown in Figure 4.51.

In conclusion, fracture of the pipe has not been occurred, however, there were significant cracks observed around the wrinkle location during the experiment. There were two main reasons of not being tearing the pipe: first one is that locking angle, 3.5°, was not enough to form enough strain reversals at the wrinkle locations under increasing axial load and second reason was that the 40% of SMYS internal pressure was not enough.

4.6. Discussion of Behavior of D20P0A5-5

The initiation and the growth of the wrinkle for D20P0A5-5 were given in Figures 4.52 and 4.53. Similar to D20P40A3.5-4, this specimen was also pressurized to 40% SMYS to form an outward bulge type wrinkle and three pairs of collars were used at each end of the pipe to push the buckle towards the midsection. However, the wrinkle was initiated between demec points Dc1 and Dc2, as shown in Figure 4.52. The buckle was formed 315 mm below the mid height of the pipe and 1215 mm below the top. Moreover, after the wrinkle has formed, the closest collars to the buckle were removed to allow the wrinkle expansion (see Figure 4.53). The average of the rotation angle of the pipe was increased up to 5° and the rotation was locked at that level. Consequently, locking the rotation was followed by the depressurization of the pipe and increase of the axial load monotonically to expand the wrinkle all the way around and finally fracture the pipe. During increasing the axial load on the pipe under constant curvature, folding of the wrinkle on the compression side was created tremendous strain reversals and a crack was observed which can be seen in Figure 4.54. In contrary, after releasing the

internal pressure the wrinkles (in south and north sides) at the 90° directions to the initial local buckling location (in west side) were deformed inward at the initial buckled section which is demonstrated in Figure 4.53. Similar to D16P0A5-2 and D20P40A3.5-4, test was terminated after the axial load carrying capacity of the pipe was started to increase again due to the folding of the wrinkle on the tension side. No visible tearing was observed during the experiment.

The reduced test results are given in Figures 4.55 to 4.62. The comparison between strain gauge and demec gauge strains at two different load levels was shown in Figure 4.55. And, good agreement was observed between two measurements. The variation of the top and bottom rotation angles during the test is shown in Figure 4.56. Up to the formation of the wrinkle, the angle at the top and bottom was similar however, after locking rotation the while the rotation of the top was 3.9°, the bottom was 6.1°.

Although D20P0A5-5 was designed to be a zero pressure test, the pipe was pressured with 40% SMYS at the beginning of the experiment to avoid the diamond type wrinkle. Under this condition, jack load was increased and the internal pressure was adjusted to keep it around 40% of p_y, until an outward bulge was formed. The corresponding critical compressive strain and the peak moment value can be obtained from Figure 4.57. The moment capacity was 658.5 kN.m and the critical compressive strain at that moment value was 4653με (0.46%). Besides, instead of using moment curvature plot if it was desired to use global curvature vs. local compressive strain curve, Figure 4.59, the change of the slope of the curve represents the critical compressive strain value which was 4746με (0.47%). The compressive strain was localized at the wrinkle location under increased curvature and hit up to 32% just before

locking the rotation (Figure 4.59). The pipe was deflected 78 mm in east direction and that deflection was introduced some P-Δ effect on the pipe. The corresponding second order moment was 621 kN.m which was obtained from Figure 4.58.

Once the wrinkle was formed on the compression side, the rotation was increased up to 5^{o} and locked at that level. The 40% internal pressure was released completely after that stage. And, the axial load was increased monotonically under constant curvature, to create strain reversals on the wrinkle location and tear the pipe. The axial load was reached to 2300 kN and then dropped to 1072 kN according to Figure 4.61. But, the tearing action could not be completed because the wrinkle on the tension side was folded completely and the axial load capacity of the pipe was increased again to 2300 kN. So, it was decided to stop the test after that point, because further increase of the axial load would probably create another wrinkle.

Finally, the change of the axial load and the jack force with respect to shortening of the pipe was given in Figures 4.62. The pipe was squashed 149 mm in axial direction without any fracture. The formation of the initial buckle and the keeping the rotation angle around a specific value during the test was achieved by adjusting the jack force. Therefore, the jack force was increase up to 587 kN (in compression) to form an outward bulge on the west side and during increasing the axial load monotonically the jack force switched into 317 kN in reverse direction to keep the locking angle constant (Figure 4.62).

4.7. Discussion of Behavior of D20P80A4.05-6

It was concluded from D20P40A3.5-4 and D20P0A5-5 that, 40% of SMYS internal pressure is not enough to form an outward type wrinkle around the

circumference of the pipe. Therefore, for this specimen it was decided to apply 80% of SMYS internal pressure until the end of the experiment. The wrinkle was formed and resulted in a form which is shown in Figure 4.63. Different than the previous two pipes, D20P80A4.05-6 was pressurized to 80% of SMYS initially to form a bulge type wrinkle on the compression side. For this pipe, wrinkle was initiated above the midsection of the pipe, between the demec points Dc5-7, as shown in Figure 4.63. The elevation of the wrinkle was 254 mm above the mid height and the 1154 mm form the bottom of the pipe. The collars above the wrinkle were removed just after realizing the formation of the wrinkle on the compression side (Figure 4.63). After removal of the collars, the end rotations on the pipe were increased up to 4.05°, at the same time internal pressure and the axial load on the system was adjusted simultaneously. The average end rotation angle of the system was locked at 4.05° and the internal pressure was kept at 80% of p_y while increasing the axial load to tear the pipe. Under monotonically increasing axial load, folding of the buckle on the compression face was created strain reversals and consequently a crack was observed under the winkle, as shown in Figure 4.64. However, at the end of the test no significant tearing was observed. The main reason for that was, as the axial load increase the crack was sealed and no water spraying action was observed.

The results obtained form the reduction of the data was given through Figures 4.65 to 4.71. In Figure 4.65, it is obvious that strain gauge and demec gauge readings showed a good agreement for two different count numbers. Prior to the buckling, strain distribution along the entire specimen exhibited a constant trend. The variation of the top and bottom rotation angles during the entire experiment is given in Figure 4.66. The

top and bottom rotations were almost same before the buckling but, the top was rotated 4.8° while the bottom was 3.3° after locking the rotation at 4.05°. In order to avoid the "cowboy hat" type buckling mode ,which was seen in D16P0A5-2, D20P40A3.5-4 and D20P0A5-5, internal pressure was increased to 80% of SMYS and kept until the end of the experiment. As a result of increasing the internal pressure the initial axial load on the pipe was also increased to 2500 kN to prevent a zip through fracture on the tension side of the wrinkle. Furthermore, moment vs. curvature relationship of the pipe was shown in Figures 4.67 and 4.68. According to the Figure 4.67, the moment capacity of the section and the critical buckling strain are 463 kN.m and 4513με (0.49%). On the other hand, it is obvious in Figure 4.69 that, the slope of the curve was changing at a strain value of 5010με (050%). The deformation was localized after formation of the wrinkle and the compressive strain was increased up to 28% before the rotation was locked (see Figure 4.69). Due to the reduction of the LVDT readings the lateral deflection of the pipe was calculated as 81mm, approximately. And the corresponding second order moment vs. curvature curve is shown in Figure 4.68.

Locking the rotation at 4.05° was followed by the increase of the axial load by keeping the internal pressure at 80% of SMYS. The axial load was increased monotonically and reached to 2800 kN which was shown in Figure 4.70. During this stage, wrinkle was extended around the circumference. But, as the axial deformation increased, wrinkle was totally folded and the axial capacity was started to increase again. Besides, the jack force was adjusted at this stage to keep the curvature at a constant value. Figure 4.71 shows that, jack force reached to 400 kN in compression and switched to 284 kN in tension to compensate the second order effects on the bending of

the pipe. D20P80A4.05-6 showed an axial shortening of 234 mm over the length of 1802 mm without fracturing.

4.8. Behavior of Pipes in the Post-buckling Region

Tearing (post-buckling) behavior of buckled pipes is one of the major objectives of this experimental program. And, in order to achieve a clear understanding of this phenomenon the tearing mechanisms will be handled according to the corresponding loading conditions.

Total of six full scale specimens were tested under different internal pressure and locking curvatures. Two types of failure modes were observed during testing. In the first failure mode, some of the pipes were buckled in such a way that they were ended up in a shape which was similar to a "cowboy hat" (see Figure 4.15). In this case, while the axial deformation was increased, wrinkle extended around the circumference and folded in such a way that wrinkle lips touched each other at north, south, east and west locations at four points. As a result this action, axial load carrying capacity of the pipe was increased again which prevents the fracture of the pipe.

On the other hand, for some specimens instead of the cowboy hat type failure mode, another type of deformation mode was governed which involves the tearing action. General mechanism of this type of failure is given in Figure 4.72. After the formation of the outward bulge type wrinkle on the compression face of the pipe, average rotation was locked. "*Locking the rotation*" is basically keeping the average curvature around a certain value during the experiment which was achieved by adjusting jack force. Consequently, axial deformation on the pipe was increased under constant

curvature and the wrinkle was expanded around the circumference. Further increase of the axial deformation leads to the folding of the wrinkles. When the wrinkle on the compression side completely folded, bottom portion of the pipe tends to go into the top part. This action continues until the tension side wrinkle lips touched each other. And during this movement, strain values at the foot of the compression side wrinkle changes from compression to tension which was defined as the strain reversal.

4.9. Summary

A total number of six full-scale pipe specimens were tested under monotonically increasing axial load and constant curvature to fail the pipes by tearing type failure. When the critical strain values for16 inches (19408, 19497 and 21181 με) and 20 inches (4941, 4653 and 4513 με) were observed, it could be concluded that in the pre-buckling stage pipes exhibit similar behavior regardless of the loading conditions. However, amount of internal pressure, end constrains and the locking rotation value has a significant effect on the post-buckling behavior of the pipes. It was realized during the experimental stages of D16P0A5-2, D20P40A3.5-4 and D20P0A5-5 that, internal pressure affects the tearing behavior of the pipes. Because, under monotonic increase of the axial deformation under 0% p_y and 40% p_y internal pressure, wrinkled section took a shape looks like a cowboy hat which is more likely known as a diamond shape buckle.

Besides, during testing of the all specimens in order to allow the expansion of the wrinkle around the circumference of the pipes, closest set of collars were removed to prevent the end constrain. And the other important conclusion is that, pipes can show significant amount of axial ductility without fracture.

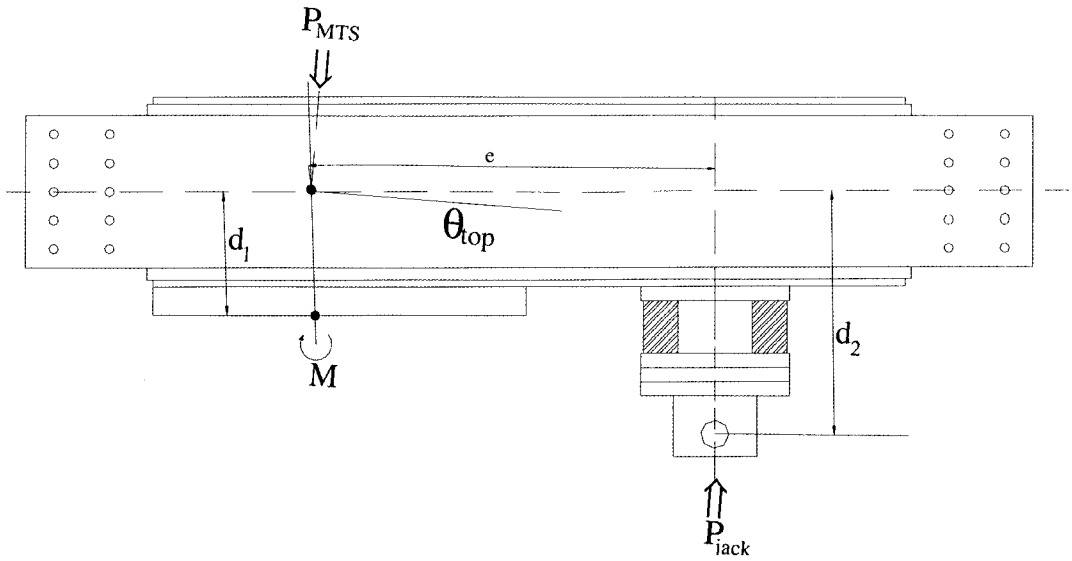

Figure 4.1 Free Body Diagram of the Moment Arm - Global End Moment

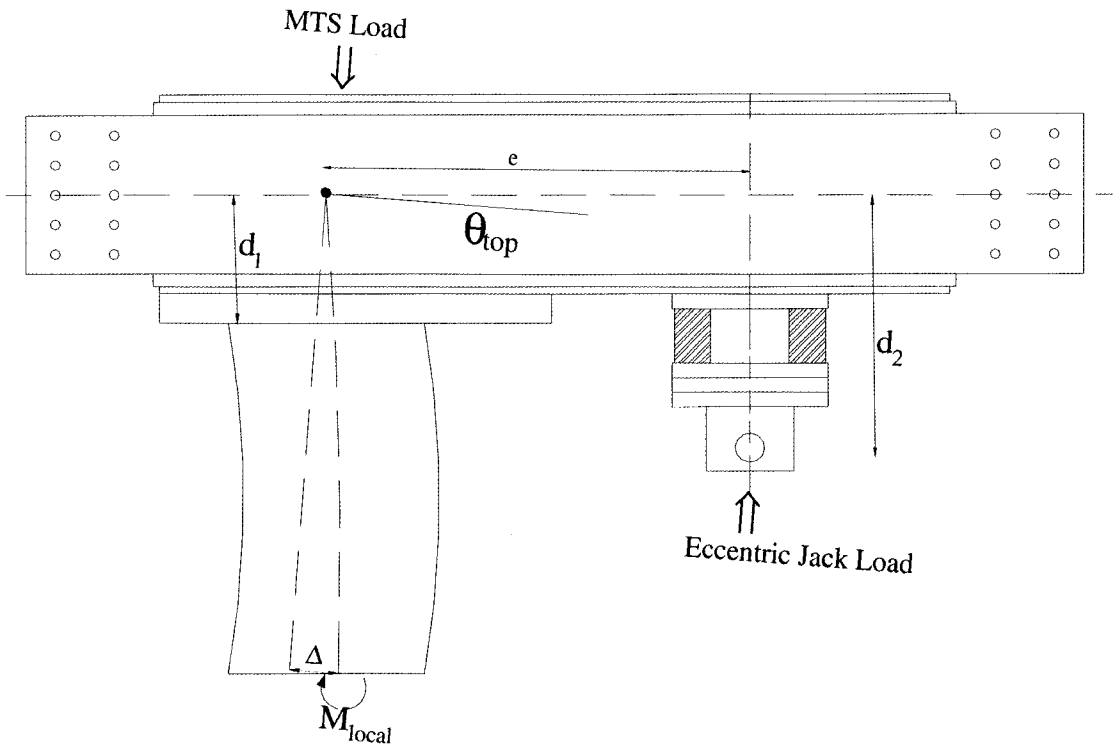

Figure 4.2 Free Body Diagram of the Moment Arm - Local Moment

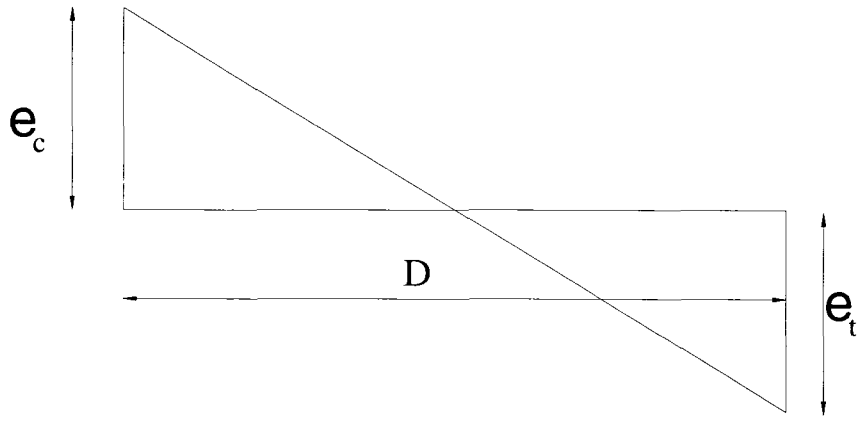

Figure 4.3 Strain Distribution to Calculate Local Curvature

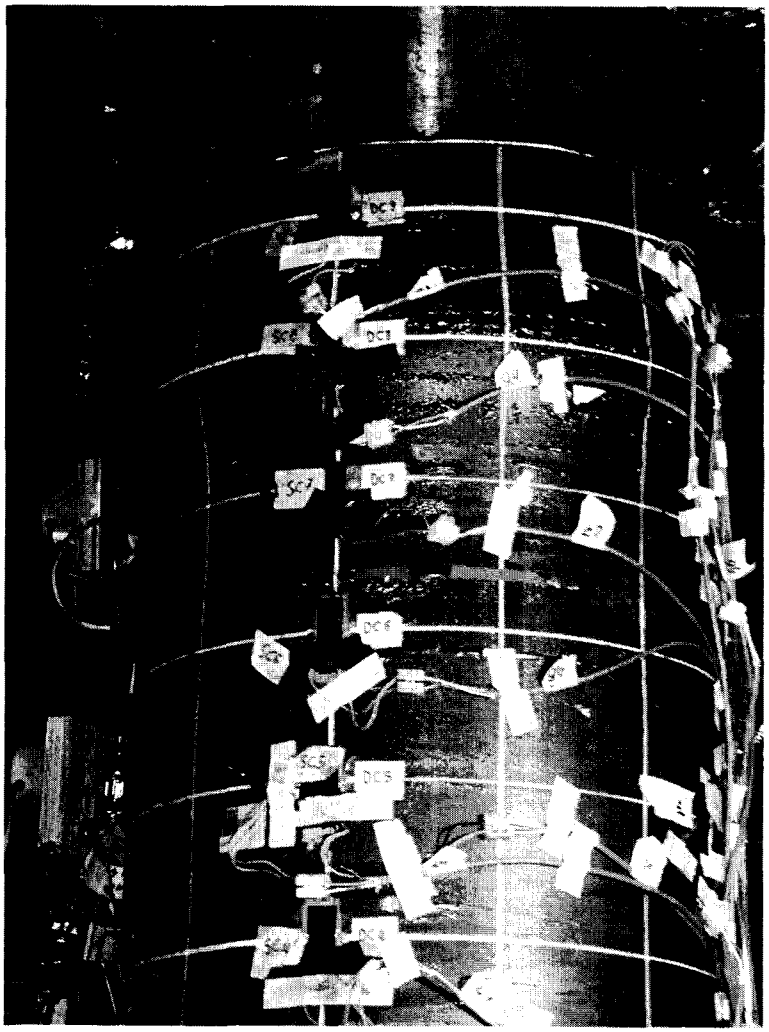

Figure 4.4 Initial Buckle Position D16P0A4.5-1

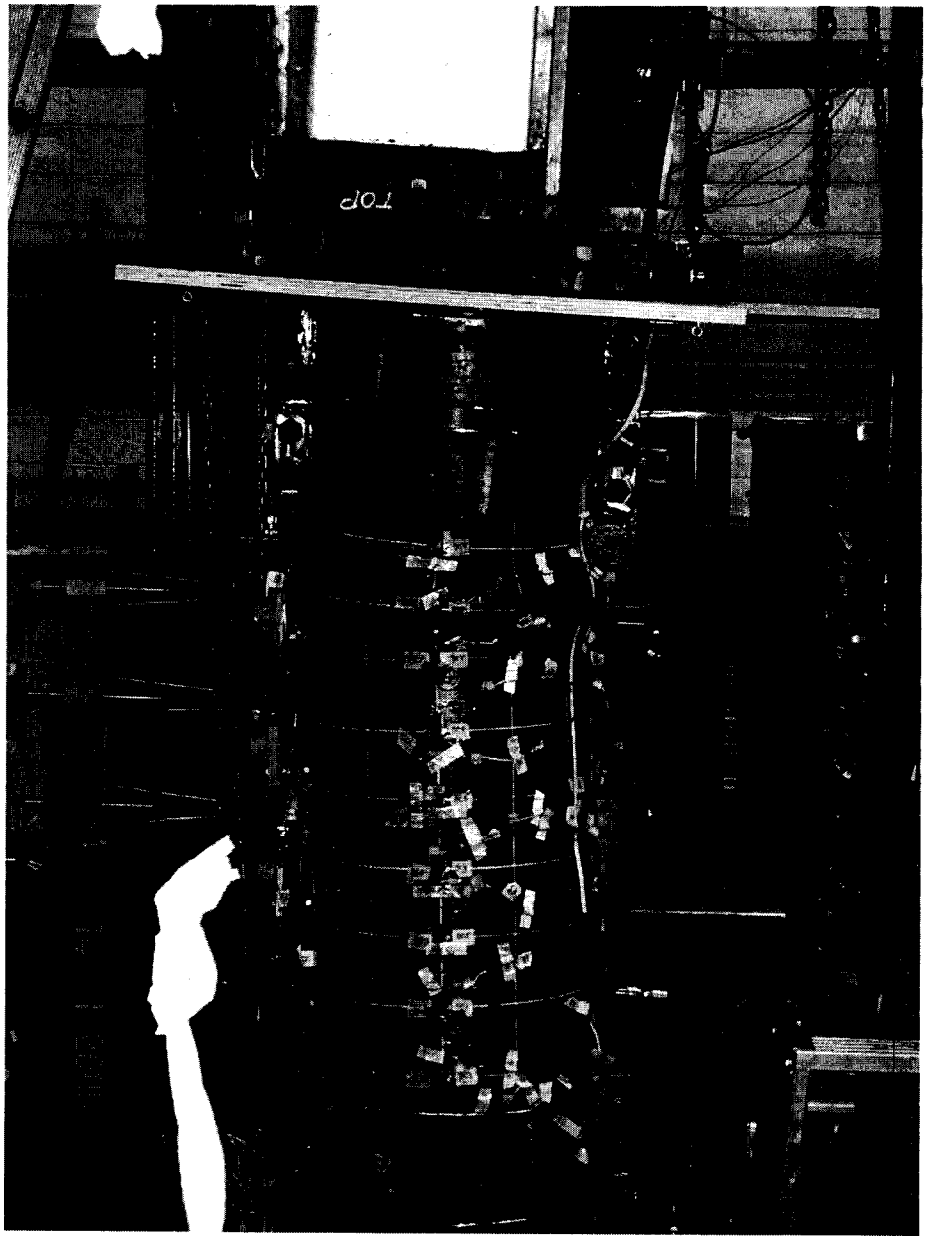

Figure 4.5 Out-of-Plane Bending D16P0A4.5-1

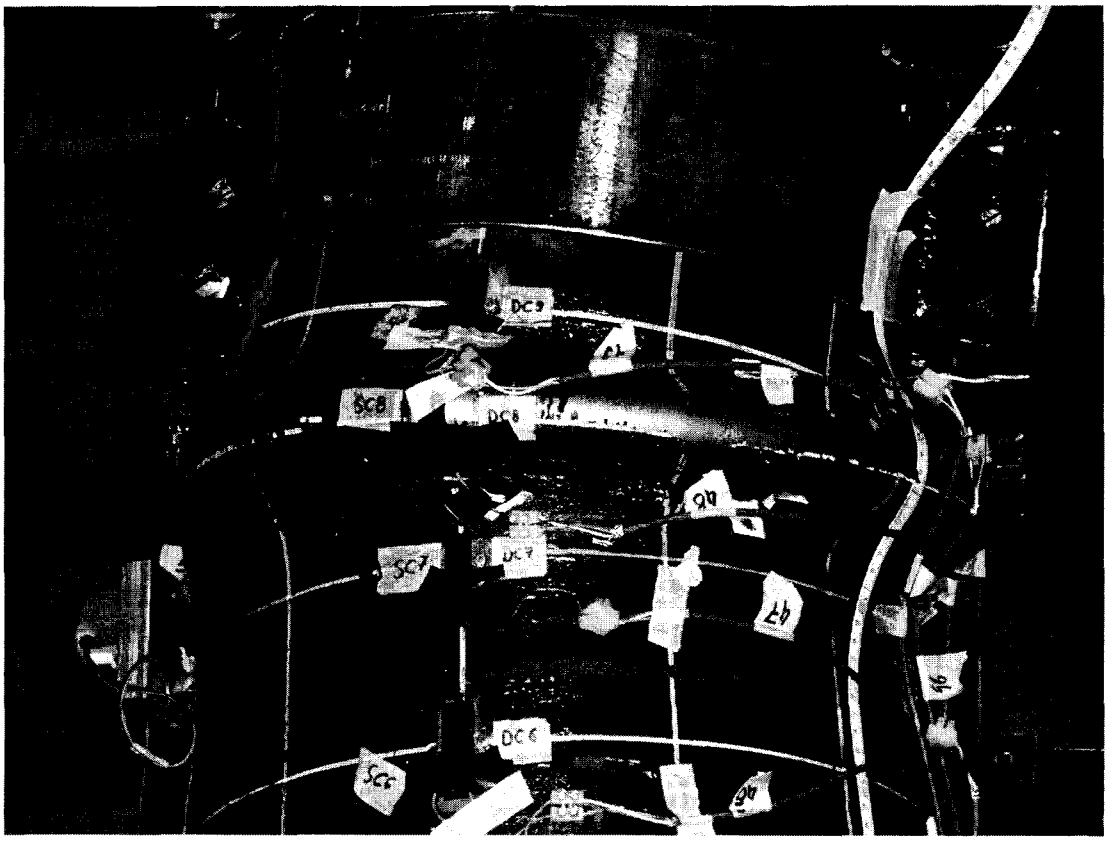

Figure 4.6 Final Shape of the Wrinkle D16P0A4.5-1

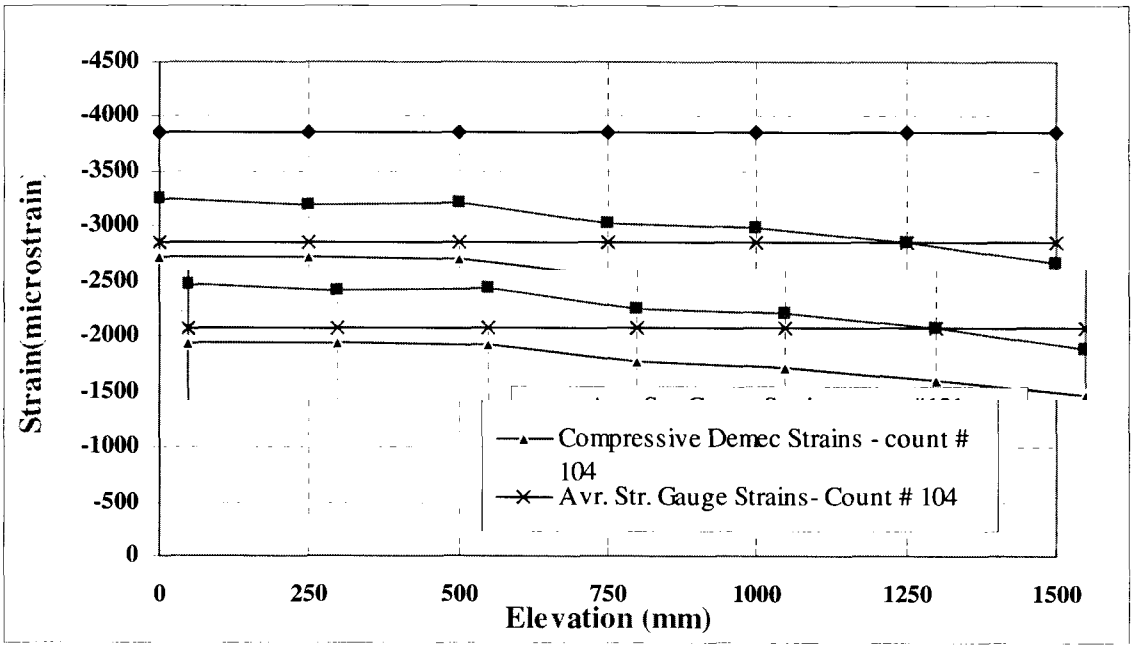

Figure 4.7 Comparison between Demec Strain and Strain Gauge Strain D16P0A4.5-1

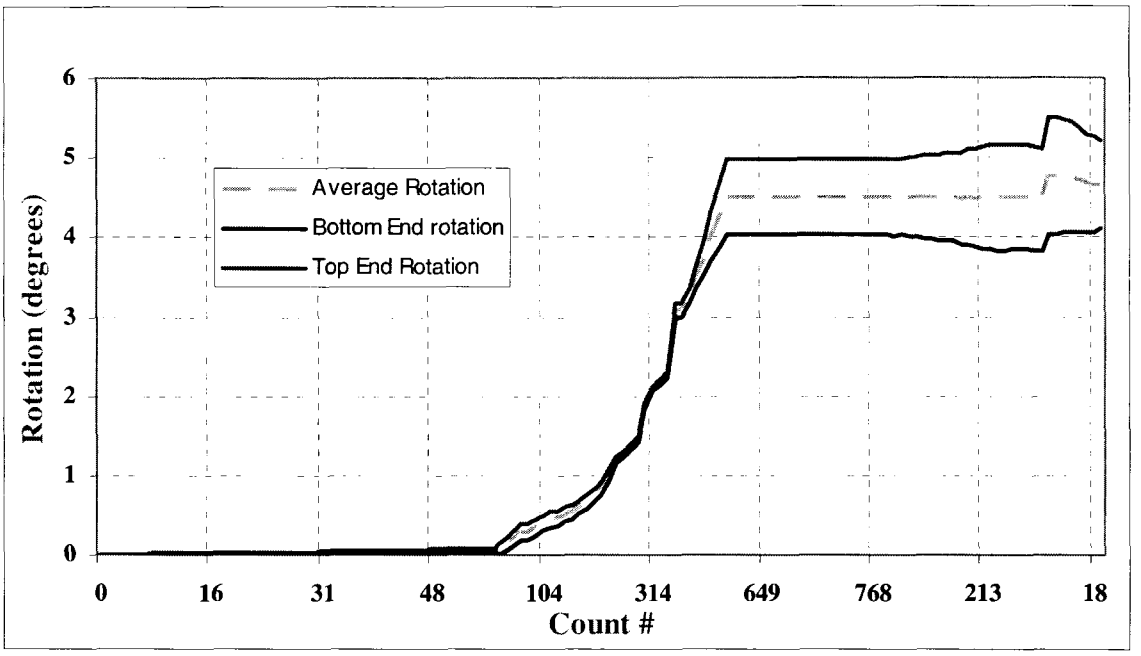

Figure 4.8 Variation of the End Rotations D16P0A4.5-1

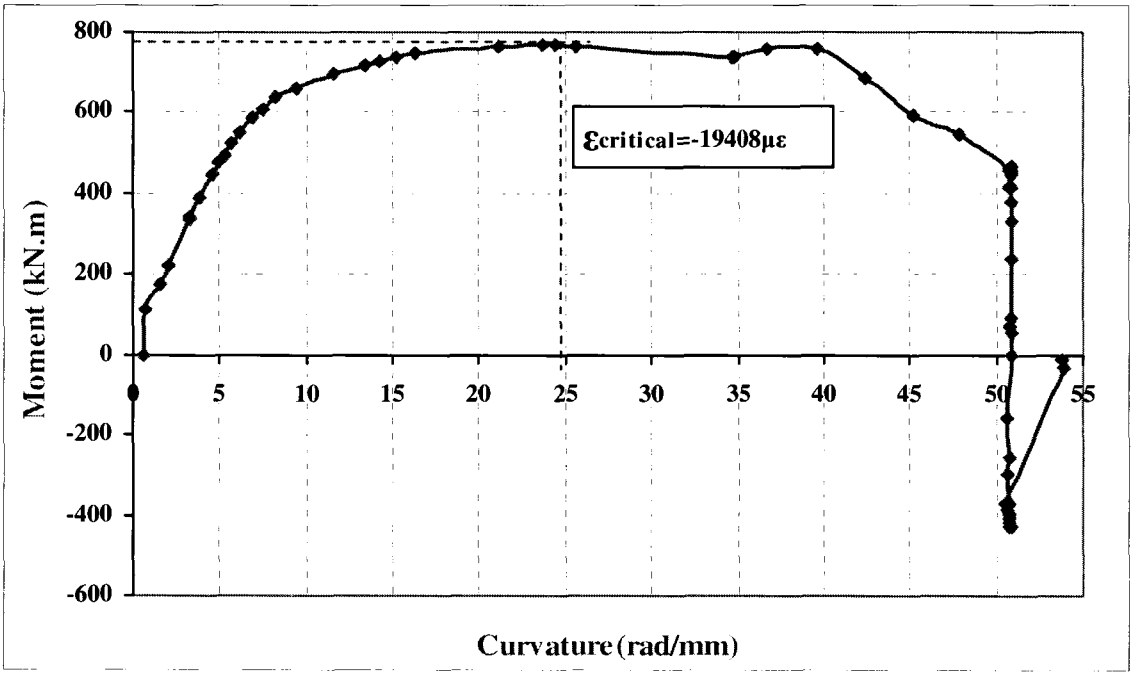

Figure 4.9 Average Global End Moment vs. Global Curvature D16P0A4.5-1

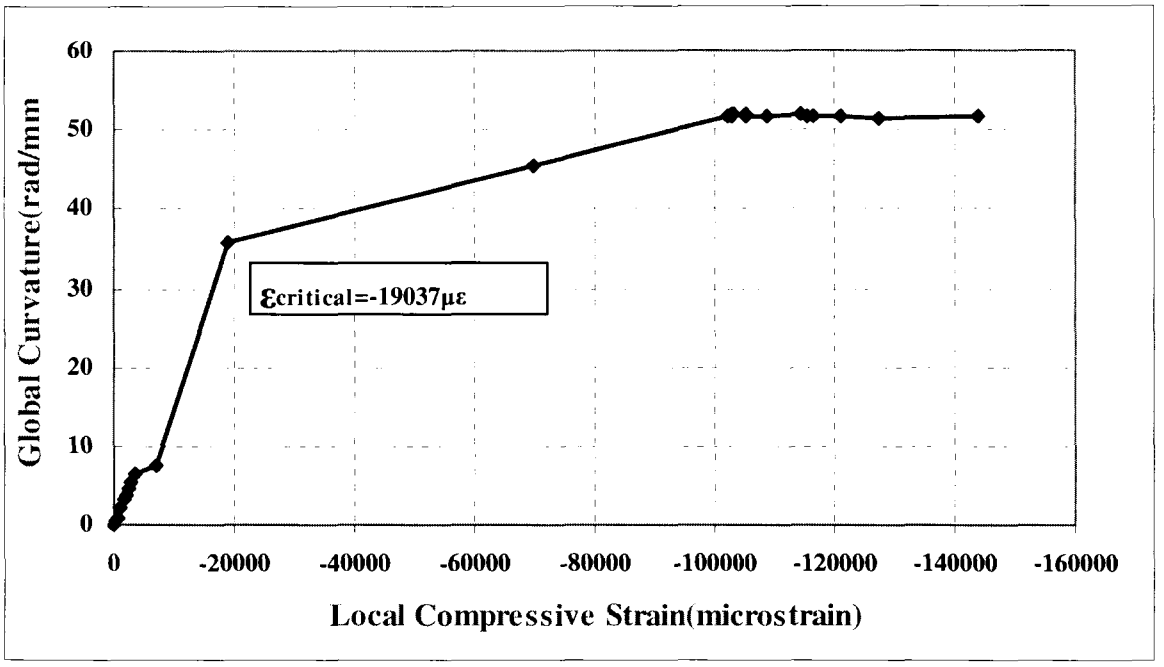

Figure 4.10: Global Curvature vs. Local Compressive Strain D16P0A4.5-1

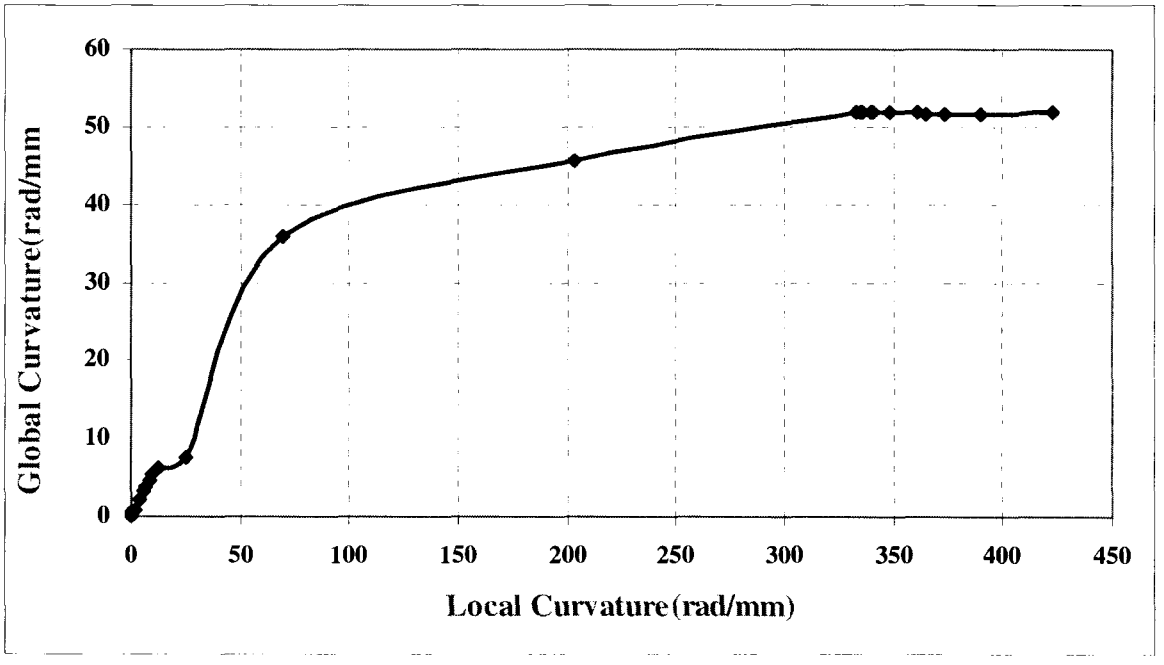

Figure 4.11 Global Curvature vs. Local Curvature D16P0A4.5-1

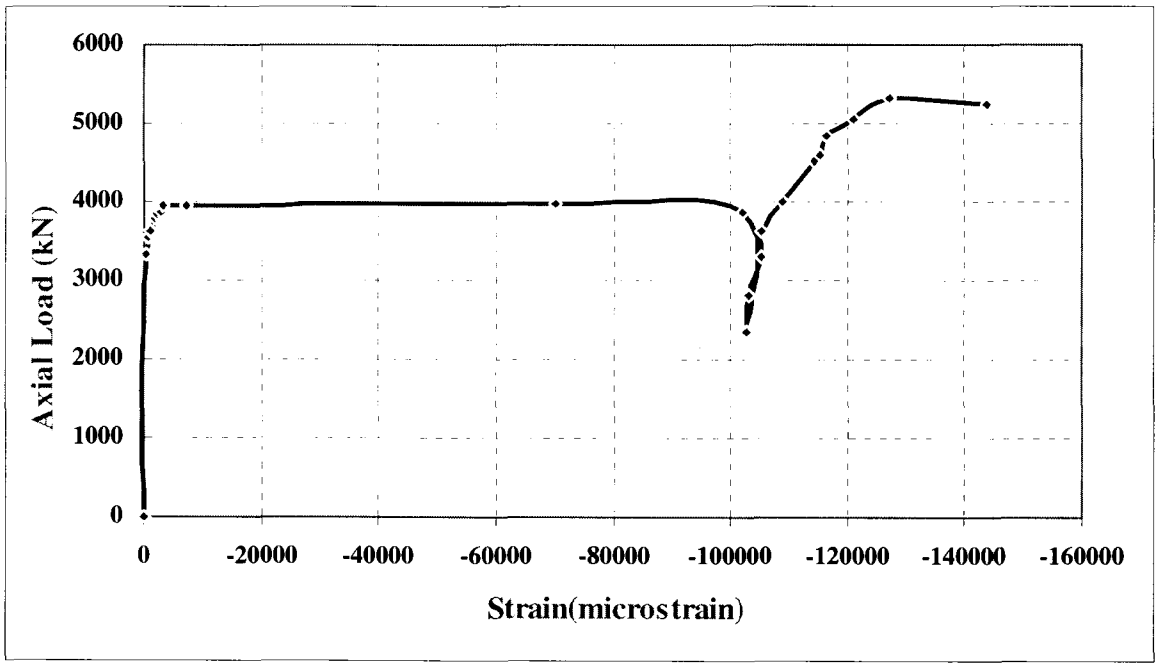

Figure 4.12 Axial Load vs. Local Compressive Strain D16P0A4.5-1

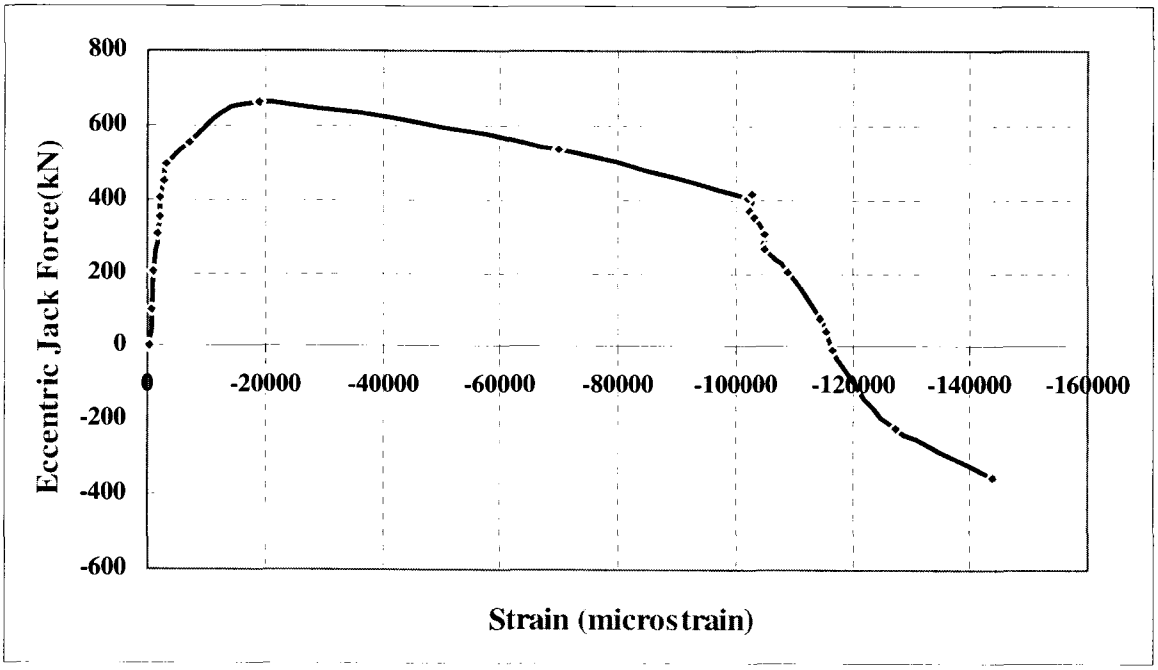

Figure 4.13 Eccentric Jack Force vs. Local Compressive Strain D16P0A4.5-1

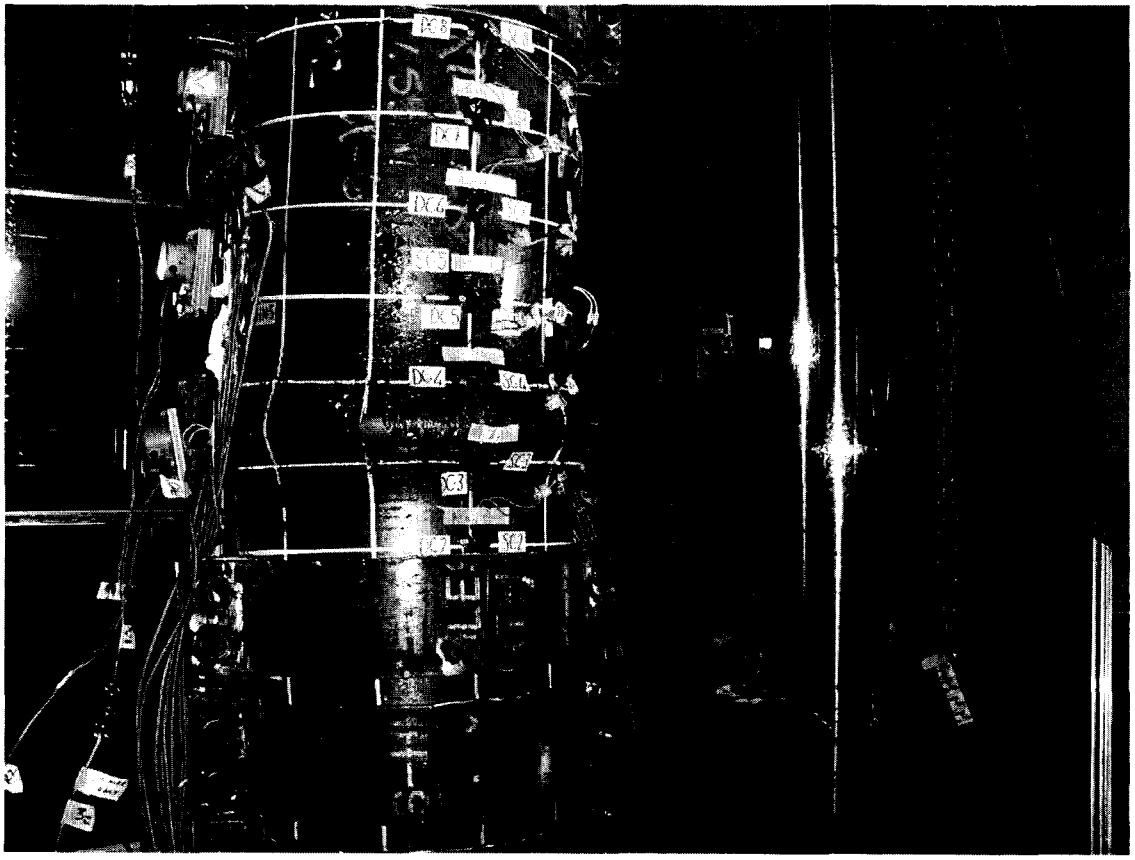

Figure 4.14 Initial Buckle Position D16P0A5-2

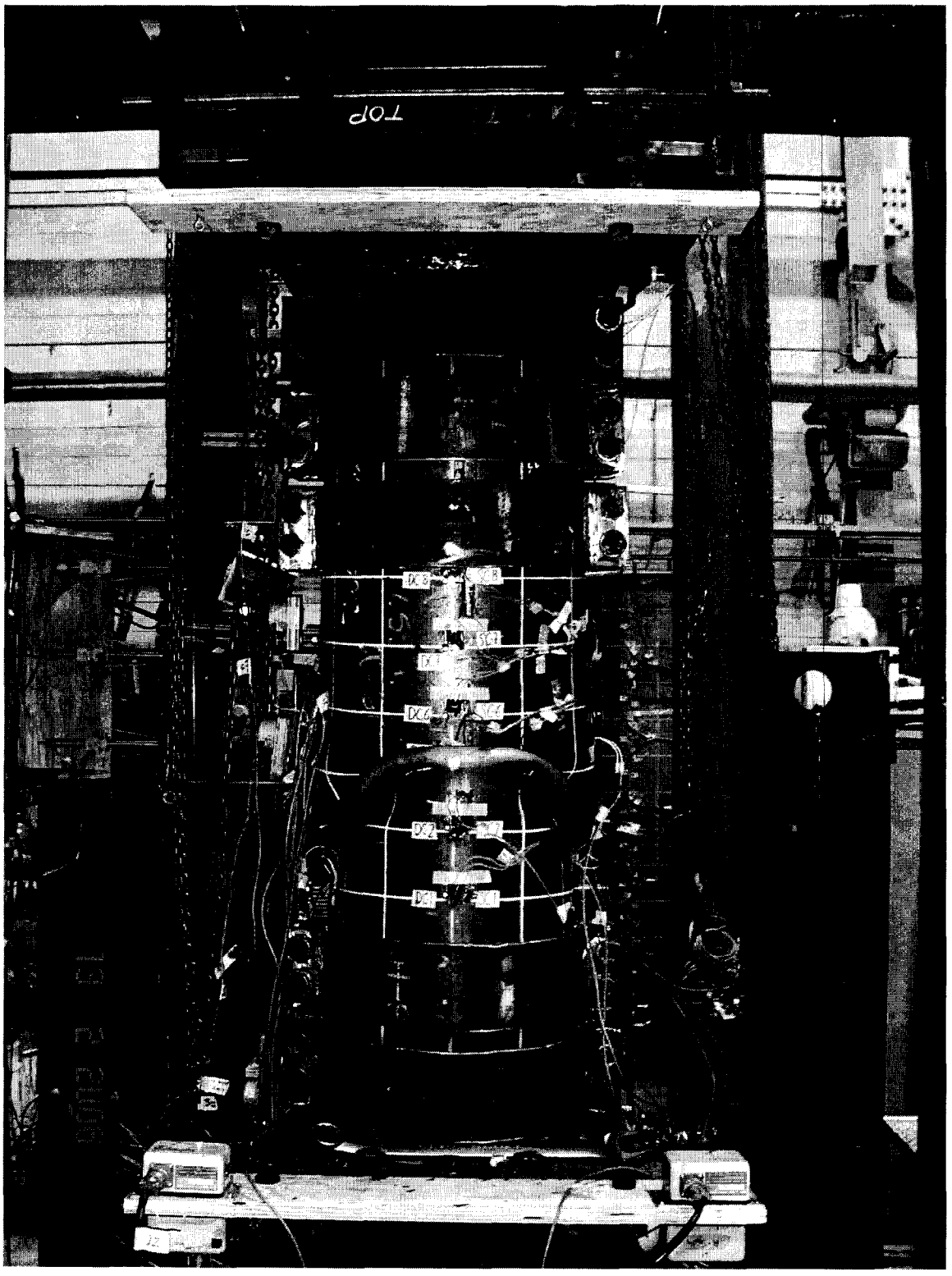

Figure 4.15 Final shape of the Buckle D16P0A5-2, Compression (west) Side

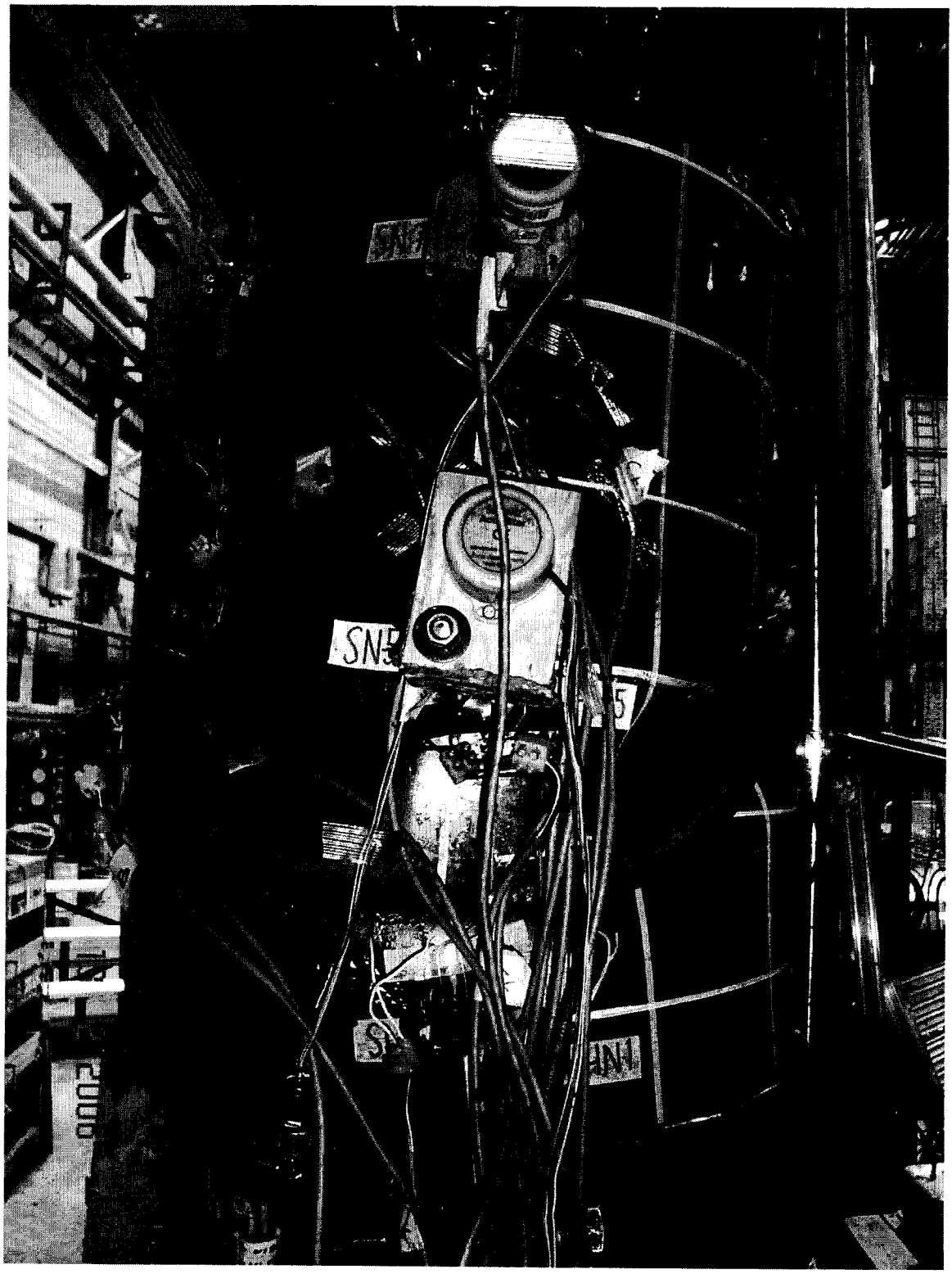

Figure 4.16 Final Shape of the Buckle D16P0A5-2, North Side

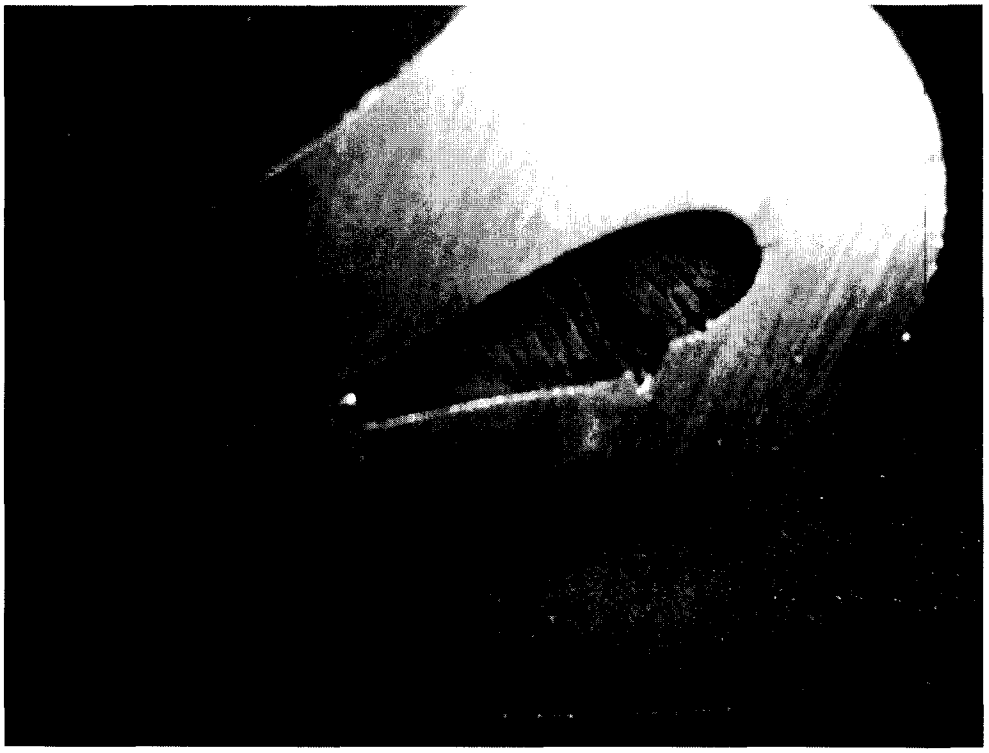

Figure 4.17 Cut Segment from Compression Side I, D16P0A5-2

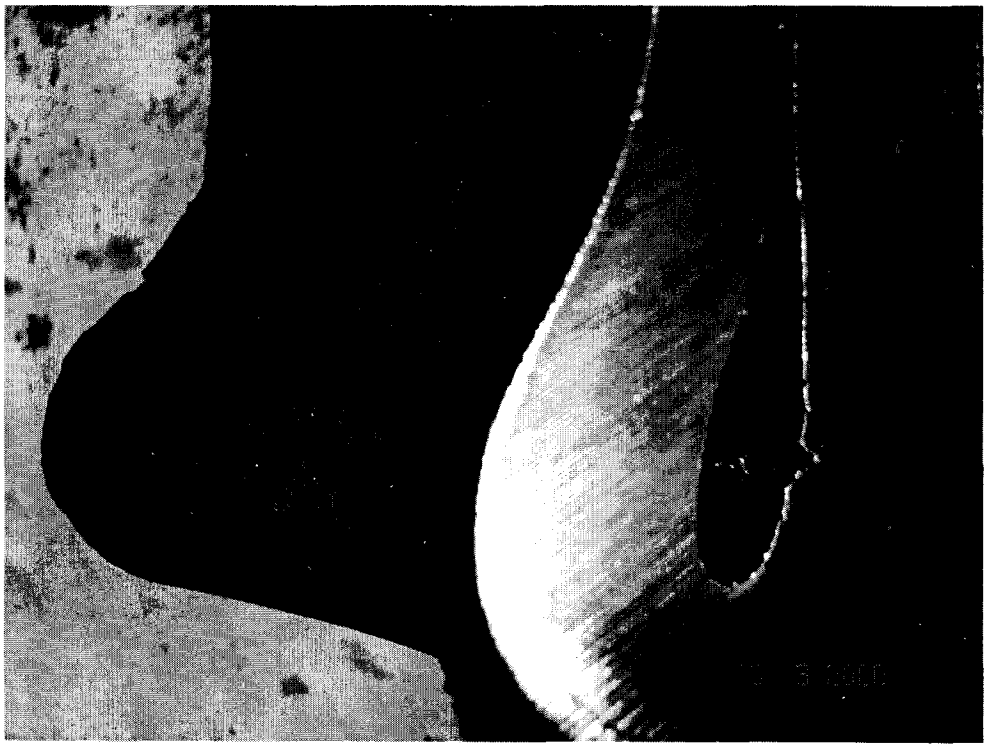

Figure 4.18 Cut Segment from Compression Side II, D16P0A5-2

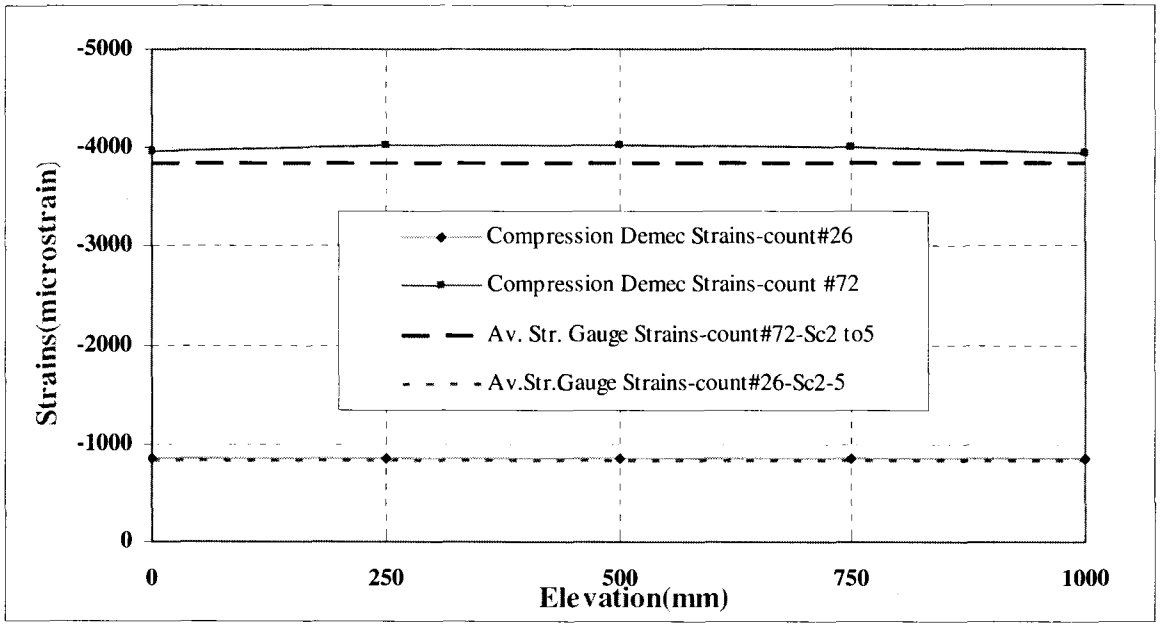

Figure 4.19 Comparisons between Demec Strain and Strain Gauge Strain D16P0A5-2

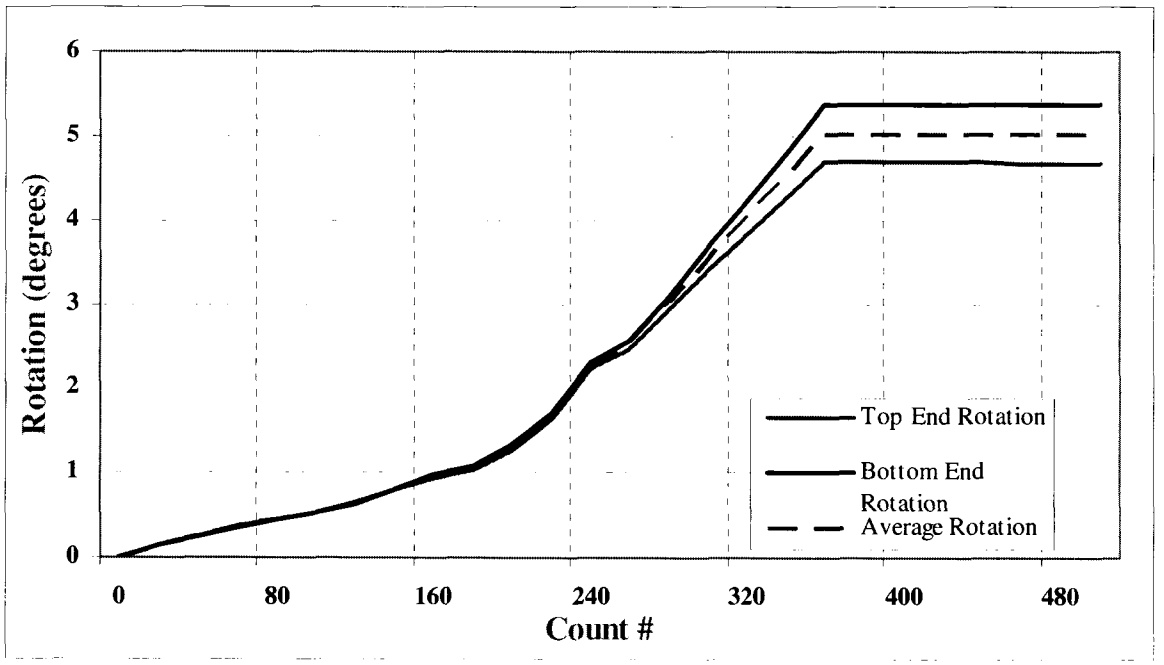

Figure 4.20 Variation of the End Rotations D16P0A5-2

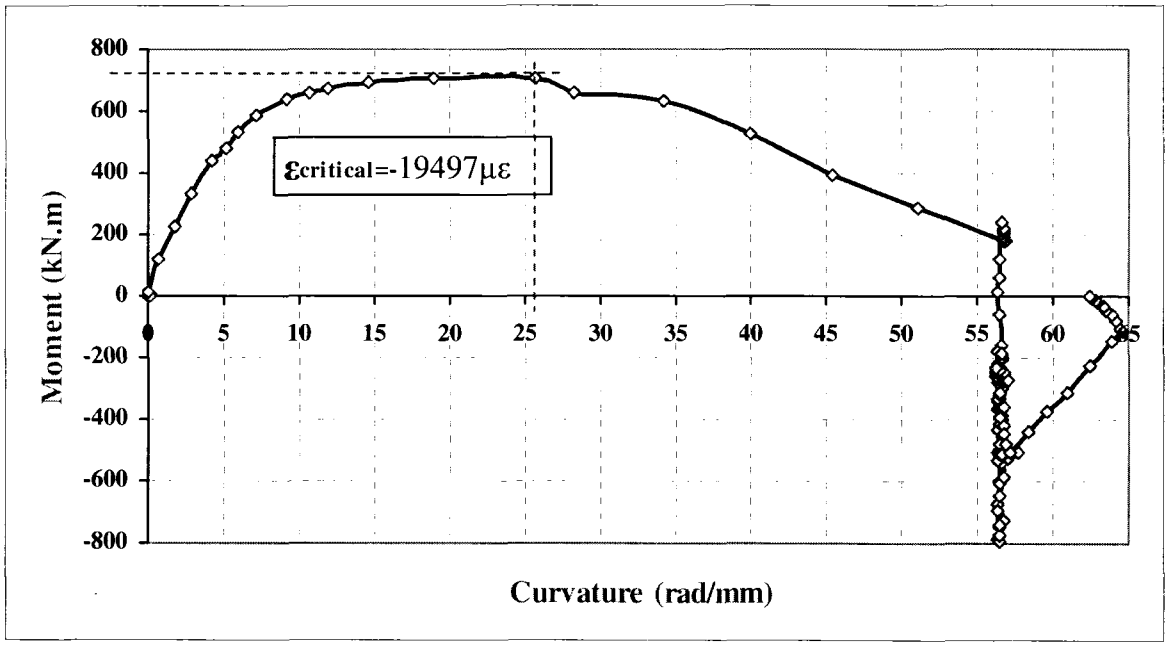

Figure 4.21 Average Global End Moment vs. Global Curvature D16P0A5-2

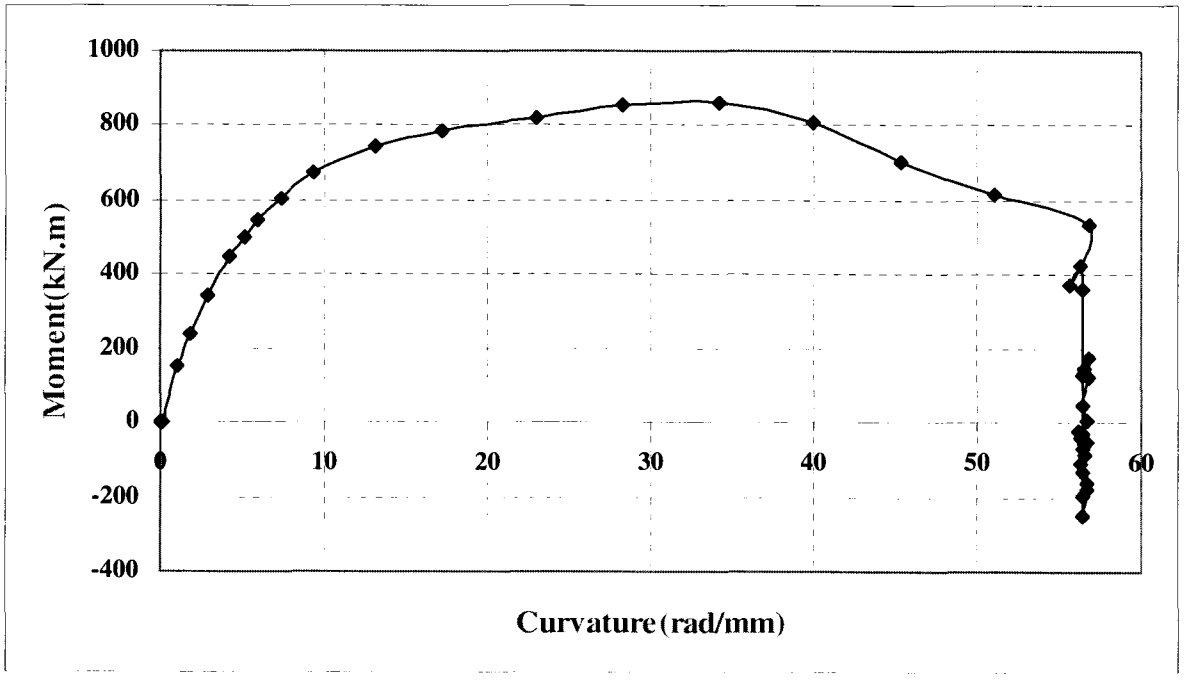

Figure 4.22 Local Moment vs. Global Curvature D16P0A5-2

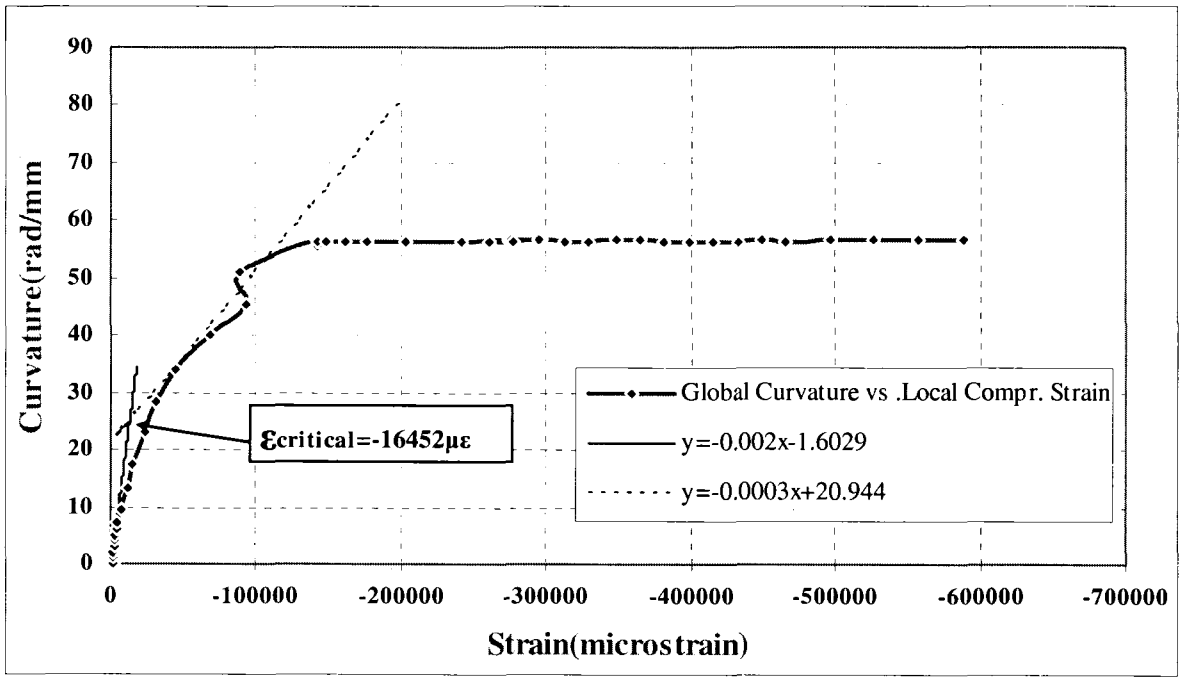

Figure 4.23 Global Curvature vs. Local Compression Strain D16P0A5-2

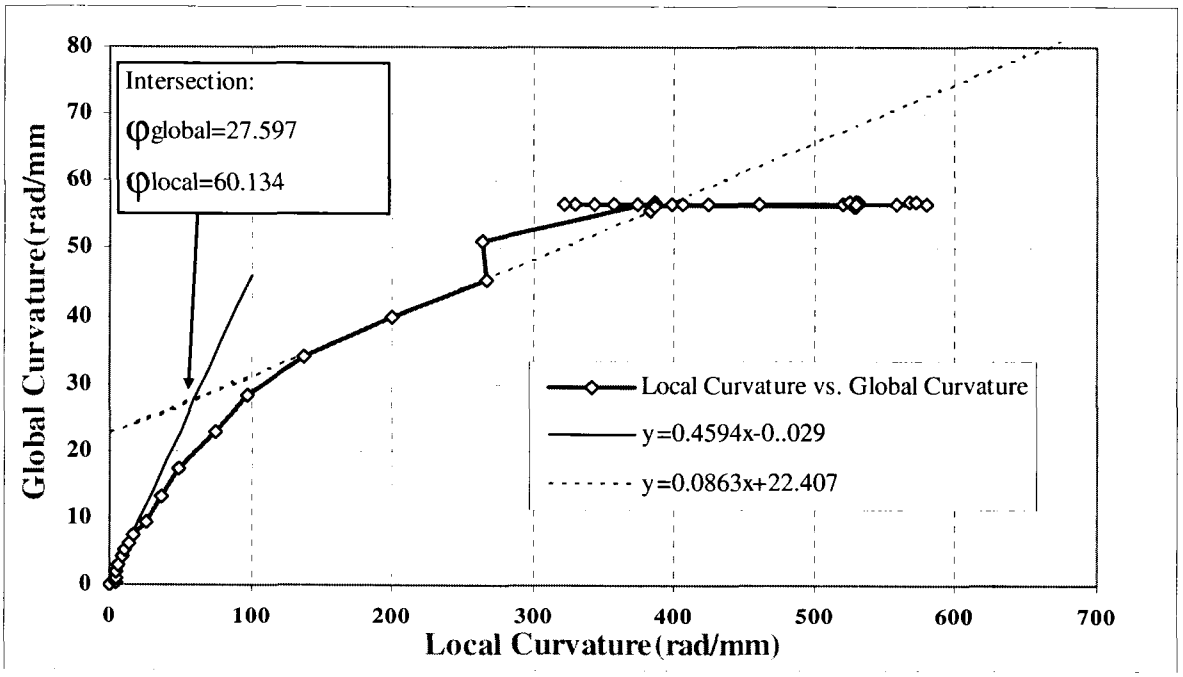

Figure 4.24 Global Curvature vs. Local Curvature D16P0A5-2

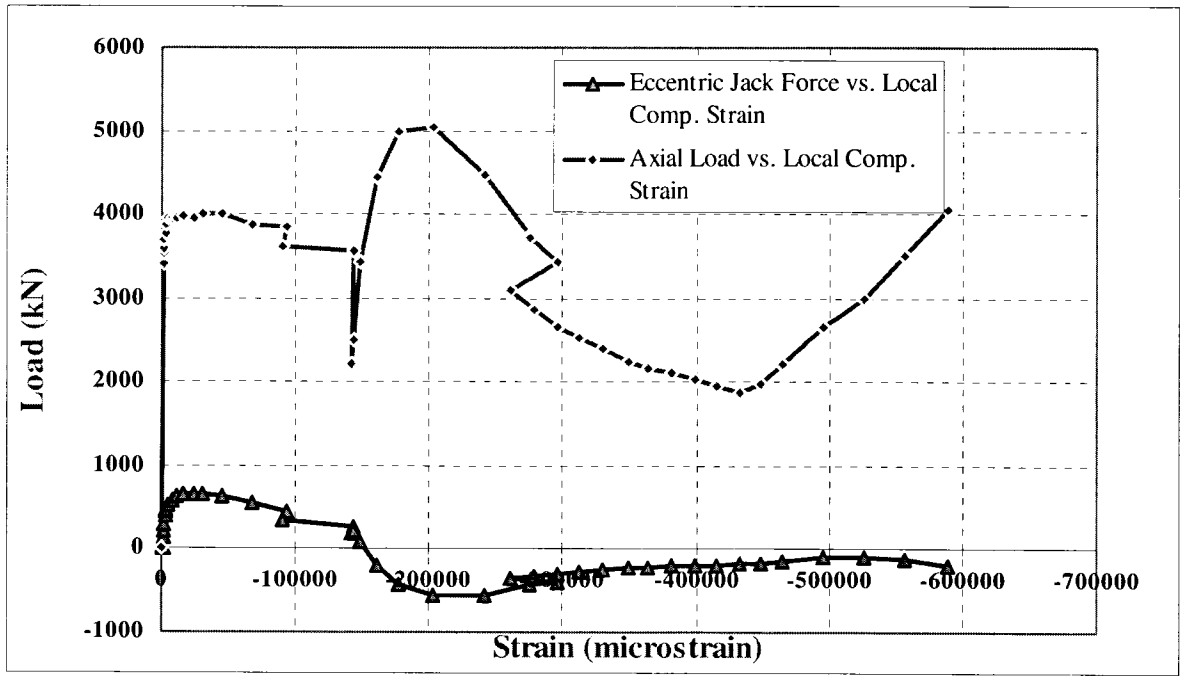

Figure 4.25 Load vs. Local Compressive Strain D16P0A5-2

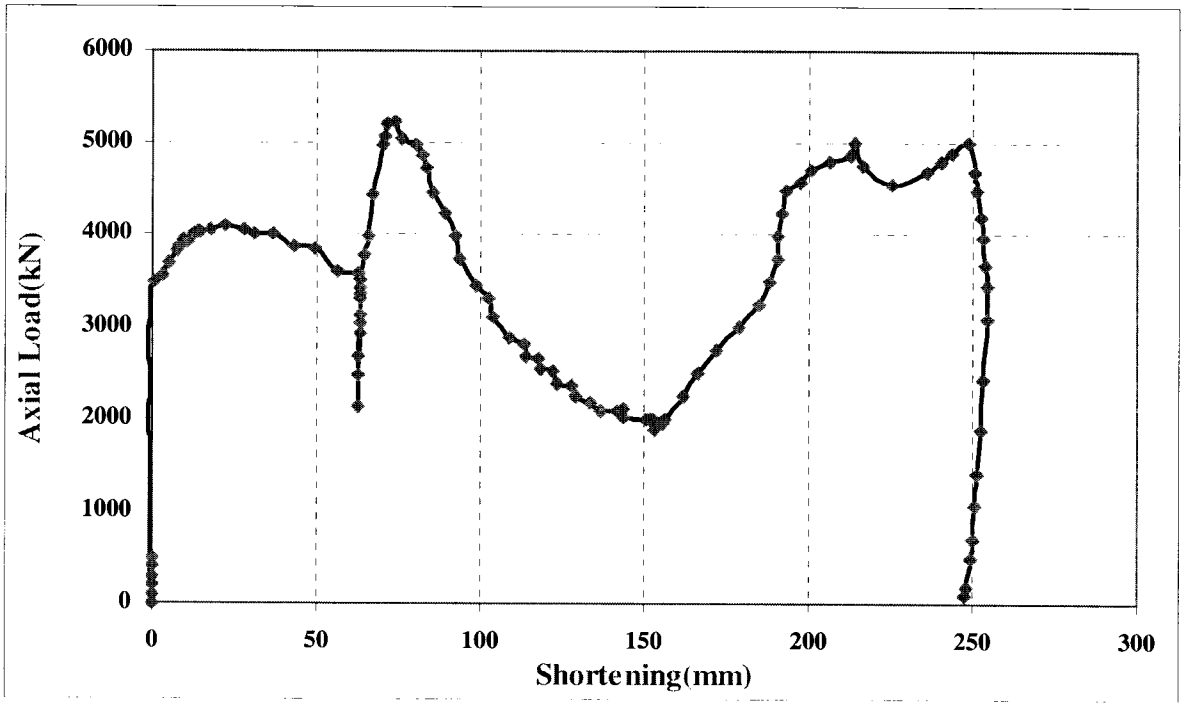

Figure 4.26 Axial Load vs. Shortening D16P0A5-2

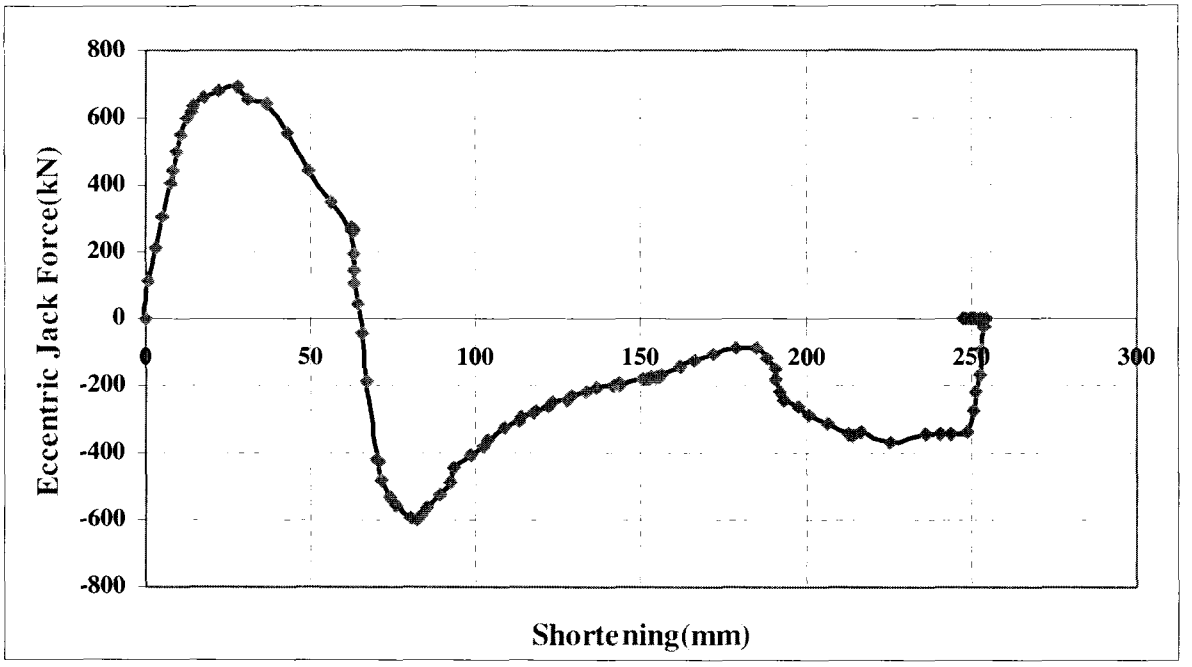

Figure 4.27 Eccentric Jack Load vs. Shortening D16P0A5-2

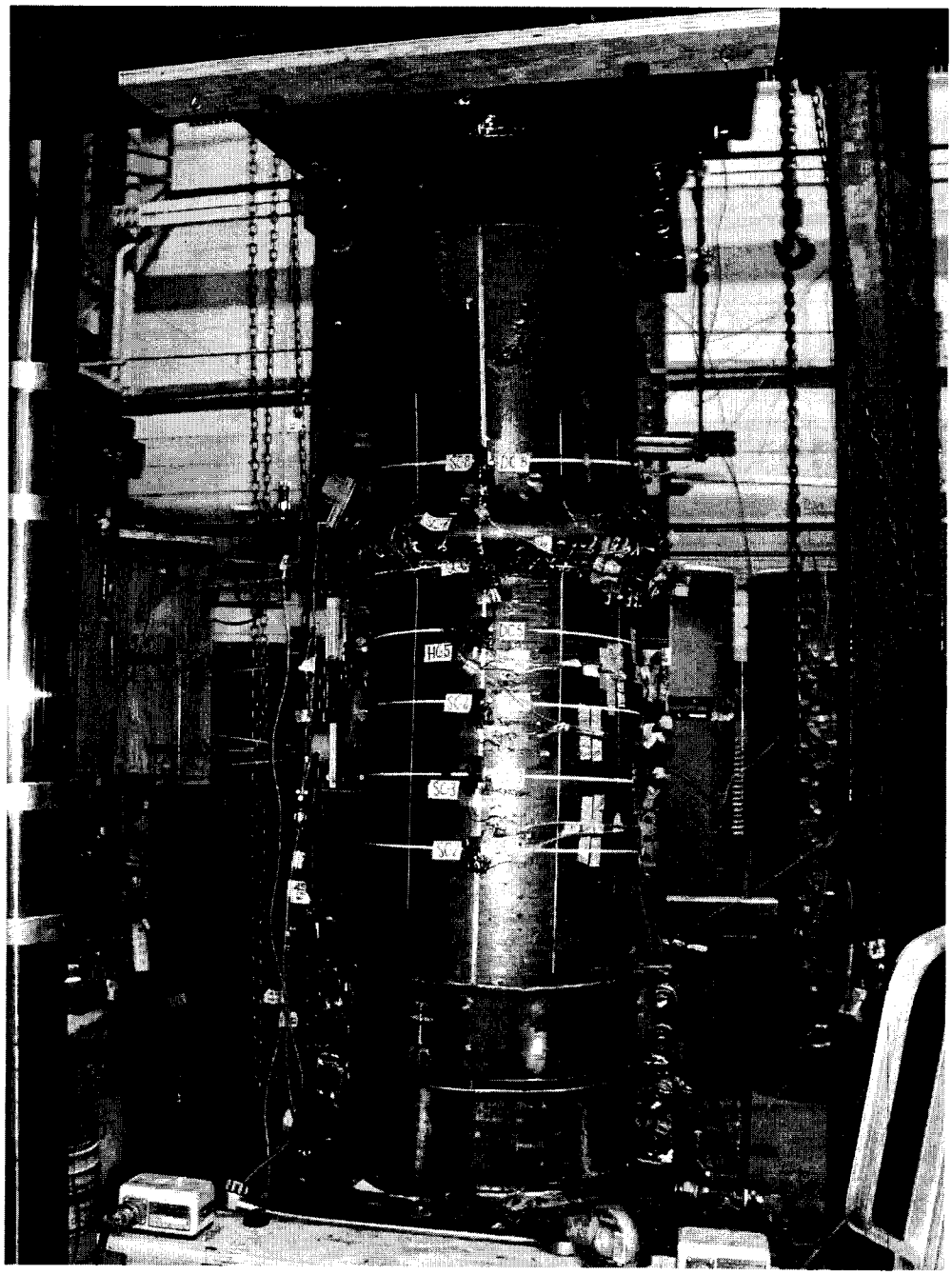

Figure 4.28 Initial Buckle Position D16P40A7-3

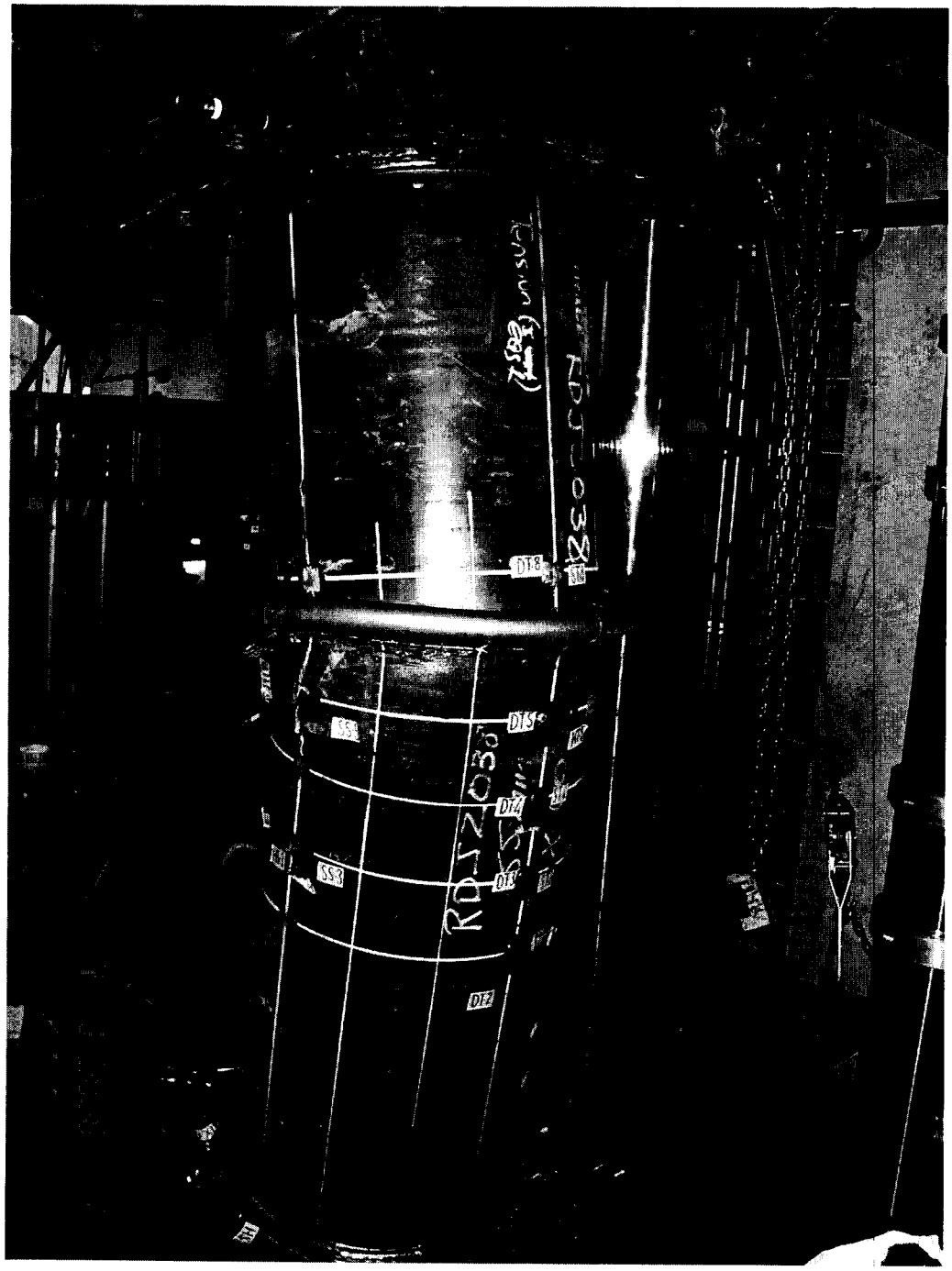

Figure 4.29 Final Shape of the Buckle D16P40A7-3

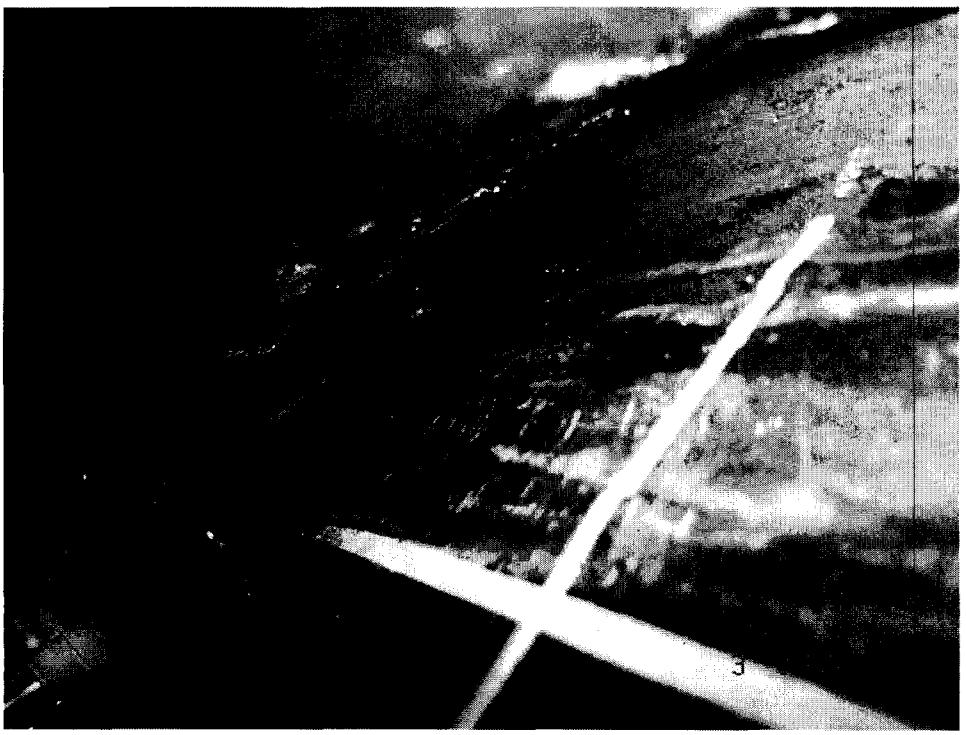

Figure 4.30 Initial Crack D16P40A7-3

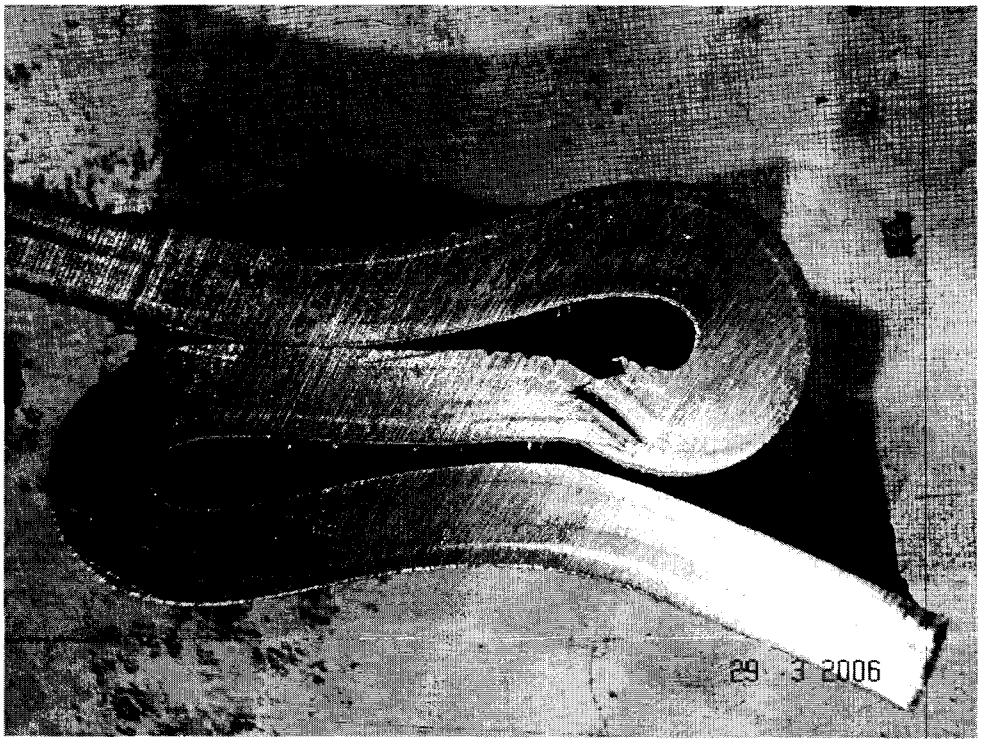

Figure 4.31 Cut Segment D16P40A7-3, Compression Side

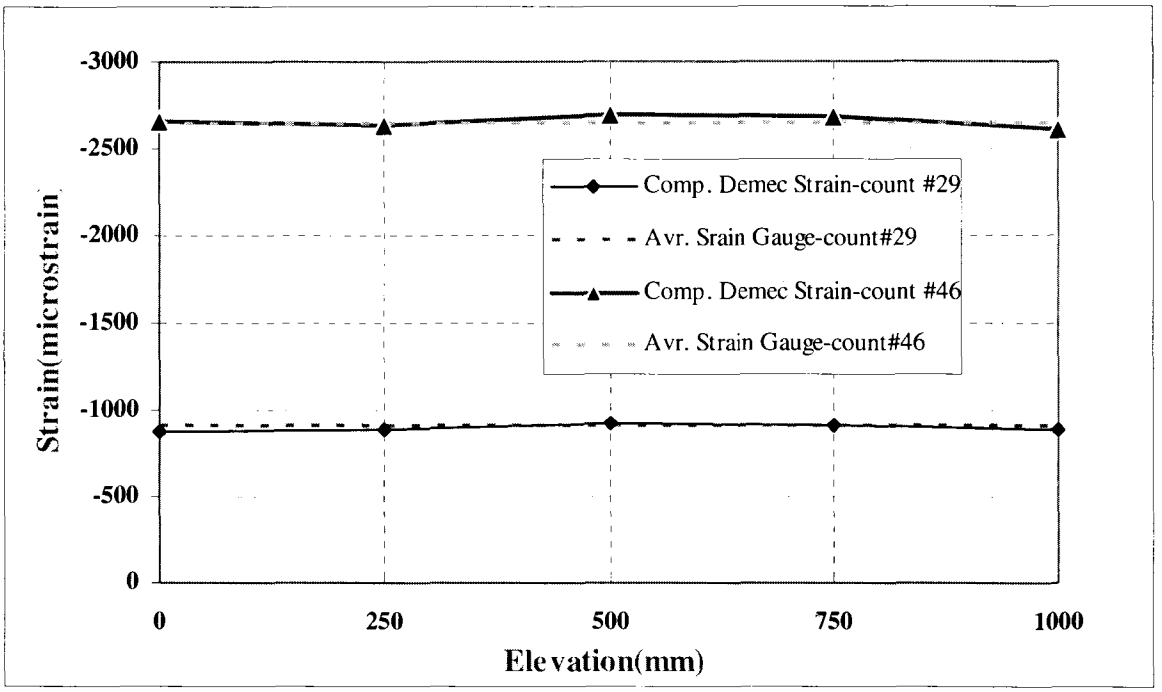

Figure 4.32 Comparison between Demec Strain and Strain Gauge Strain D16P40A7-3

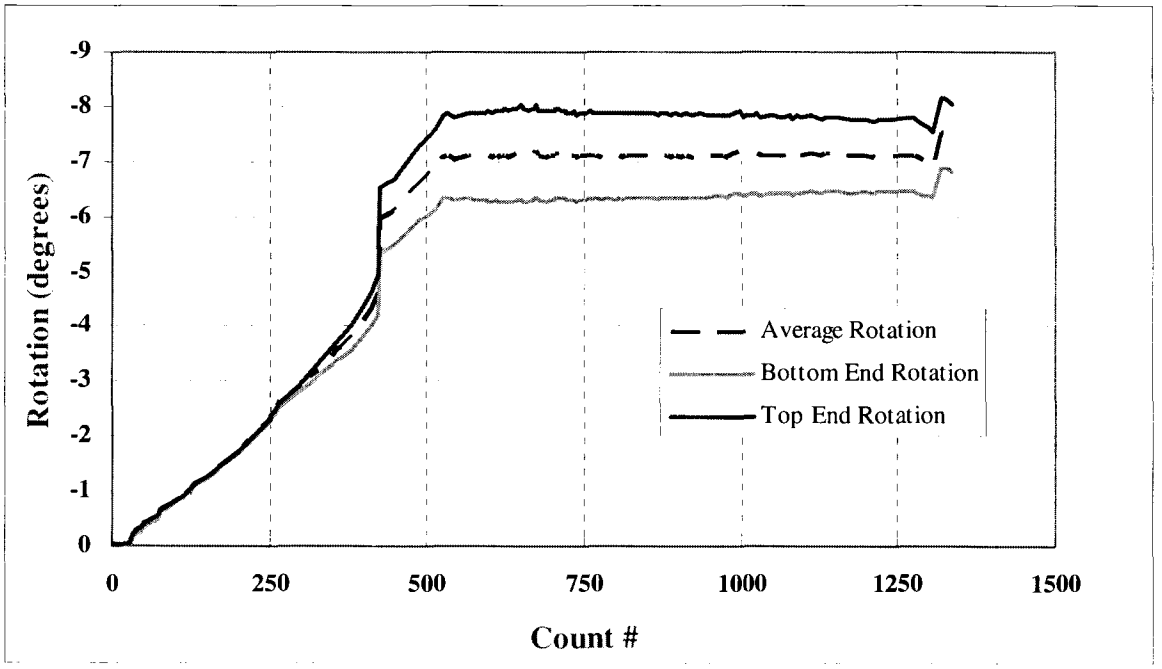

Figure 4.33 Variation of the End Rotations D16P40A7-3

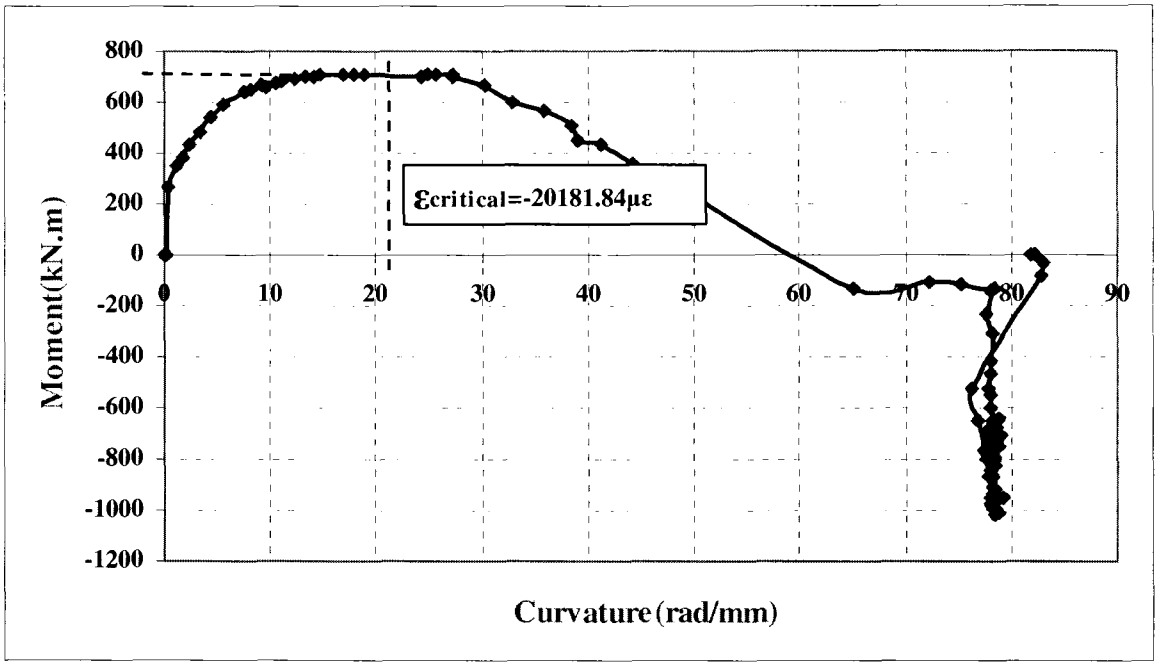

Figure 4.34 Average Global End Moment vs. Global Curvature D16P40A7-3

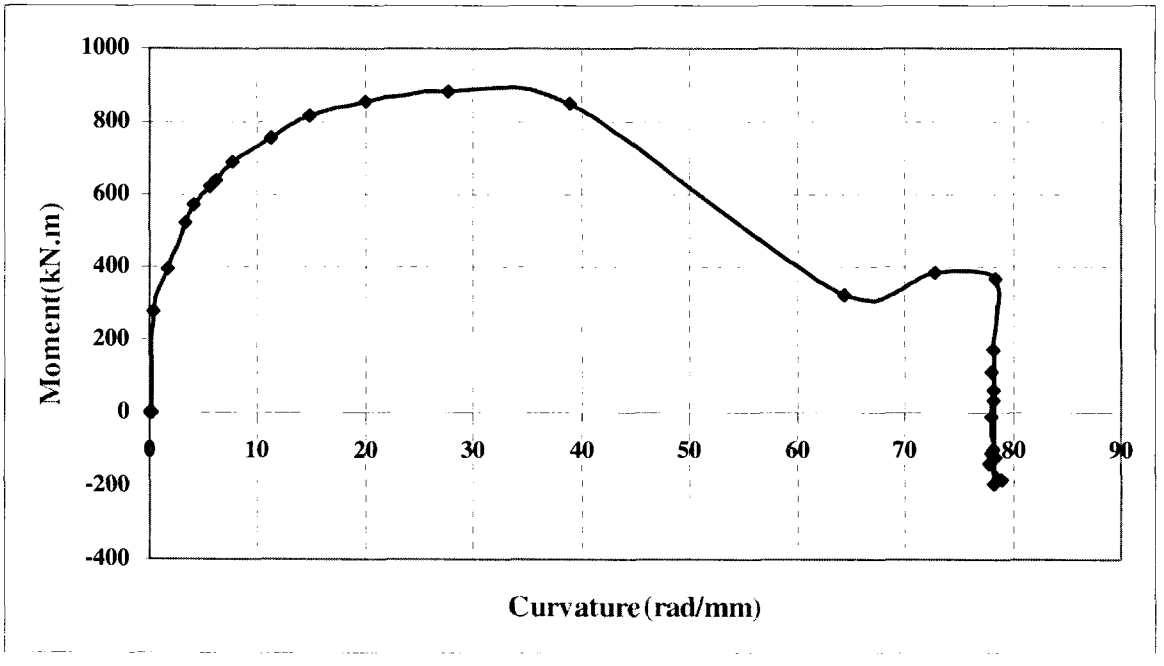

Figure 4.35 Local Moment vs. Global Curvature D16P40A7-3

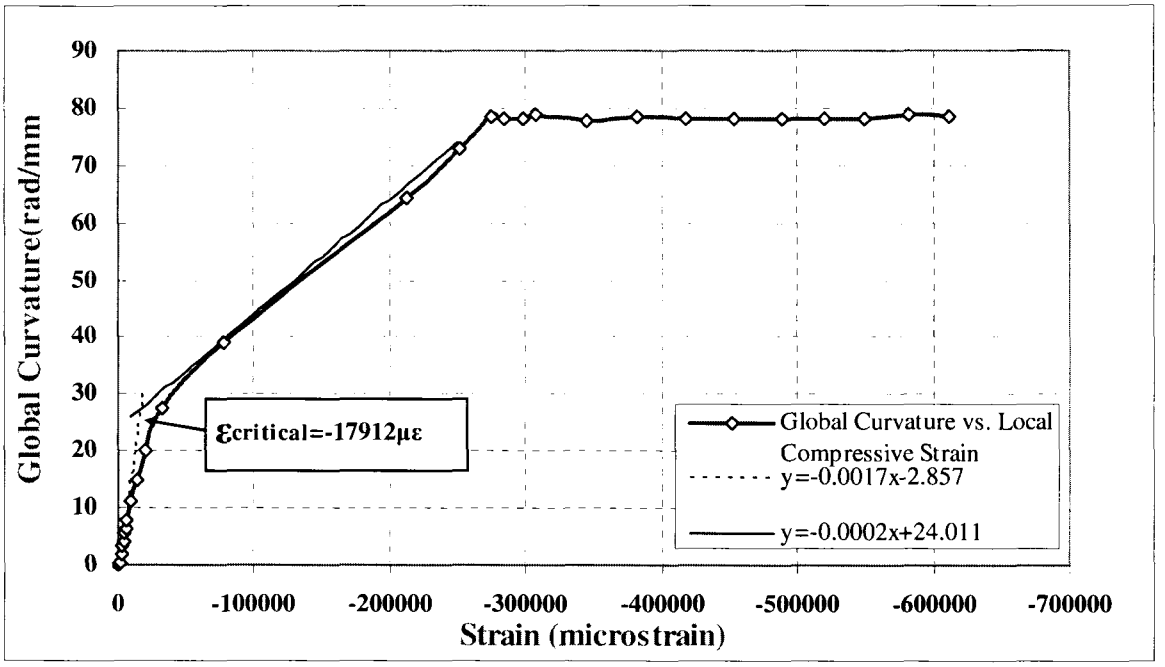

Figure 4.36 Global Curvature vs. Local Compressive Strain D16P40A7-3

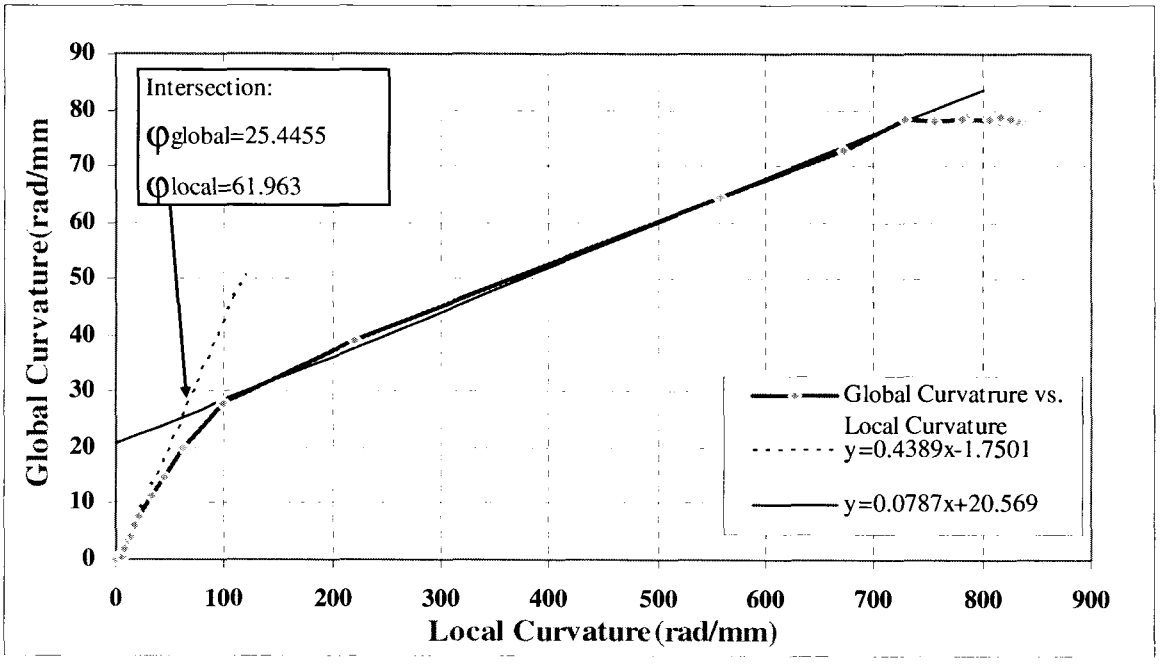

Figure 4.37 Global Curvature vs. Local Curvature D16P40A7-3

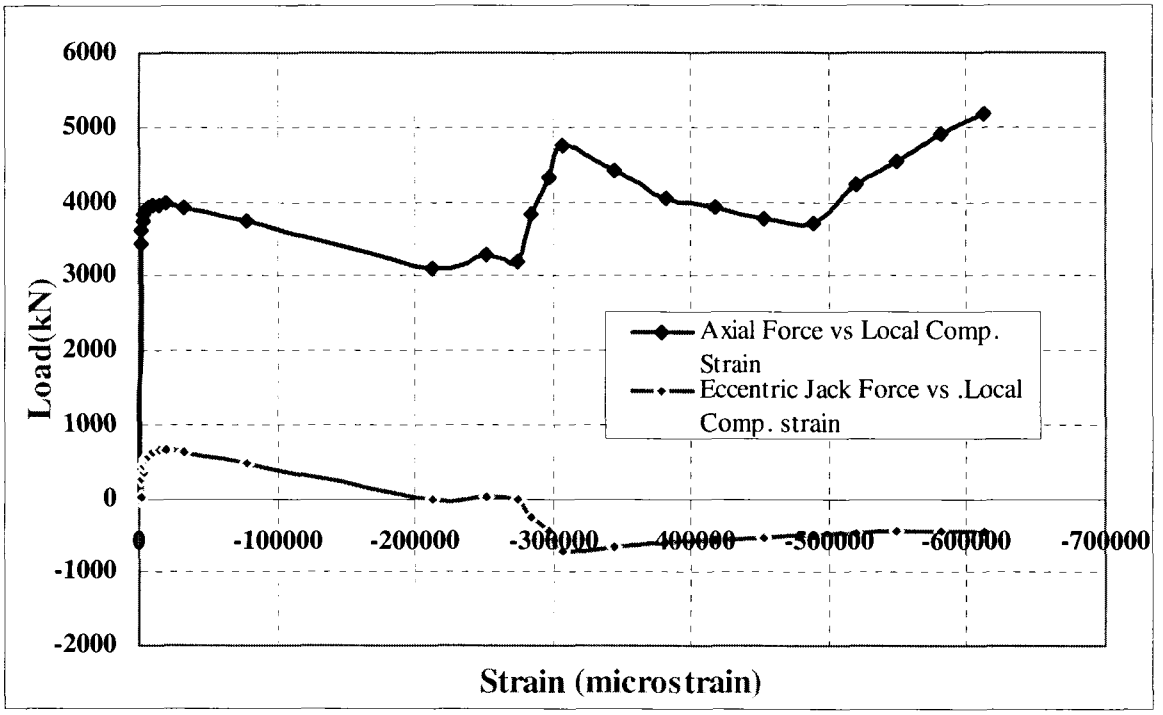

Figure 4.38 Load vs. Local Compressive Strain D16P40A7-3

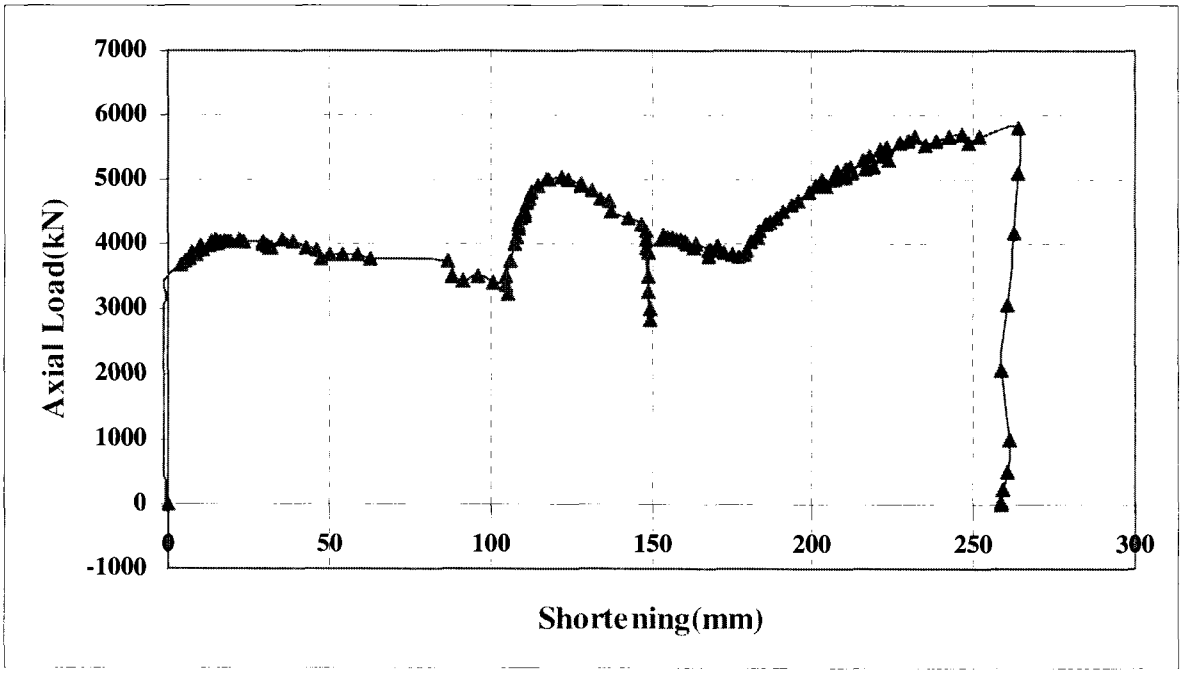

Figure 4.39 Axial Load vs. Shortening D16P40A7-3

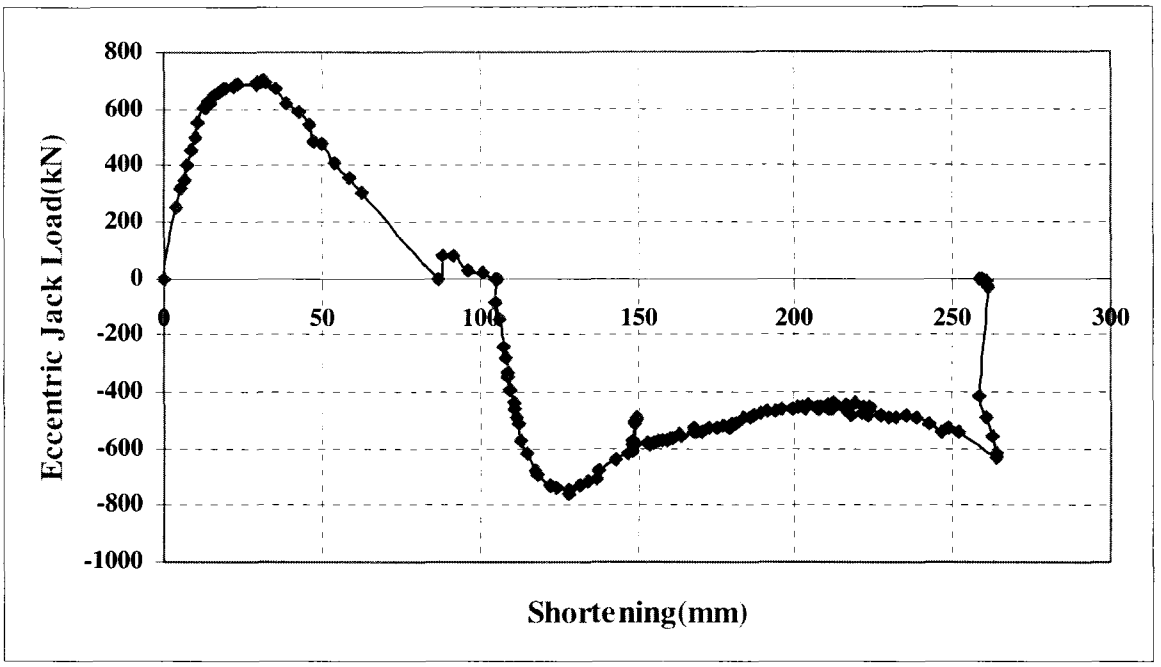

Figure 4.40 Eccentric Jack Load vs. Shortening D16P40A7-3

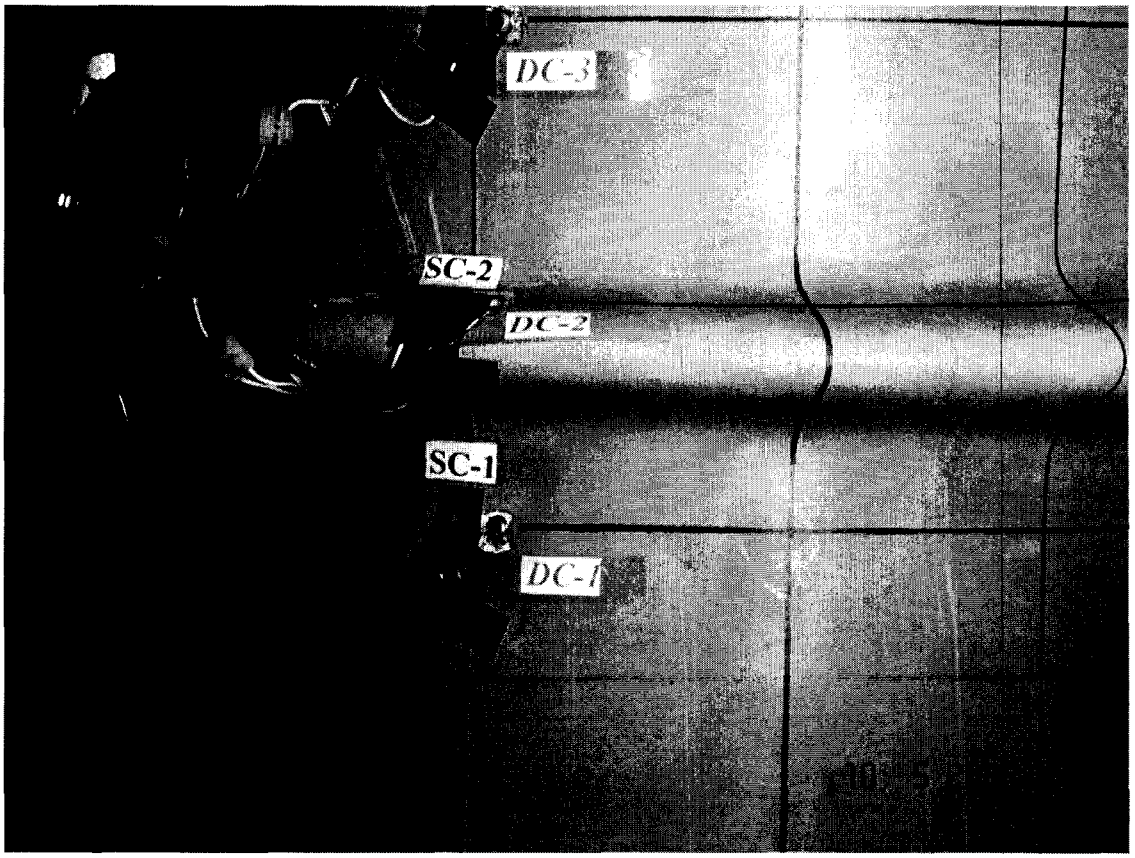

Figure 4.41 Initial Buckle Position D20P40A3.5-4

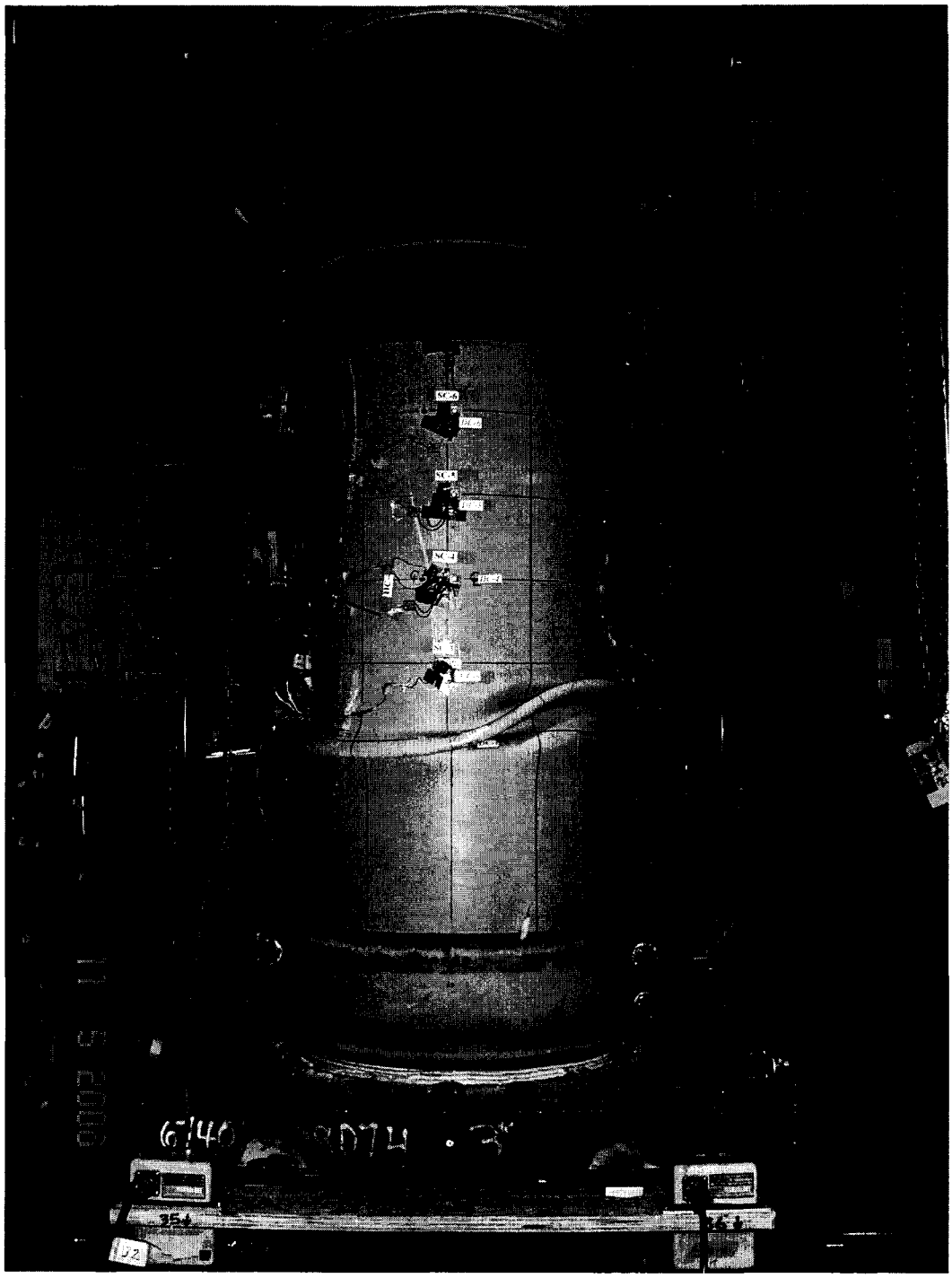

Figure 4.42 Final Shape of the Buckle D20P40A3.5-4

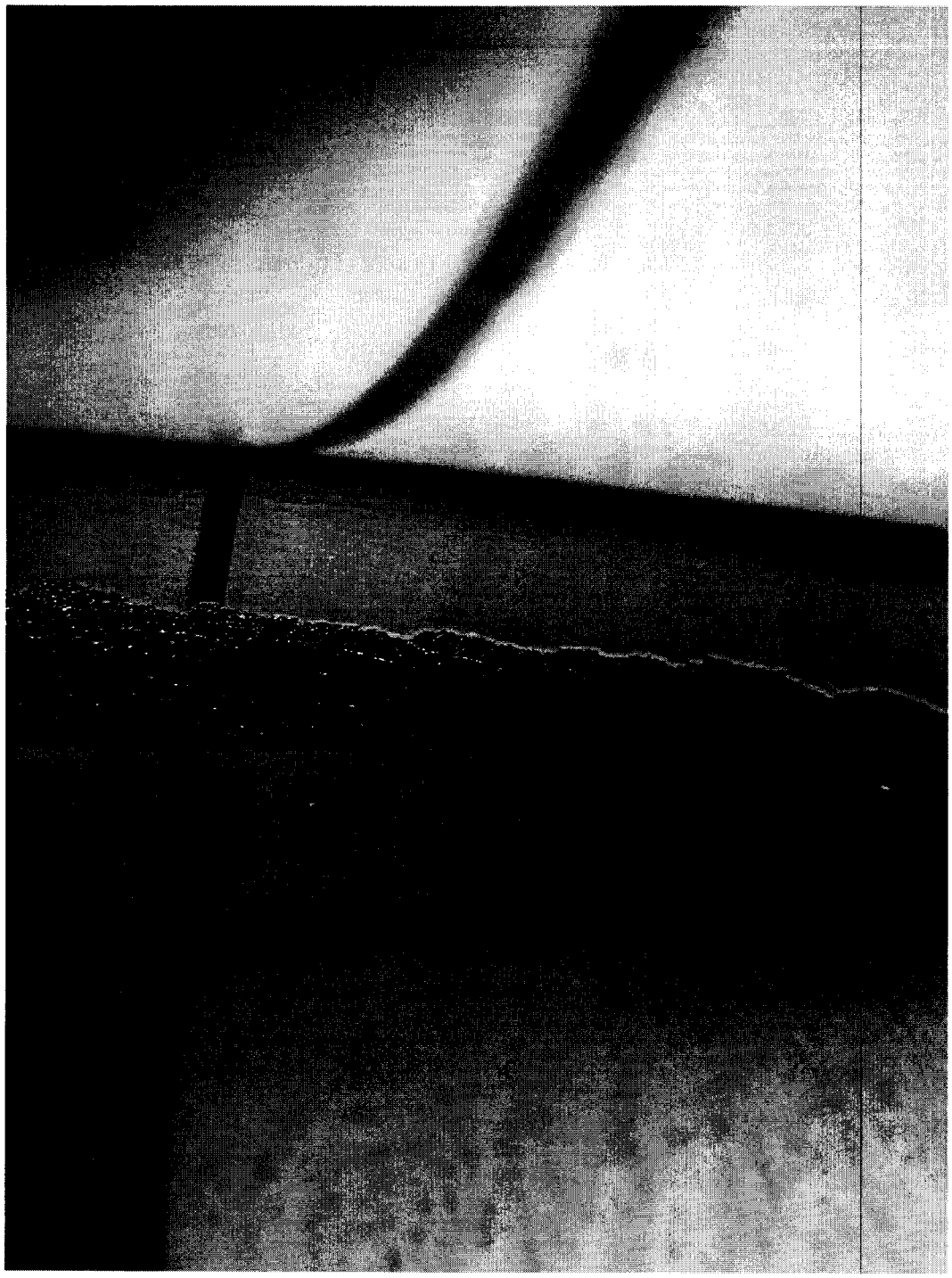

Figure 4.43 Initial Crack D20P40A3.5-4

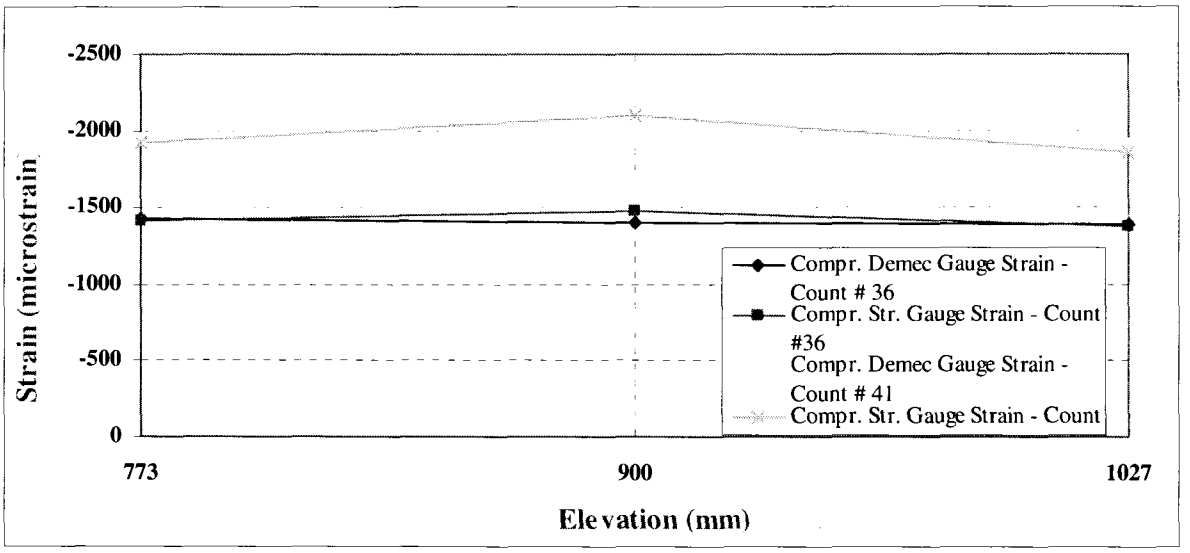

Figure 4.44 Comparison between Demec Strain and Strain Gauge Strain D20P40A3.5-4

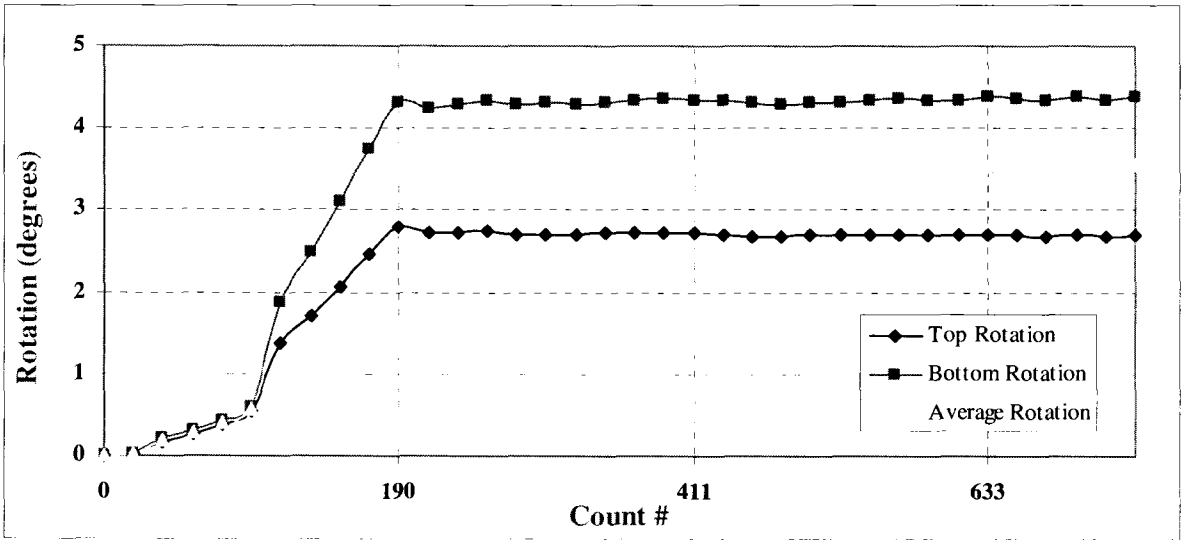

Figure 4.45 Variation of the End Rotations D20P40A3.5-4

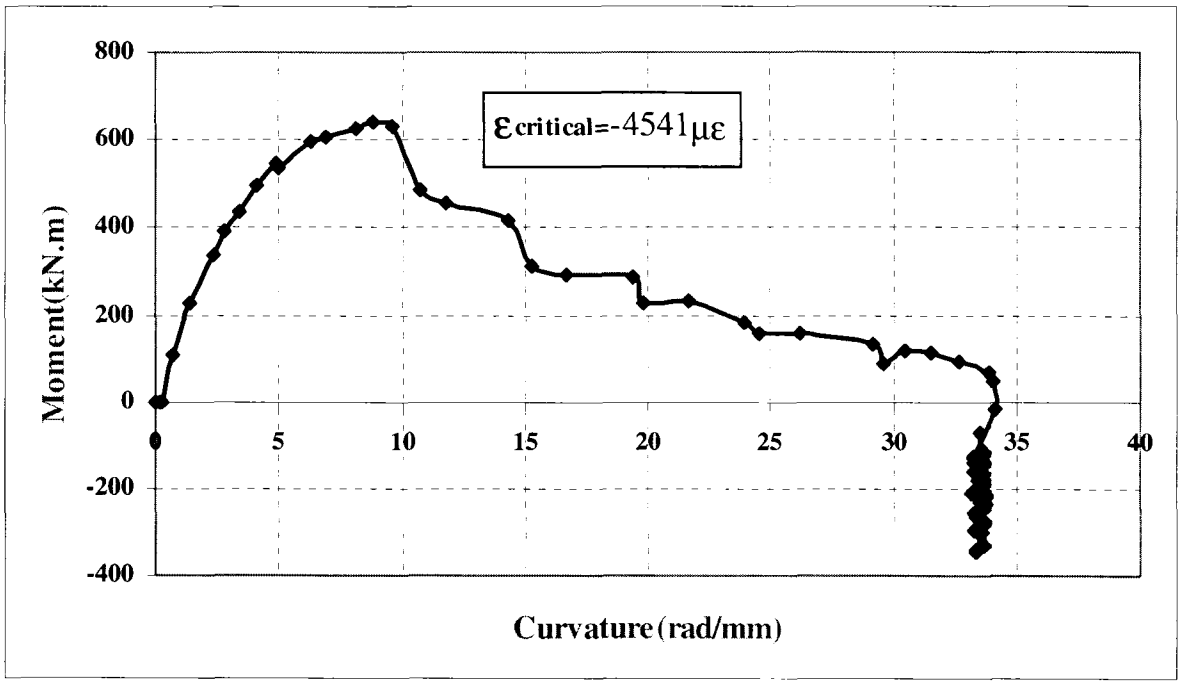

Figure 4.46 Average Global End Moment vs. Global Curvature D20P40A3.5-4

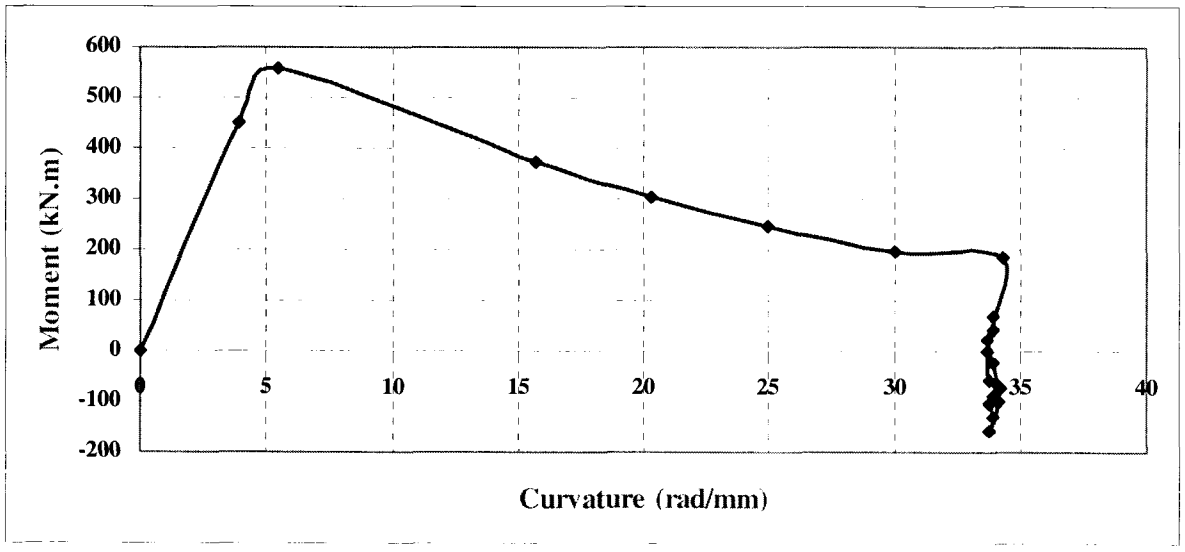

Figure 4.47 Local Moment vs. Global Curvature D20P40A3.5-4

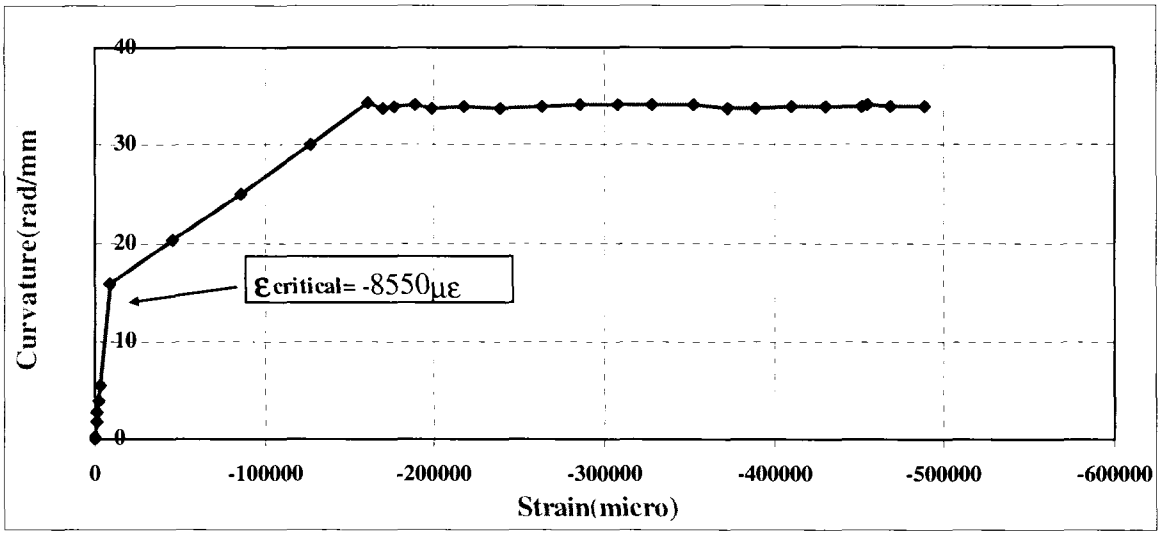

Figure 4.48 Global Curvature vs. Local Compressive Strain D20P40A3.5-4

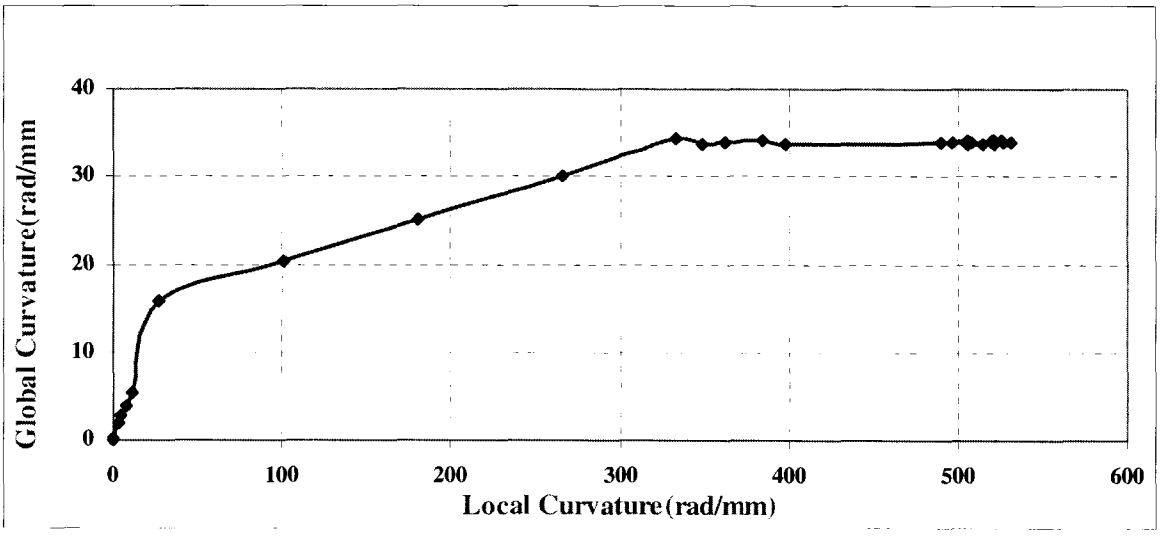

Figure 4.49 Global Curvature vs. Local Curvature D20P40A3.5-4

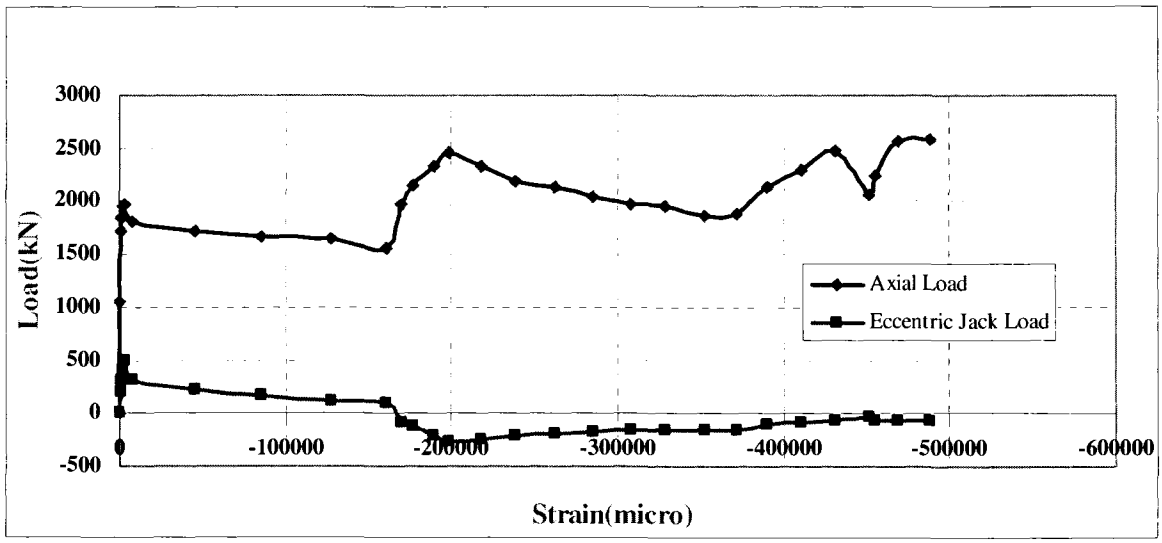

Figure 4.50 Load vs. Local Compressive Strain D20P40A3.5-4

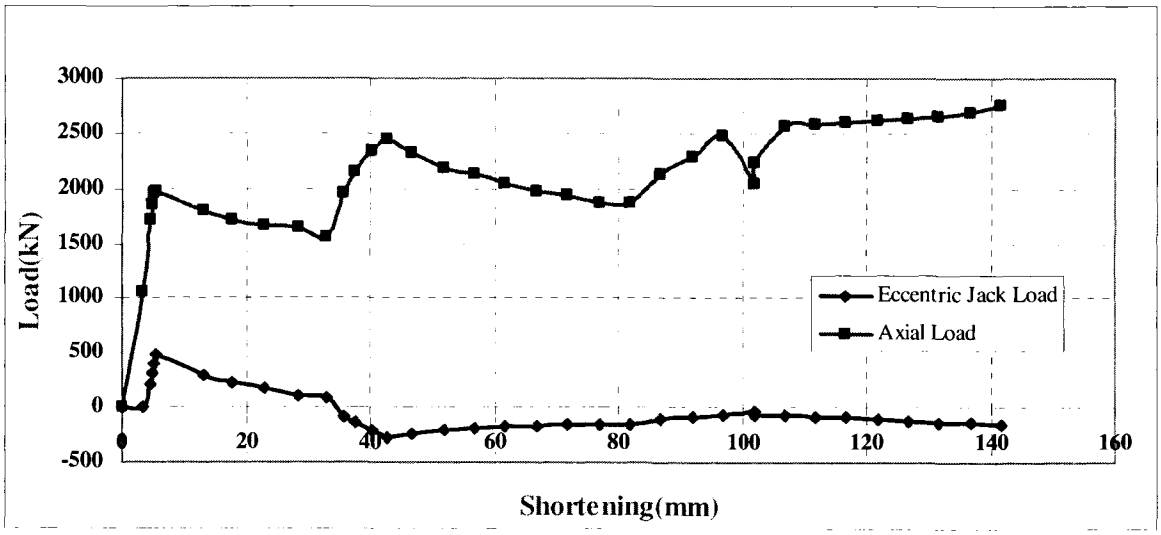

Figure 4.51 Load vs. Shortening D20P40A3.5-4

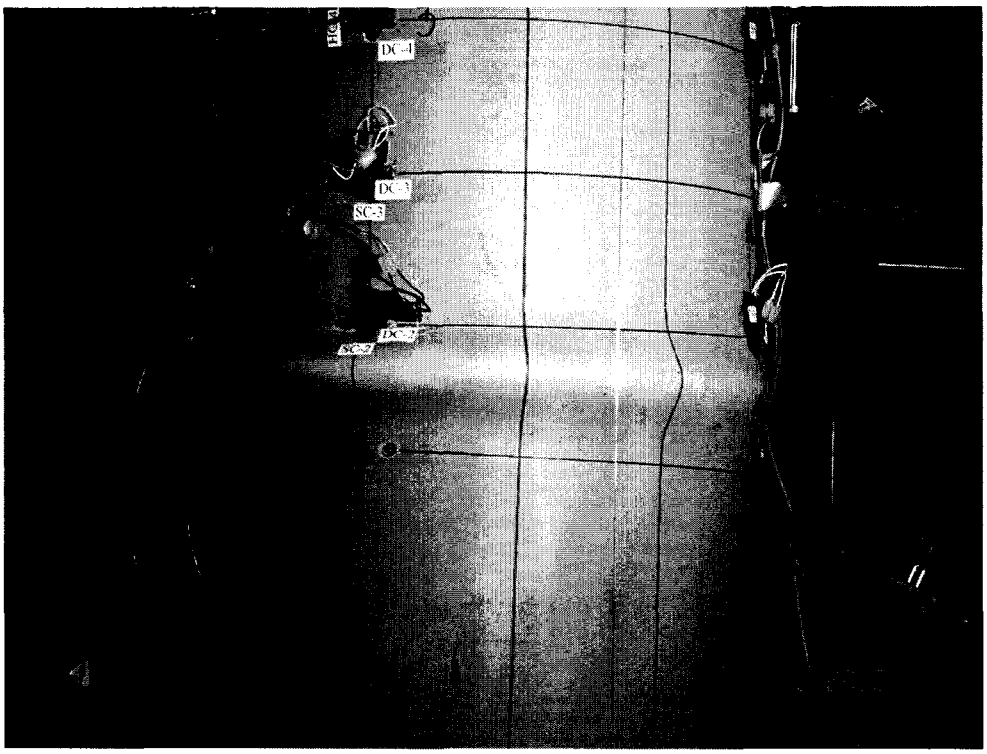

Figure 4.52 Initial Buckle Position D20P0A5-5

Figure 4.53 Final Shape of the Buckle D20P0A5-5

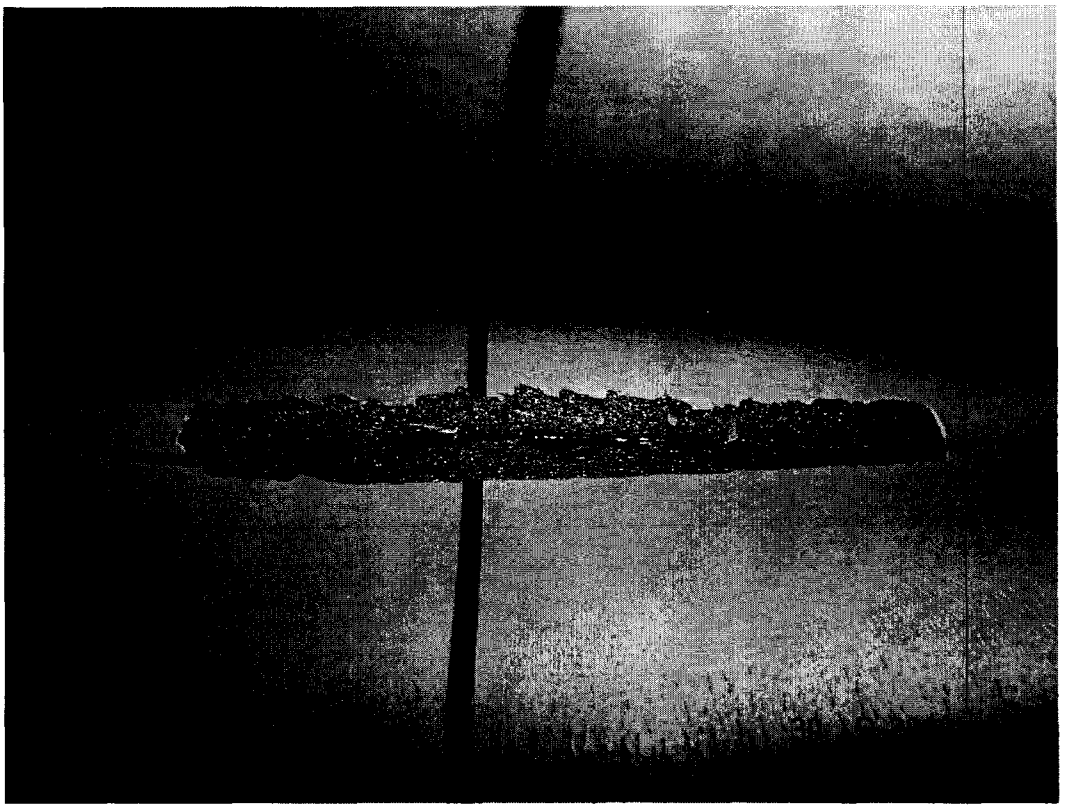

Figure 4.54 Initial Crack D20P0A5-5

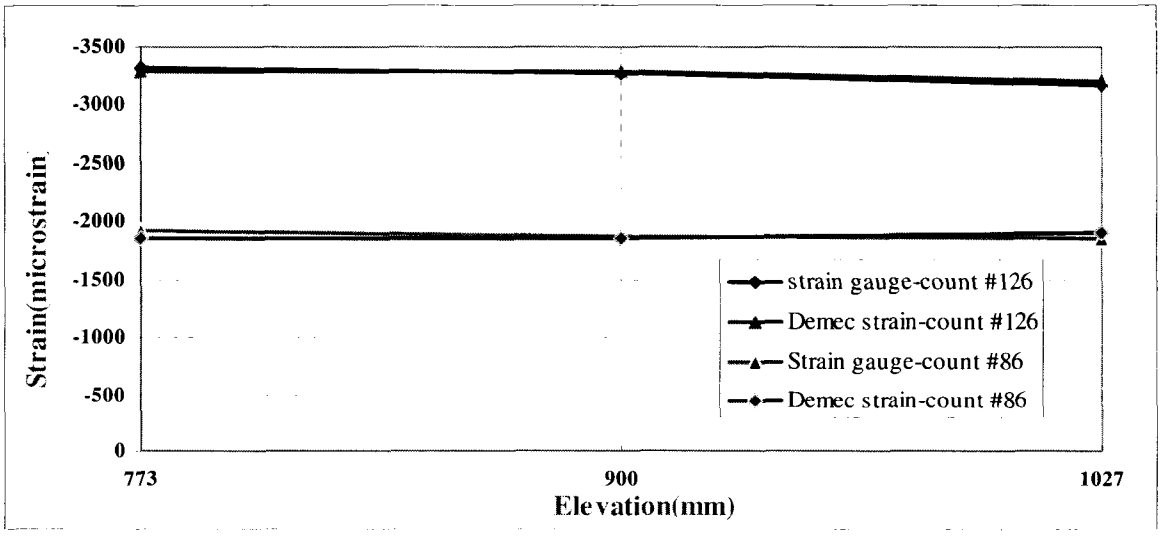

Figure 4.55 Comparison between Demec Strain and Strain Gauge Strain D20P0A5-5

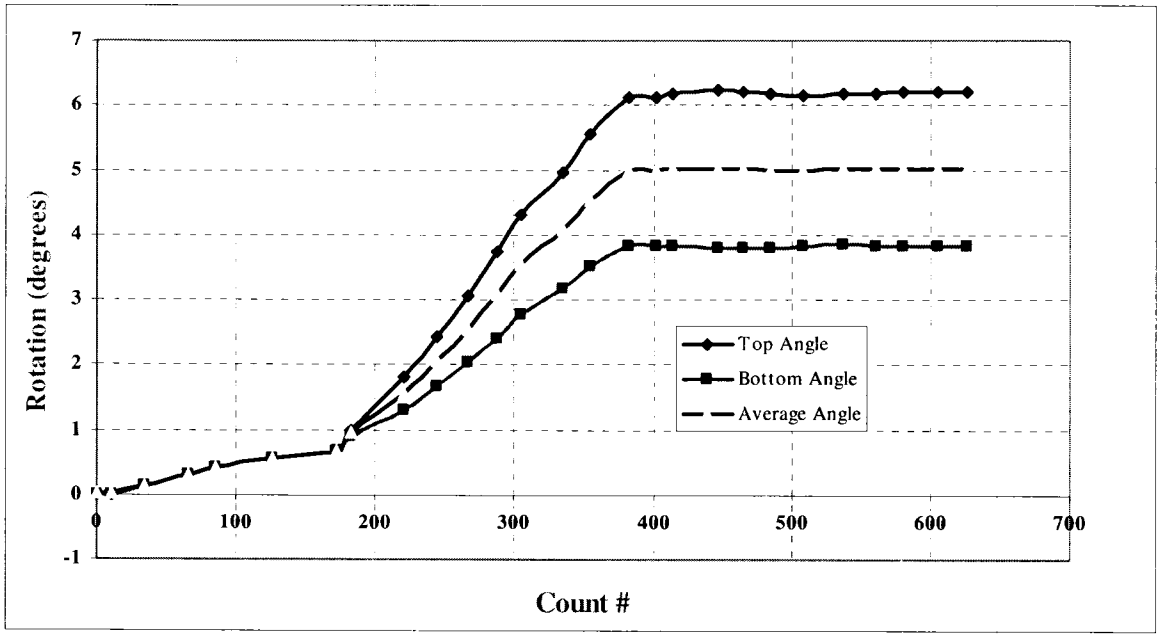

Figure 4.56 Variation of the End Rotations D20P0A5-5

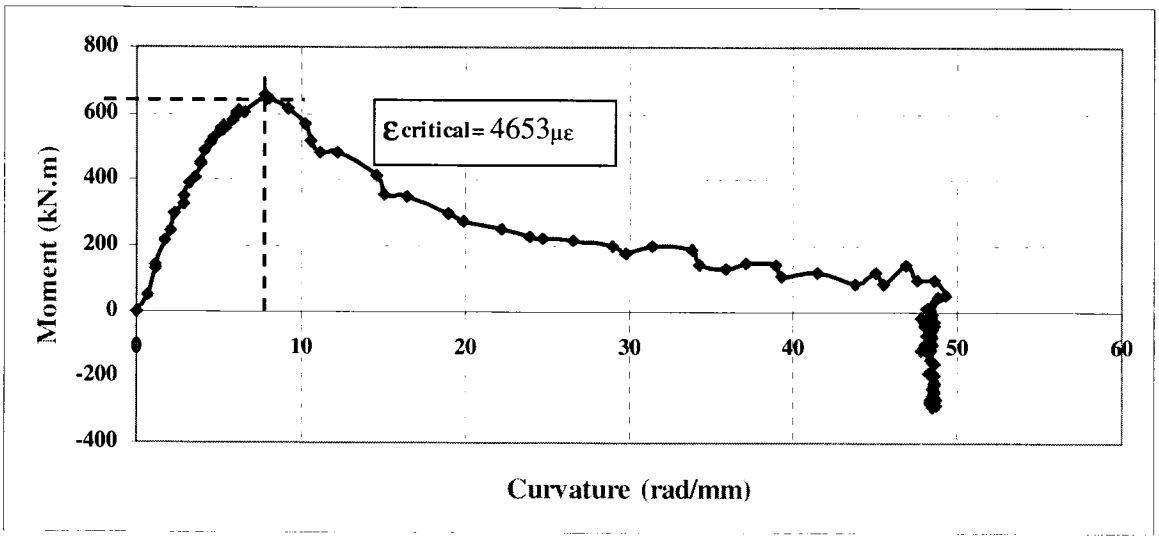

Figure 4.57 Average Global End Moment vs. Global Curvature D20P0A5-5

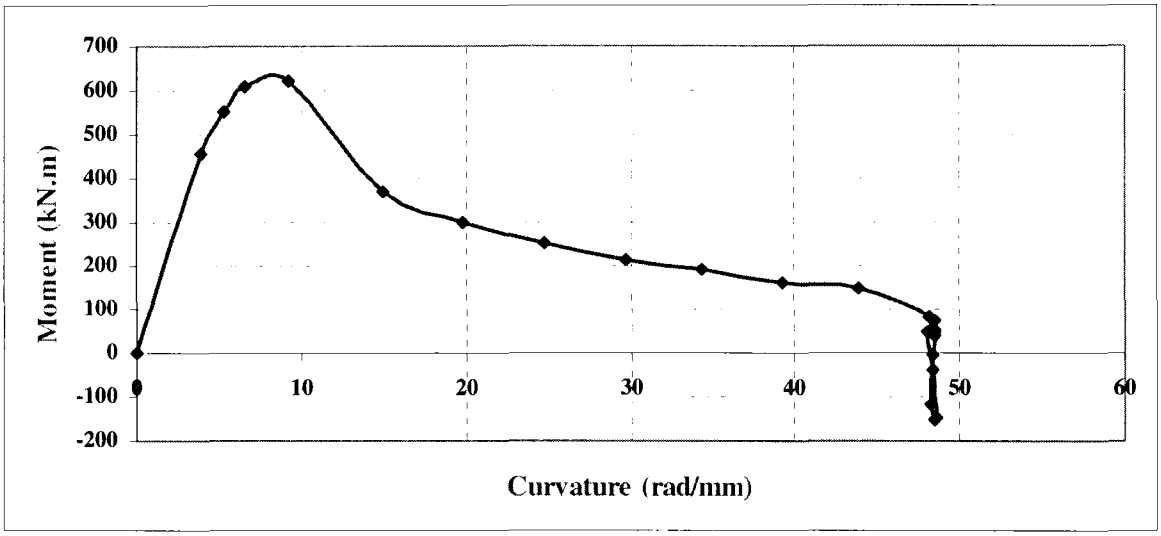

Figure 4.58 Local Moment vs. Global Curvature D20P0A5-5

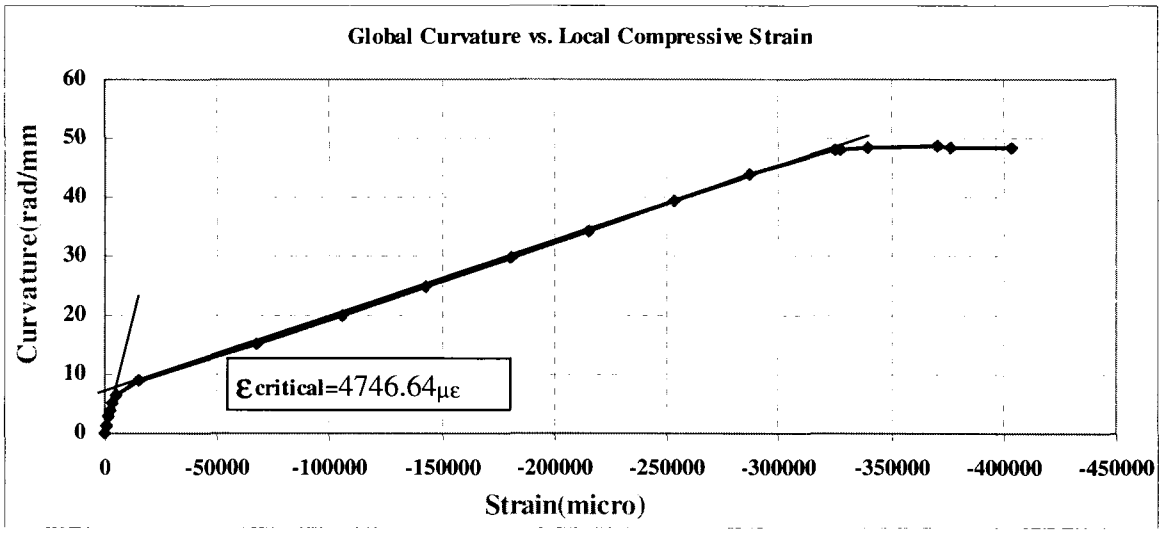

Figure 4.59 Global Curvature vs. Local Compressive Strain D20P0A5-5

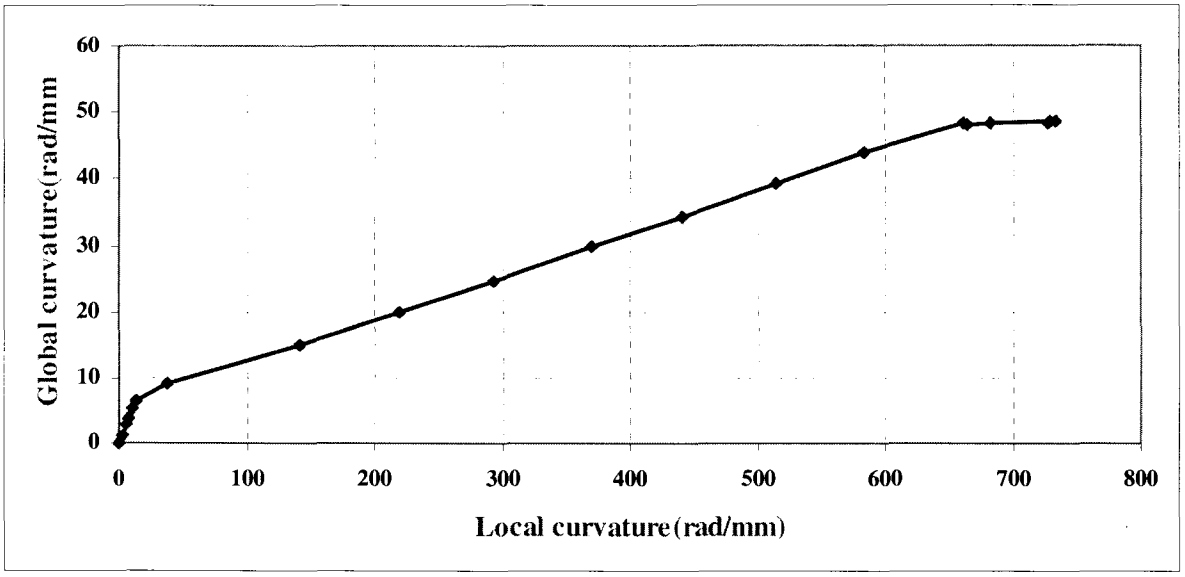

Figure 4.60 Global Curvature vs. Local Curvature D20P0A5-5

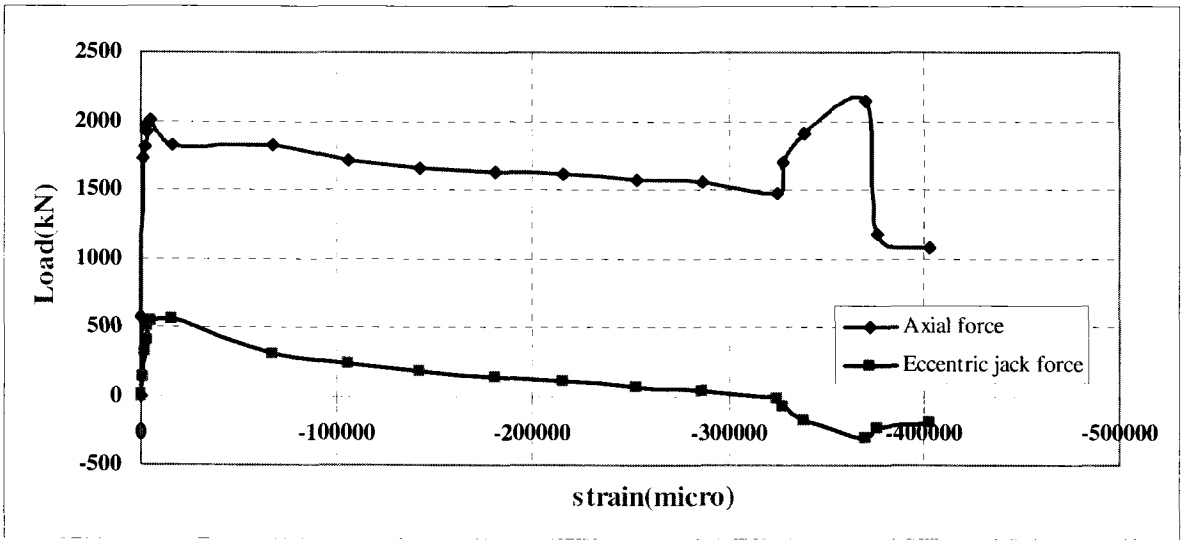

Figure 4.61 Load vs. Local Compressive Strain D20P0A5-5

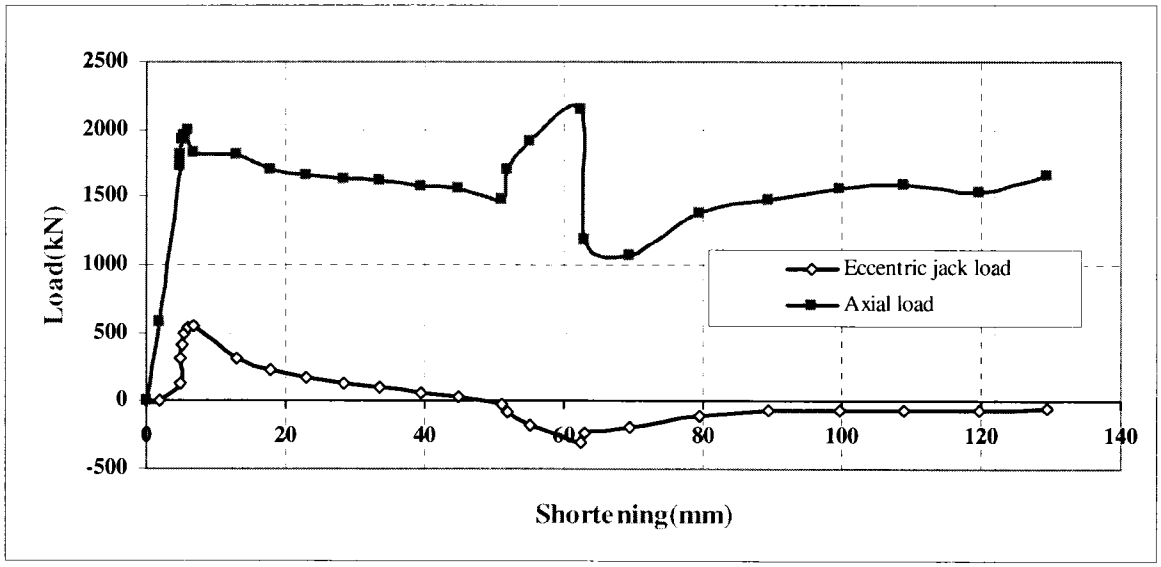

Figure 4.62 Load vs. Shortening D20P0A5-5

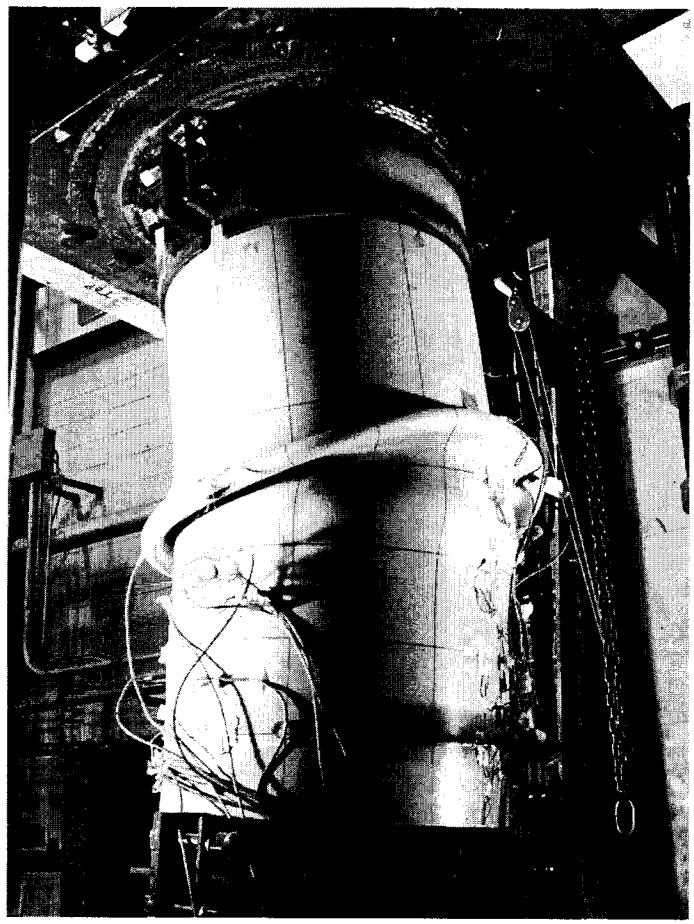

Figure 4.63 Final Shape of the Wrinkle D20P80A4.05-6

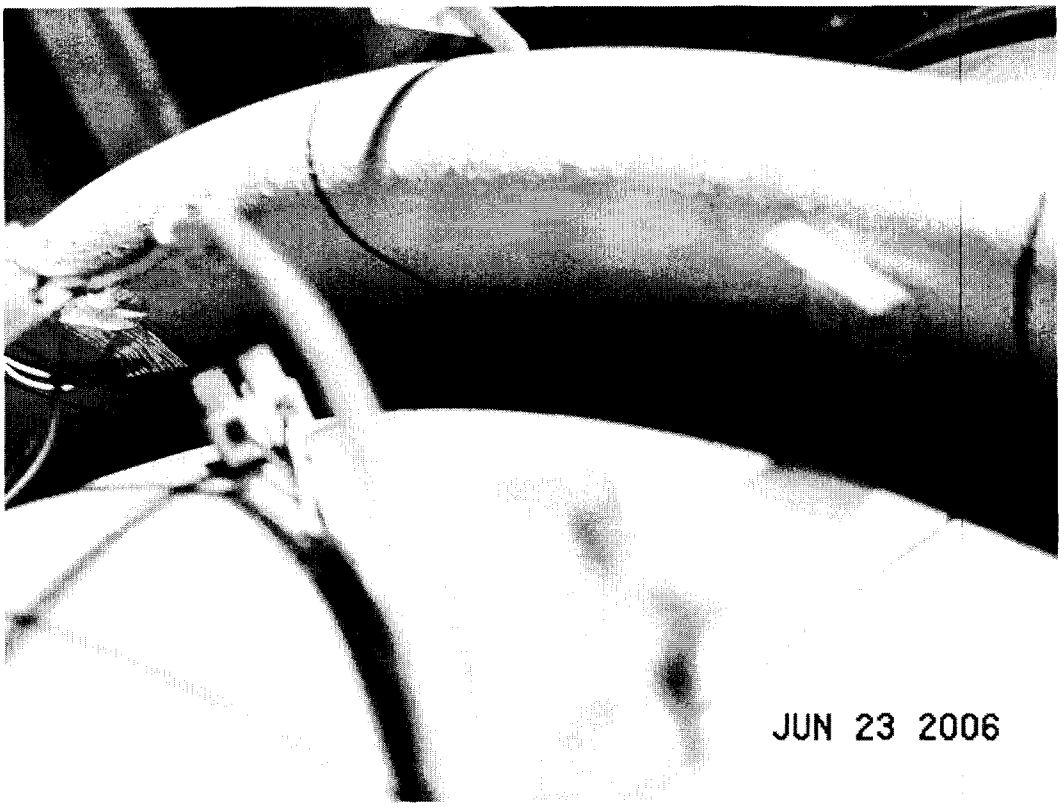

Figure 4.64 Initial Crack D20P80A4.05-6

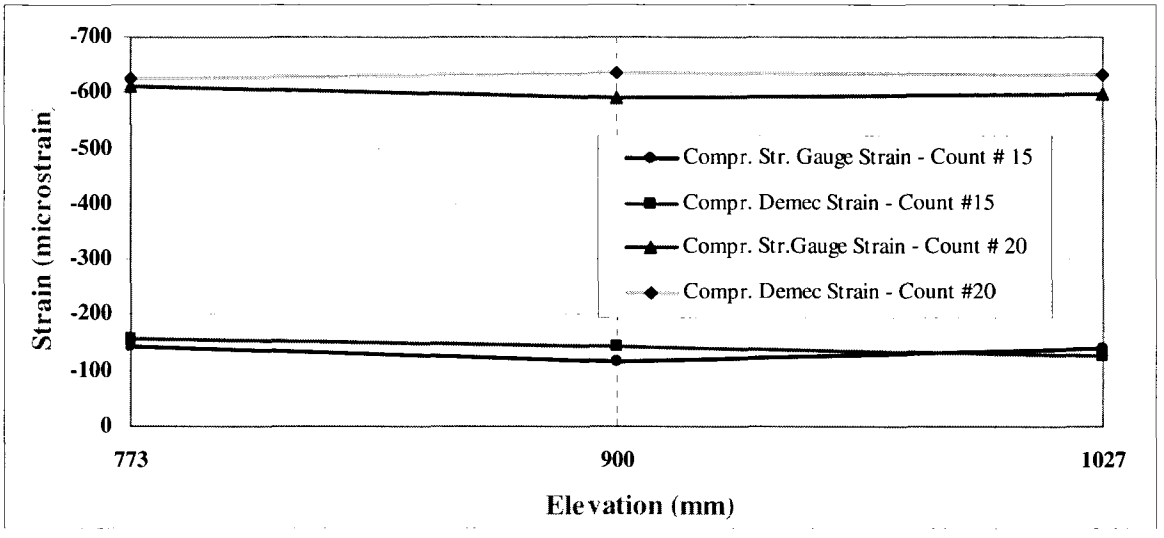

Figure 4.65 Comparison between the Demec Strain and Strain Gauge Strain D20P80A4.05-6

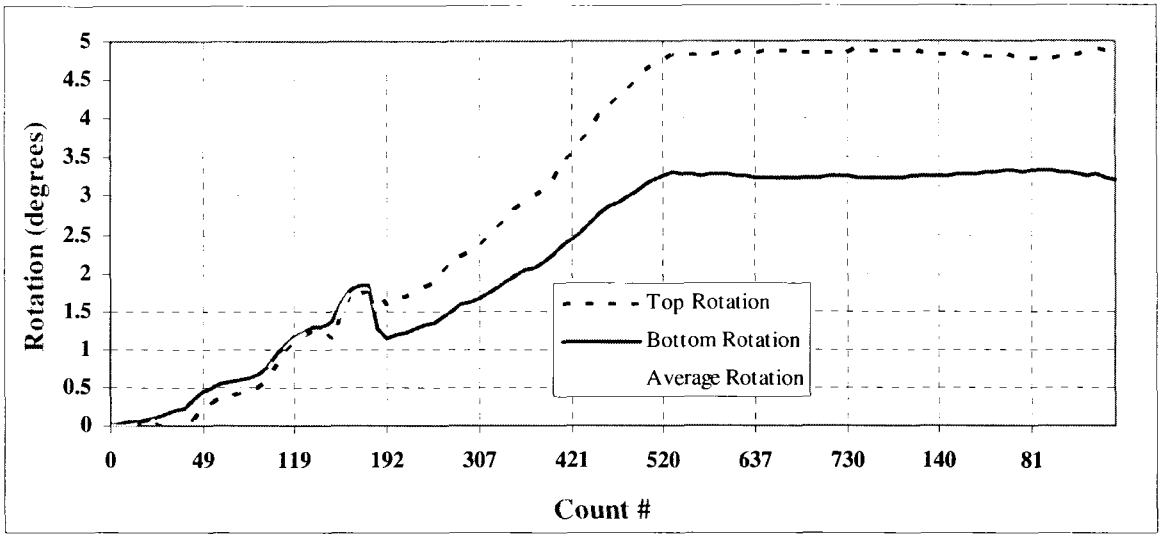

Figure 4.66 Variation of the End Rotations D2-P80A4.05-6

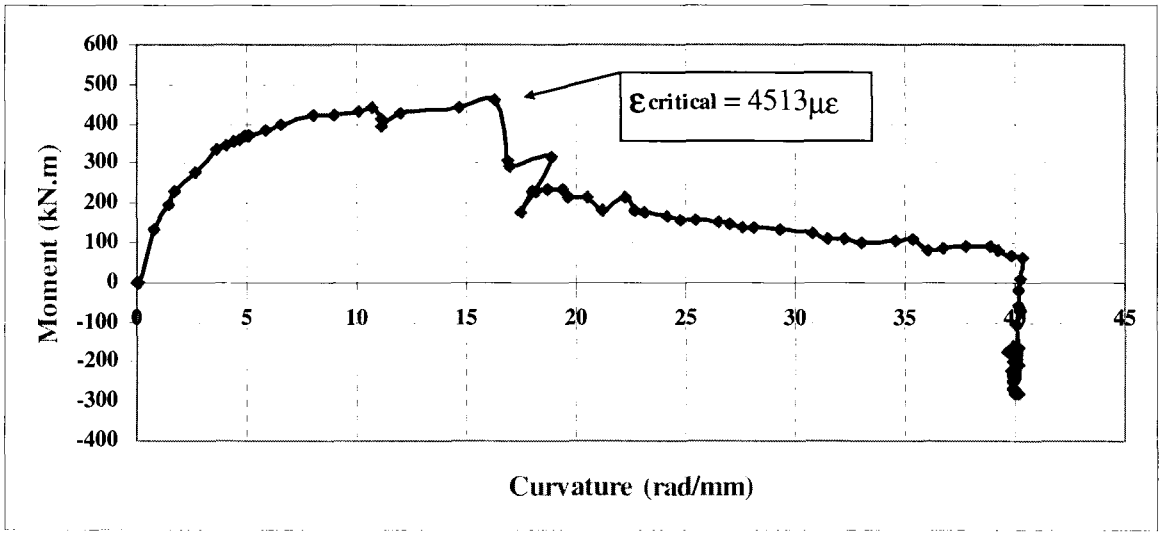

Figure 4.67 Average Global End Moment vs. Global Curvature D20P80A4.05-6

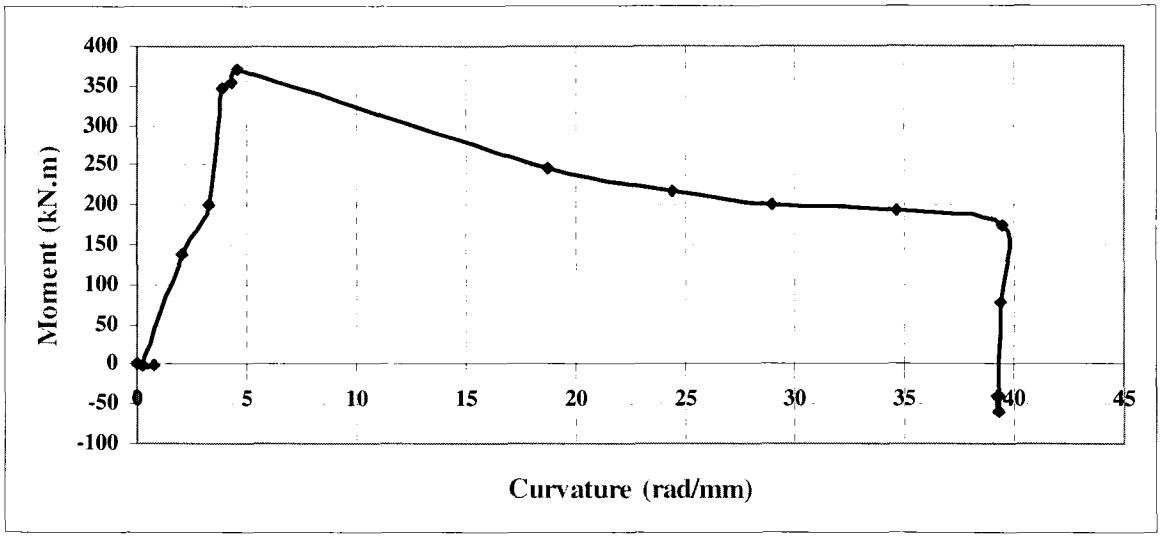

Figure 4.68 Local Moment vs. Global Curvature D20P80A4.05-6

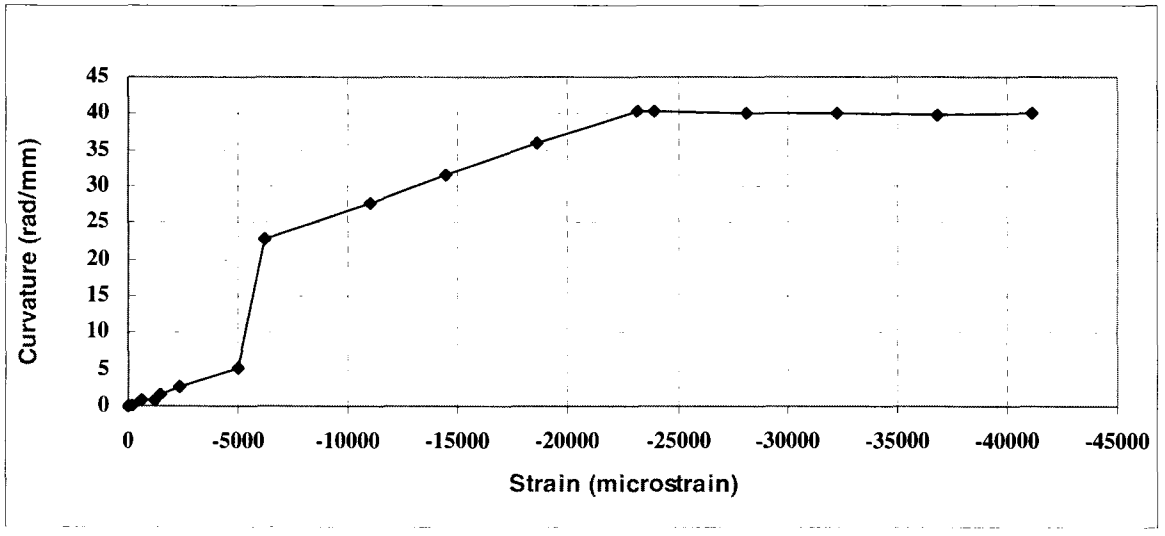

Figure 4.69 Global Curvature vs. Local Compressive Strain D20P80A4.05-6

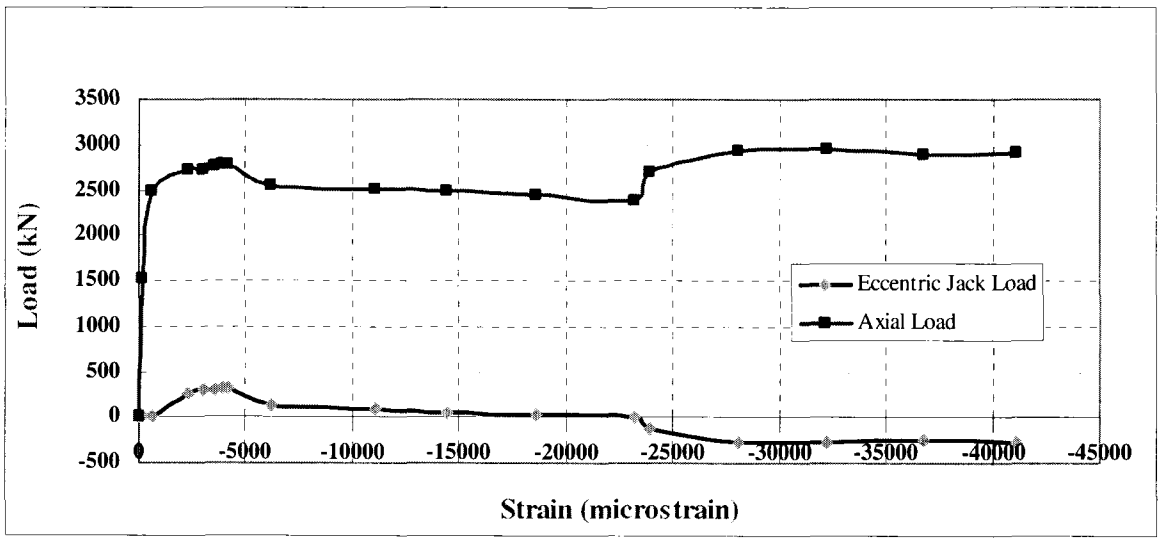

Figure 4.70 Load vs. Local Compressive Strain D20P80A4.05-6

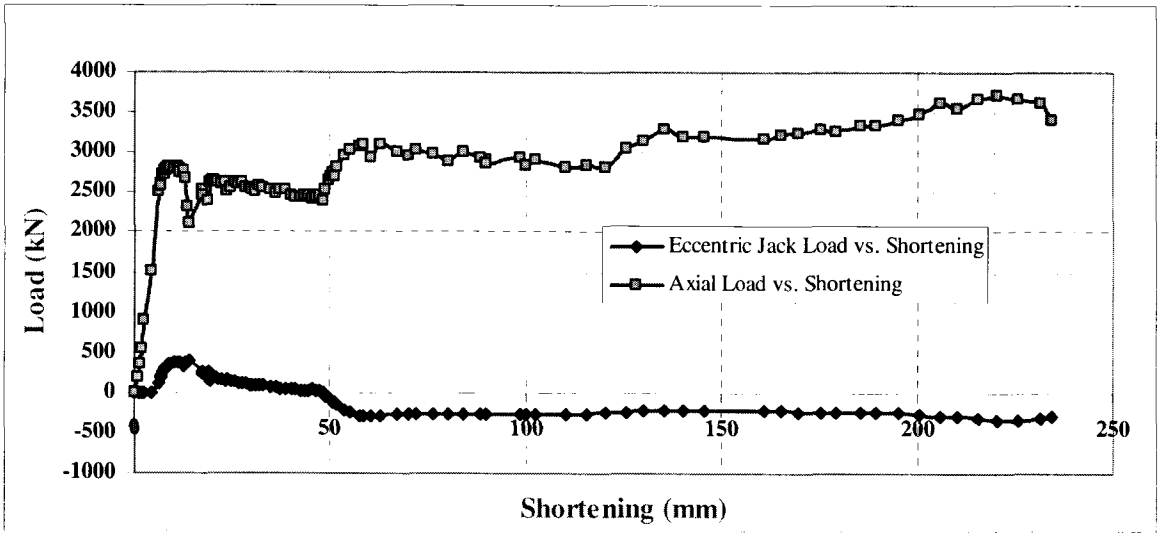

Figure 4.71 Load vs. Shortening D20P8-A4.05-6

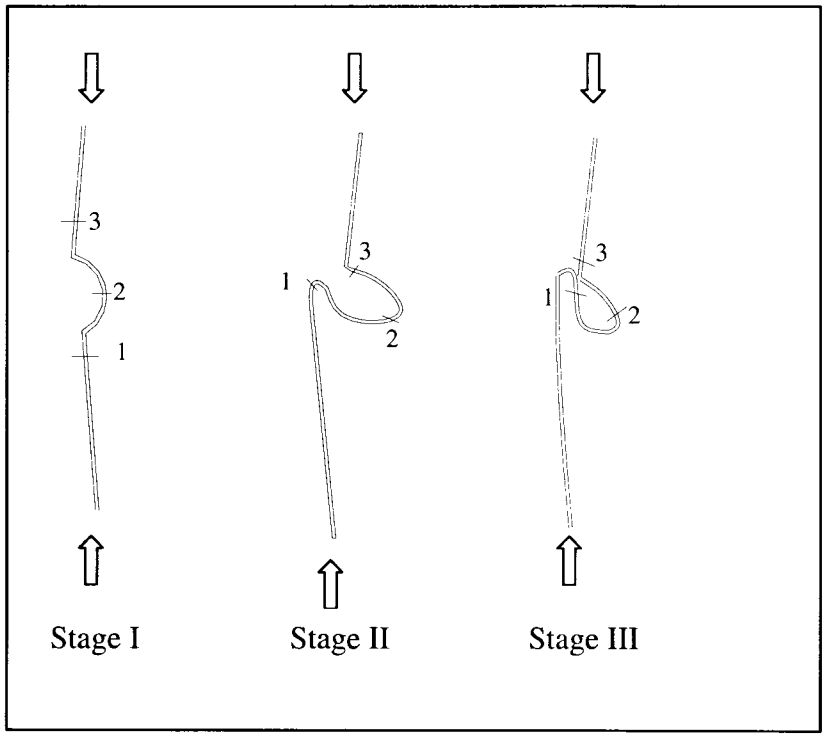

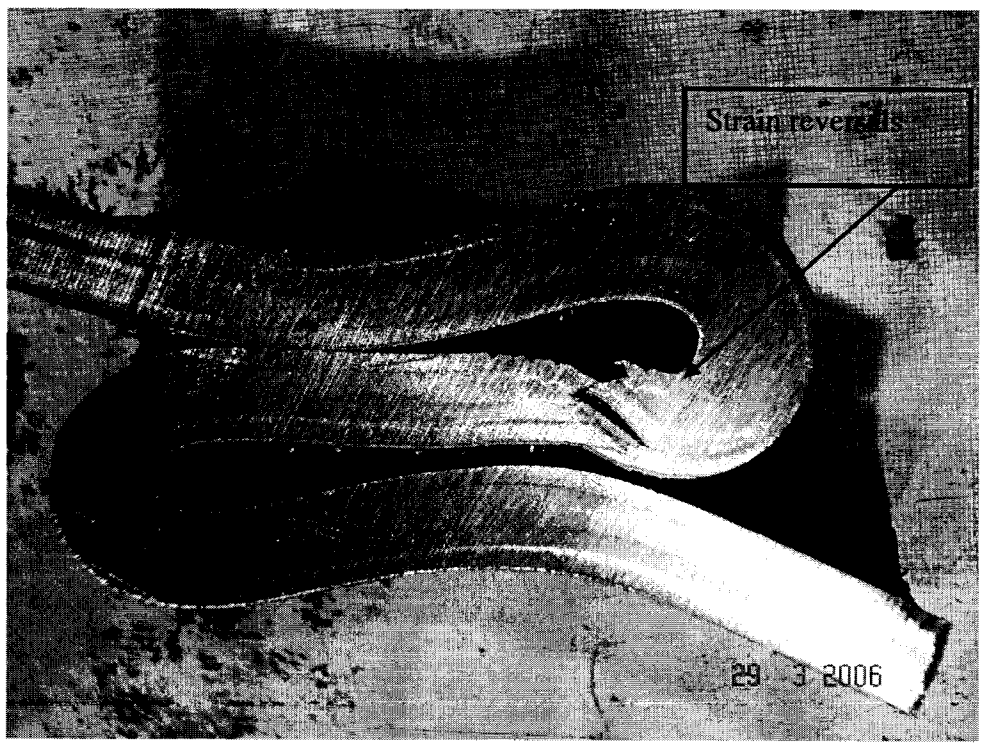

Figure 4.72 Tearing Mechanism

5. SUMMARY, CONCLUSIONS AND RECOMMENDATIONS

The summary of the fundamental objectives and the scope of this research project and the conclusions are provided in this section. Besides, recommendations to extend and improve the results of the future research work on this particular area were provided as well.

5.1. Summary

Field observations of buried pipelines indicate that geotechnical movements, temperature effects and fluid pressure in the pipe may impose large displacements on buries pipelines resulting in large local deformations of the pipe wall. During the operational life of a pipeline, the soil settlement forces the pipe to bend which may develop a wrinkle along the pipe wall. On the other hand, radial expansion of the cross-section is restrained by the surrounded soil (resulting from the internal pressure), and the longitudinal expansion (resulting from the temperature difference) of the pipeline is restrained by the soil friction and end conditions of the pipe. Both these pressure and temperature effects impose axial load on the deformed pipe which may result fracture at wrinkled location. However, limited amount of information is available about the loading history to fracture a wrinkled pipe and the deformation capacity during the post buckling period. Therefore, this project was designed to simulate the field behavior of pipelines which may fail by tearing under monotonically increasing axial load with a combination of constant internal pressure and curvature.

A total of six pipes with two different D/t ratios were tested. First three set of pipes were having 16 inches (406.4 mm) outside diameter and a D/t ratio of 34. The D/t

for the remaining pipes was 79 with an outside diameter of 20 inches (508 mm). On the other hand, 16 inches pipes were having an overall length of 1550 mm and the 20 inches were 1800 mm. During the testing of these pipes, three different levels of internal pressures were used: 0% p_y, 40% p_y and 80% p_y. As a first step, pipes were pressurized with 40% p_y (80% p_y only for the last 20 inches pipe) during increasing the curvature to create an outward bulge type wrinkle. Every specimen was pressurized initially, regardless of the type of the experiment (pressurized or unpressurized). As a second step, internal pressure was released if the test was planned as an unpressurized experiment. And for the last step, pipes were loaded axially by keeping the curvature and the pressure constant until tearing.

5.2. Conclusions

A several number of conclusions can be drawn from the experimental results obtained from this research project.

a) The pipes are highly ductile and can exhibit significant plastic deformation when they are subjected to monotonically increasing axial load under constant curvature.

b) After formation of a bulge wrinkle on the compression side, while increasing the axial load to grow the wrinkle around the circumference, the loading setup aimed to move in the out-of-plane direction. Therefore, system has to be supported laterally during testing.

c) The post-buckling behavior and tearing fracture of a wrinkled pipe are dependent on the amount of the curvature (locking angle), internal pressure and the end constrains (collars). Higher locking rotation angle and higher internal pressure will encourage

the pipe failed in the tearing failure. Also, closest collars to the wrinkle have to be removed immediately while extending the wrinkle around the circumference.

d) All three 16 inches specimens showed almost identical peak moment and critical buckling strains regardless of the loading procedure. This is also valid for the 20 inches pipes.

e) Based on the results from other research program, low-cycle fatigue of wrinkled pipes, conducted by the Pipeline Research Group at the University of Alberta, it can be concluded that if cyclic loading (or strain reversal) exists in a buried pipes under accumulated axial strain the tearing fracture will more likely to occur.

5.3. Recommendations

To the knowledge of the author, this research project is the first and the only type of its kind. Therefore, experimental results obtained from this work will provide valuable enhancement to the objectives of the project. However, better understanding of this phenomenon, which is tearing type failure, can be achieved by conducting more experiments.

First of all, it is recommended to do additional experiments to examine the influence of the internal pressure and the level of the rotation angle (curvature). Also, a FEA simulation of the specimens including the effect of the end collars, initial imperfections and detailed deformational behavior in the wrinkle region should be modeled.

REFERENCES

Bouwkamp, G. and Stephen, R.M., 1973, "Large Diameter under Combined Loading." Transportation Engineering Journal, Vol. 99, no. TE3, pp. 521-536.

Das, S., Cheng, J.J.R., and Murray, D.W., 2002, "Fracture in Wrinkled Linepipe under Monotonic Loading." ASME International Pipeline Conference, Calgary, AB, Canada, Paper No. IPC02-27097

Das, S., Cheng, J.J.R. and Murray, D.W., 2003, "Fracture of Wrinkled Energy Pipelines" Structural Engineering Report 247, Department of civil and Environmental Engineering, University of Alberta, Canada

Dorey, A.B., Cheng, J.J.R. and Murray, D.W., 2001, "Critical Buckling Strains for Energy Pipelines." Structural Engineering Report No. 237, Department of Civil and Environmental Engineering, University of Alberta, Edmonton, Canada.

Cheng, J.J.R., Aydin, M., Behbahanifard, M., Zhang, J.M. and Murray, D.W., 2006, " Tearing Fracture of 16 inch Pipes under Monotonic Loading Conditions", Report prepared for Tokyo Gas and TransCanada Ltd., Department of Civil and Environmental Engineering, University of Alberta, Edmonton, Alberta

Mohareb, M.E., Alexander, S.D.B., Kulak, G.L. and Murray, D.W., 1993, "Laboratory Testing of Line Pipe to Determine Deformation Behavior." Proceedings of the 12th International Conference on OMAE, Vol. 5-Pipeline Technology, ASME, pp. 109-114

Mohareb, M.E., Kulak, G.L., Elwi, A. and Murray, D.W., 2001, " Testing and analysis of Steel Pipeline Segments", Journal of Transportation Engineering, Vol. 127, pp.408-417

Myrholm, B.W., 2001, "Local Buckling and Fracture Behavior of Line Pipe under Cyclic Loading." Master of Science Thesis, Department of Civil and Environmental Engineering, University of Alberta, Edmonton, Canada.

Murray, D.W., 1997, "Local Buckling, Strain Localization, Wrinkling and Post-Buckling Response of Line Pipes." Engineering Structures, Vol. 19, No. 5, pp. 360-371